Investigating the molecular mechanisms of microtubule catastrophe

By

Veronica Jeanne Farmer

Dissertation

Submitted to the Faculty of the

Graduate School of Vanderbilt University

in partial fulfillment of the requirements

for the degree of

DOCTOR OF PHILOSOPHY

in

Cell & Developmental Biology

May 13, 2022

Nashville, Tennessee

Approved:

Ian Macara, PhD

Brandt Eichman, PhD

Alissa Weaver, MD, PhD

Dylan Burnette, PhD

Marija Zanic, PhD

ACKNOWLEDGMENTS

To my mentor, Dr. Marija Zanic, thank you for your scientific guidance. You successfully provided an environment to engage in rigorous, yet fun, science. I appreciate your love for critical thinking, and your dedication to mentoring. I feel incredibly privileged to be able to call you a mentor, and friend.

To my committee members, Dr. Ian Macara, Dr. Brandt Eichman, Dr. Alissa Weaver, and Dr. Dylan Burnette, thank you for your thoughtful input throughout my graduate career. I appreciate your willingness to meet and your insightful feedback.

The Zanic lab has been my home for the past six years, and I would not be the scientist, or person, I am today without having this enriching environment to engage with on a daily basis. To all the Zanic lab members, both past and present, thank you for your scientific and personal support. I am grateful to have been surrounded by exceptionally talented scientists, who were never afraid to be critical, pushing each other to do the best science possible. To the sassier grad students (Claire, Nikki, and Caye), thank you for creating a fun work environment and for all the conversations about life and lab. To Goker, thank you for your patience throughout all these years as I developed my computational skillset. I am so thankful we had each other to work with and learn from.

To the Department of Cell & Developmental Biology, specifically all the administrators who keep the department running, thank you for working behind the scene so I could focus on my research. I am so grateful to have joined such a

collaborative and fun department. Thank you to the Microtubules & Motors Club for the endless discussions and helpful feedback on preliminary data. It was a pleasure to be surrounded by so many excellent cytoskeleton-scientists.

I am grateful for the support from the Molecular Biophysics Training Program that I have received. It broadened my understanding of structural biology and immersed me in a community that I was previously intimidated by.

To my first scientific mentor, Dr. Amy Camp, thank you for giving me the opportunity to do research in your lab and provide a positive research environment. To my postbac mentor, Dr. Jadranka Loncarek, thank you for taking a chance on me. I fell in love with microscopy in your lab and I would not be the scientist I am today without that experience.

To my support network, the work detailed in this dissertation would have not been possible without you. To my best friends from Vanderbilt, Kayla, Luda, and Frankie, thank you for the dinner dates, nights out, and laughs. You were there when I needed a shoulder to cry on and there to celebrate the wins. To Dara, Caddy, and Roma, thank you for your support and unconditional love. I would have not made in through this journey without the hours-long phone calls and yearly trips to look forward to. To my family, thank you for your support and encouragement. To Carolyn & Will, thank you for always giving me a hard time while simultaneously being my biggest cheerleaders, because what else are siblings for. To my parents, Bill & Mary Jo, thank you for teaching me to persevere and your endless support.

TABLE OF CONTENTS

LIST OF FIGURES

LIST OF APPENDIX FIGURES

LIST OF ABBREVIATIONS

MT	microtubule
MTOC	microtubule organizing center
MAPs	microtubule associated proteins
γ-TURC	γ-tubulin ring complex
GTP	guanosine triphosphate
GDP	guanosine diphosphate
DIC	differential interference contrast
GMPCPP	guanosine-5'-[(α,β)-methyleno]triphosphate
UV	ultra-violet
MTBP	microtubule binding protein
XMAP215	xenopus microtubule-associated protein of 215 kDa
TOG	tumor overexpressed gene
CKAP2	cytoskeleton-associated protein 2
TPX2	targeting protein for Xklp2
CAMSAP	calmodulin-regulated spectrin-associated protein 2
CLASP	cytoplasmic linker-associated protein
SPR2	SPIRAL2
MAP2	microtubule associated protein 2
MAP4	microtubule associated protein 4
SSNA1	Sjögren's Syndrome nuclear autoantigen 1
MCAK	mitotic centromere-associated kinesin
EGTA	ethylene glycol-bis(β-aminoethyl ether)-N,N,N′,N′-tetraacetic acid

TIRF	total internal reflection fluorescence
PIPES	piperazine-N,N′-bis(2-ethanesulfonic acid)
KOH	potassium hydroxide
TAMRA	tetramethylrhodamine
Sf9	clonal isolate of Spodoptera frugiperda Sf21 cells (IPLB-Sf21-AE)
KCl	potassium chloride
DTT	dithiothreitol
EM-CCD	electron-multiplying charge-coupled device
GFP	green fluorescent protein
CAP-Gly	cytoskeleton-associated protein-glycine-rich
CH	Calponin homology
SEM	standard error of the mean
CE	counting error
CI	confidence interval
SD	standard deviation
FPS	frames per second
SSR	sum of squared residuals
MSD	mean squared displacement
Cryo-EM	cryo-electron microscopy
Cryo-ET	cryo-electron tomography
CLEM	correlative light and electron microscopy

CHAPTER 1

1. Introduction

Microtubules are dynamic polymers found in all eukaryotic cells. They are one of the major components of the cytoskeleton and are essential for a number of dynamic cellular processes; from forming the mitotic spindle and axoneme, to acting as tracks for molecular motors to facilitate intracellular transport. The dynamic nature of the polymer facilitates formation of architectures which are necessary for the cellular processes the microtubule network supports. In the absence of microtubules, cells suffer from defects in spindle formations, cell cycle arrest, and eventually cell death (Strome et al., 2001)(Hannak et al., 2002)(Yuba-Kubo et al., 2005).

Microtubules are stiff, hollow tubes typically containing 13 protofilaments that are formed through self-assembly of αβ-tubulin heterodimers that join longitudinally in a head-to-tail fashion (Figure 1)(Tilney et al., 1973)(Margolis and Wilson, 1978)(Desai and Mitchison, 1997). This arrangement results in structurally distinct polymer ends, with α-tubulin exposed at one end (termed the minus end), and β-tubulin exposed at the other (termed the plus end) (Fan et al., 1996)(Nogales et al., 1999). The biochemical and structural polarity is fundamental to microtubule function and dynamics. It is typically thought that microtubule minus ends are anchored to microtubule organizing centers (MTOCs), while the plus ends are free to explore the

cytoplasm, however this is not always the case. Some microtubule-associated molecular motors recognize the structural polarity of microtubules and use it as a directional signal. Microtubule-associated proteins (MAPs) can differentially regulate microtubule dynamics at the two ends, helping to change the overall microtubule architecture. While the basic mechanism underlying dynamic instability has been identified, many of the observed impacts MAPs have on dynamics are not explained within this simple model. Thus, despite being an intrinsic property of microtubules, dynamic instability is not fully understood. In order to understand how MAPs can change microtubule dynamics in order to regulate microtubule organization and function, we must understand all of the characteristics of microtubules that play a role in defining its stability.

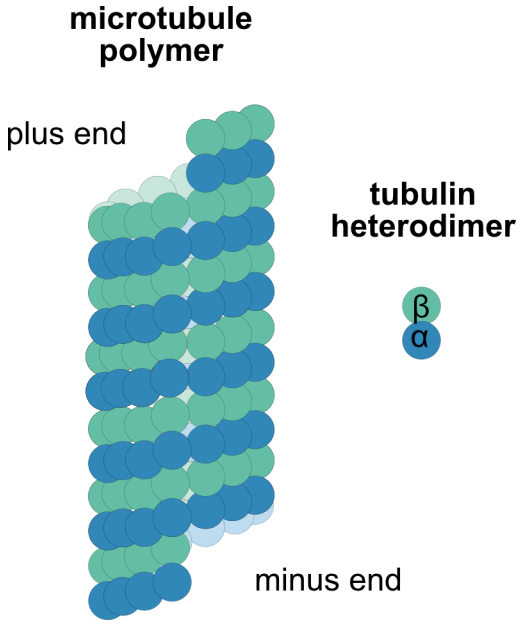

Figure 1. Schematic of the microtubule polymer structure. Microtubules are built out of tubulin heterodimers that polymerize head-to-tail, where β-tubulin is exposed at the plus end and α-tubulin is exposed at the minus end.

1.1. The microtubule network adapts distinct architectures in support of its cellular functions

Microtubule dynamics are regulated both spatially and temporally to dramatically change the overall microtubule architectures in cells. There are two major types of microtubule networks, centrosomal and noncentrosomal arrays. While arrays can be classified broadly into these two types, there are many cell-type-specific arrays that are essential for proper cellular functions (Figure 2). The regulation of microtubule dynamics at an individual microtubule level is required to drive the formation, and evolution, of these larger architectures to adapt to the needs of the cell.

1.1.1. Centrosomal arrays

Centrosomal microtubule arrays, found in many cell types such as mesenchymal cells, form when the centrosome, or spindle pole body, is the major microtubule organizing center (MTOC) and microtubules nucleate radially towards the cell cortex. Microtubules nucleate from microtubule nucleation complexes such as the γ-tubulin ring complex (γ-TURC), the most abundant nucleator in mammalian cells, with microtubule minus ends attached and the plus ends free to explore the cytoplasm (Martin and Akhmanova, 2018) (Liu et al., 2021). De novo nucleation and elongation are not an energetically favorable process, thus microtubule nucleation complexes, and their associated regulatory factors, help overcome this energy barrier by providing

templates for microtubule nucleation (Zheng et al., 1995)(Moritz et al., 2000)(Aldaz et al., 2005)(Kollman et al., 2010)(Roostalu and Surrey, 2017)(Liu et al., 2021). The α-tubulin of an incoming $\alpha\beta$-dimer binds head-to-tail off of the 13-protofilament template to begin polymerization (Aldaz et al., 2005) (Kollman et al., 2010). The placement of these complexes is a mechanism employed by the cell to regulate microtubule organization (Kollman et al., 2011). The location of γ-TURC complexes move throughout the cell cycle with the centrosomes, even increasing in number at the onset of mitosis, suggesting cell cycle dependent regulation of MTOCs and regulatory proteins (Khodjakov and Rieder, 1999). Although the microtubule network dramatically reorganizes throughout the cell cycle and specifically at the onset of mitosis, these shape changes are all still centered around centrosomal microtubule arrays. While the centrosome is the major MTOC in centrosomal microtubule arrays, microtubules are also nucleated from other MTOCs located throughout the cell. Other MTOCs during mitosis include the spindle microtubules themselves, kinetochores, and around the chromatin (Heald et al., 1996)(Maiato et al., 2004)(Petry et al., 2013). In interphase cells, it is now well established that the nuclear envelope, Golgi, and plasma membrane can serve as MTOC locations (Tassin et al., 1985)(Mogensen and Tucker, 1987)(Chabin-Brion et al., 2001)(Efimov et al., 2007). It is when these MTOCs overtake nucleation, compared to the centrosome, that the formation of noncentrosomal arrays dominates.

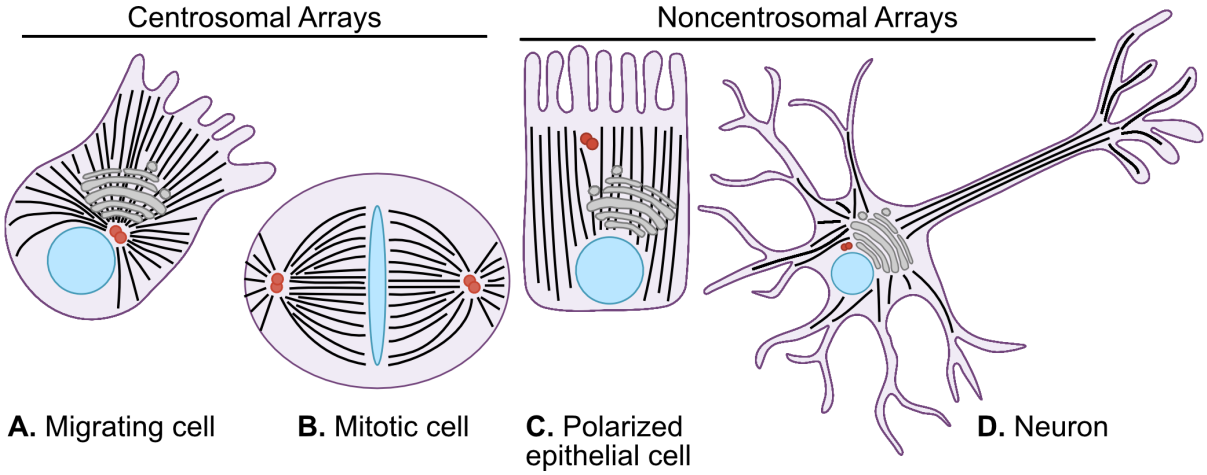

Figure 2: Cartoon of different microtubule arrays. Microtubules are in black, nuclear material in blue, centrosomes in red, Golgi apparatus in grey, and cell membrane in purple.

1.1.2. Noncentrosomal arrays

Noncentrosomal arrays are found in many cell types including plant cells, blood cells, polarized epithelial cells, and neurons. Noncentrosomal microtubule arrays can be formed in cells that contain centrosomes, just the centrosomes are not the primary location of microtubule nucleation in the cell. Similar to centrosomal arrays, nucleation of microtubules in noncentrosomal arrays occurs from nucleation complexes such as the γ-TURC and is regulated by a number of accessory proteins (Petry and Vale, 2015). MTOCs that form noncentrosomal arrays include the plasma membrane, the Golgi, and frequently the microtubule networks itself. It is important to note that as mentioned above, cells with centrosomal arrays will still have a subpopulation of microtubules that are nucleated from other MTOCs. Despite centrosomes being the

classic MTOC example, these other arrays are equally important for a number of essential cellular processes. The nucleation of Golgi-derived microtubules is highly regulated (Sanders and Kaverina, 2015). They can help direct cell migration, regulate insulin secretion, and help define overall cell and Golgi morphology (Efimov et al., 2007)(Ori-McKenney et al., 2012)(Zhu et al., 2015). Moreover, the cortical microtubule network in plants is highly organized and responsive to environmental cues (Cyr, 1994). Similarly, during differentiation, mesenchymal cells undergo a transition where the microtubule networks are reorganized into polarized noncentrosomal microtubule arrays (Datta et al., 2021).

Many general pathways needed to elicit these changes are known, however, the exact mechanisms that facilitate the spaiotemporal regulation of MTOCs are not well understood. The formation and regulation of these imperative microtubule networks is an area of active research in the field and it is already known that regulation of microtubule dynamics plays a significant role in defining these networks. Uncovering the keys to regulation of microtubule dynamics will contribute to understanding the mechanisms driving reorganization of microtubule arrays.

1.2. The GTP-cap model describes microtubule dynamic instability

Ever since it was first observed, the mechanisms behind microtubule dynamics have fascinated researches. Microtubules display dynamic instability, the ability of individual microtubules to stochastically switch between phases of growth and

shrinkage (Figure 3)(Walker et al., 1988). Dynamic instability is an intrinsic property of tubulin. While many key principles of dynamic instability have been identified, some fundamentals of the process are still not understood.

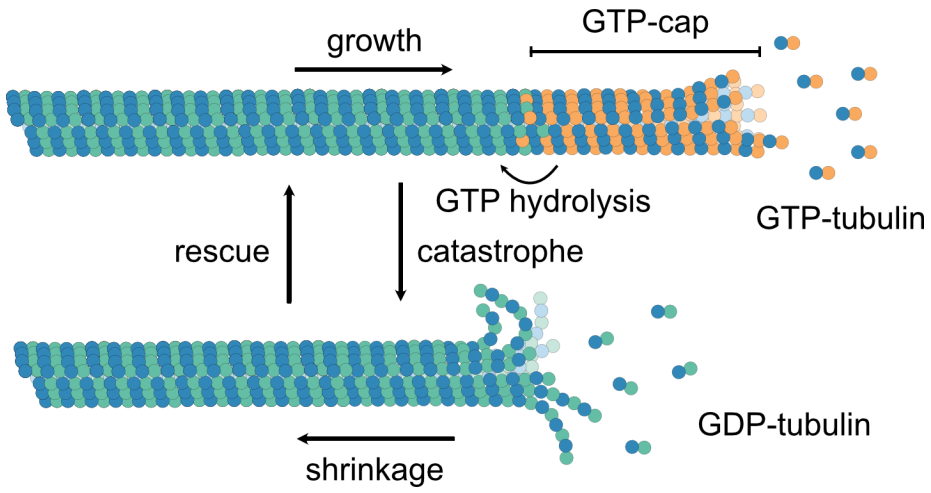

Figure 3. Microtubules undergo dynamic instability. Dynamic instability is characterized by stochastic periods of microtubule growth and shrinkage. During growth, GTP-tubulin dimers add onto the microtubule end. Shortly after incorporation, GTP hydrolyzes into GDP, creating a lattice of GDP-tubulin. The difference between the growth and GTP hydrolysis rate produces a GTP-cap at the growing end. Loss of this cap results in a catastrophe event and the microtubule switching to a phase of shrinkage. Transition from shrinkage to growth is a rescue.

1.2.1. Microtubule dynamics require GTP hydrolysis

The building block of microtubules, tubulin, is a GTPase, thus having the ability to bind and hydrolyze GTP. While both α- and β-tubulin bind GTP, only the nucleotide

associated with β-tubulin undergoes hydrolysis (Jacobs et al., 1974)(Kobayashi, 1975)(Weisenberg et al., 1976)(David-Pfeuty et al., 1977). GTPase activity in tubulin requires completion of the catalytic site, which occurs when an adjacent α-tubulin from another dimer provides an essential residue to β-tubulin (Nogales et al., 1998). The catalytic site of α-tubulin can never be completed because the essential residue needed from β -tubulin is missing, indicating why hydrolysis cannot occur in the α-tubulin subunit within a heterodimer (Löwe et al., 2001). For this reason, GTP associated with β-tubulin is considered to be in the exchangeable site, while GTP associated with α-tubulin is in the non-exchangeable site. Therefore, the nucleotide state of a tubulin dimer refers to the nucleotide state of the β-subunit.

In order to grow, αβ-tubulin heterodimers associated with GTP add on to microtubule ends (Figure 3)(Maccioni and Seeds, 1977). Once a dimer is incorporated, GTP in the β-subunit undergoes hydrolysis and phosphate release, resulting in a microtubule lattice of GDP-tubulin dimers (Linse and Mandelkow, 1988)(Carlier et al., 1989). Hydrolysis does not occur instantaneously but after a delay, resulting in a 'cap' of GTP-tubulin dimers at the growing end (Carlier and Pantaloni, 1981). This GTP-cap is stabilizing, protecting a growing microtubule from undergoing a catastrophe event and switching into a phase of rapid shrinkage (Hyman et al., 1992)(Caplow and Shanks, 1996). This GTP-cap model of dynamic instability provides an explanation for the observed characteristics of microtubule dynamics, the ability of individual microtubules to stochastically switch between phases of growth and shrinkage through transitions known as catastrophe and rescue (Mitchison and Kirschner, 1984). This unique microtubule behavior is the result of GTP hydrolysis.

Hydrolysis induces a number of conformational changes within the tubulin dimer, resulting in a lattice of unstable GDP-tubulin (Alushin et al., 2014)(Zhang et al., 2015). It is thought that these structural changes introduce strain into the microtubule lattice that is released upon depolymerization.

1.2.2. A lattice of GTP-tubulin is stable and protective, while one of GDP-tubulin is unstable

Soon after the proposal of the GTP-cap model by Mitchison & Kirshner, microtubule dynamics at the level of individual microtubules were observed thanks to the use of dark field and video-enhanced DIC (differential interference contrast) microscopy (Horio and Hotani, 1986). These methods were utilized to perform a number of pivotal experiments to support the claim that GTP-tubulin is stable and protective in polymer form while GDP-tubulin is unstable. First, microtubules polymerized with a slowly hydrolysable analogue of GTP, GMPCPP, are stable against catastrophe, indicating that hydrolysis is needed for dynamics, but not polymerization (Hyman et al., 1992). Second, severing microtubules in the middle of the lattice, using either UV-laser or a microneedle, results in rapid depolymerization from the site of severing, suggesting that the GDP-lattice is unstable and when exposed, cannot protect itself against catastrophe (Walker et al., 1989)(Tran et al., 1997). Third, dilution of soluble tubulin dimers during growth results in microtubule catastrophe and rapid depolymerization, but only after a small portion of the tip slowly shrinks (Walker et al., 1991)(Duellberg et al., 2016). Finally, the presence of a single

layer of GTP-tubulin is sufficient to protect a microtubule against catastrophe (Caplow and Shanks, 1996). These results support the conclusion that while GDP-tubulin is not stable in polymer form, GTP-tubulin is, and has the ability to protect microtubules against depolymerization.

1.2.3. The GTP-cap model predicts slow dynamic, or fast persistent growth

The GTP-cap is the result of the balance between GTP-tubulin addition, the microtubule growth rate, and the GTP hydrolysis rate. Thus, a faster growing microtubule is expected to have a larger GTP-cap, while a slower growing microtubule will have a smaller GTP-cap (Figure 4). This is under the assumption that the GTP hydrolysis is constant, and is not coupled to the microtubule growth rate. While there have been estimations of the GTP hydrolysis rate, it is still unknown what the GTP hydrolysis rate at the level of an individual microtubule is, and if this rate is coupled to the microtubule growth rate (O'Brien et al., 1987)(Flyvbjerg et al., 1996)(Bowne-Anderson et al., 2013). Due to the protective nature of the GTP-cap, it is predicted that a larger GTP-cap results in a more protected microtubule, whereas a smaller GTP-cap results in a less protected microtubule, as it is more likely to lose its cap and undergo a catastrophe (Figure 4)(Mitchison and Kirschner, 1984). There are many reports that increasing microtubule growth rate correlates with increased microtubule stability (Walker et al., 1988)(Drechsel et al., 1992)(Gardner et al., 2011b). However, confirming the prediction that a larger GTP-cap correlates with increased lifetime was not possible for decades because visualizing the GTP-cap on live microtubule is

presents many challenges (discussed in more detail in Chapter 6). It wouldn't be until a proxy for the GTP-cap on dynamic microtubules was determined that the correlation between GTP-cap size, microtubule growth rate, and stability could be elucidated. The ability to measure these three parameters on dynamic microtubules has facilitated investigations into how robust this correlation is, and how other proteins that interact with microtubules could alter it.

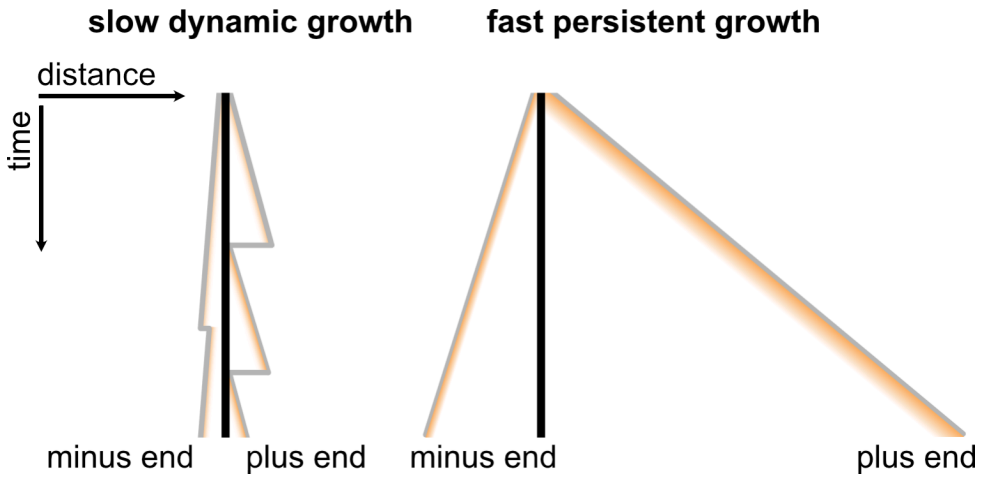

Figure 4: The GTP-cap model predicts slow dynamic growth, or fast persistent growth. Schematic kymographs of dynamic plus and minus microtubule ends growing off of stabilized seeds (black line). Microtubule end position is indicated by the grey line and GTP-cap size is depicted in yellow.

1.3. Microtubule associated proteins

In cells there is a myriad of microtubule associated proteins (MAPs) that tune and regulate microtubule dynamics. MAPs can be very broadly categorized into two

major categories based on their impact on microtubules; stabilizers or destabilizers (Goodson and Jonasson, 2018). Proteins can be further classified based on their specific function, localization, or shared domain structure. MAPs encompass one group of microtubule binding proteins (MTBP), while other groups interact with microtubules but do not directly affect microtubule dynamics. These include nucleation complexes, molecular transport motors, microtubule bundlers, and intracellular transport roadblocks. Certain MAPs have the ability to recognize and target specific structures within the microtubule lattice, such as the nucleotide state of tubulin, or differentially regulate the two microtubule ends. This very diverse set of microtubule regulators has the ability to define and regulate microtubule networks, allowing them to be as dynamic, or stable, as required for their function.

1.3.1. Stabilizers

Microtubule stabilizers are classified as proteins that positively impact microtubule growth, either by promoting growth or inhibiting shrinkage. Stabilization of the polymer can occur through two major mechanisms; it can manifest as increasing microtubule growth rate, or, decreasing the rate of depolymerization and increasing the microtubule's ability to live through pausing events. Microtubule polymerases are proteins that promote faster elongation. The most well-known microtubule polymerase is XMAP215, which is a potent polymerase conserved across species (Vasquez et al., 1994). Details on the mechanisms of action driving XMAP215 can be found in Chapter 5, however in brief, XMAP215 is a processive polymerase that uses an array of

tubulin-binding TOG (tubulin overexpressed gene) domains to increase microtubule growth rate. In addition to increasing growth rates, two other polymerases, Kinesin-5 and CKAP2, simultaneously decrease catastrophe frequency (Chen and Hancock, 2015)(McAlear and Bechstedt, 2022). It is hypothesized that Kinesin-5 does this by stabilizing lateral interactions between protofilaments, thus holding the polymer together (Chen and Hancock, 2015). The EB protein family has an overall stabilizing effect as a result of the recruitment and action of other proteins it brings to the microtubule end. While EB1 can mildly increase microtubule growth rate and catastrophe frequency *in vitro*, because depletion of EB results in decreased stability in cells, it is considered to have an overall stabilizing effect (Tirnauer et al., 2002)(Vitre et al., 2008). Some polymerases, such as XMAP215, are also considered to be nucleation factors because they promote either templated or de novo microtubule nucleation (Roostalu and Surrey, 2017). There are a number of proteins that can associate with nucleating complexes, such as γTURC, to promote/enhance microtubule nucleation. Some of these include TPX2, CAMSAP, and CLASP. All of these proteins are thought to promote growth by stabilizing lateral and/or longitudinal interactions between dimers within the microtubule polymer (Zhang et al., 2017)(Atherton et al., 2017)(Majumdar et al., 2018).

Other types of stabilizers do not promote microtubule growth, but inhibit shrinkage by increasing rescue frequency, decreasing catastrophe frequency, or decreasing shrinkage rate. Thus, it is possible for MAPs to have his stabilizing effect on microtubule dynamics without significantly impacting the microtubule growth rate (Roostalu et al., 2015)(Lawrence et al., 2018). The CLASP family of proteins decrease

the frequency of catastrophe and increase the frequency of rescue, overall promoting microtubule lifetime (Lawrence et al., 2018)(Aher et al., 2018)(Lawrence et al., 2020). TPX2 has been shown to decrease catastrophe frequency and the rate of shrinkage (Roostalu et al., 2015). Tau is a thin unstructured protein that binds between protofilaments through electrostatic interactions to sterically stabilize microtubules (Ramirez-Rios et al., 2016). Some of the first MAPs identified were MAP2 and MAP4, both of which stabilize the microtubule lattice similarly to tau (Dehmelt and Halpain, 2004). Stathmin blocks the ends of protofilaments, decreasing the overall catastrophe frequency and increasing the time microtubules spend in a pause state (Gupta et al., 2013). All of these proteins listed, and others, have the intrinsic ability to stabilize microtubules and play an important role in regulating the microtubule network in cells. Their stabilization of microtubules is often counteracted by destabilizers, resulting in a very dynamic microtubule network.

1.3.2. Destabilizers

There are many families of destabilizers, each defined by their overall function and mechanism, but a commonality is that they all have the ability to promote microtubule shrinkage. Destabilizers can be broadly subcategorized as depolymerases or severing enzymes. MCAK is a kinesin-13 motor protein that uses its ATPase activity to pull tubulin dimers off protofilament ends, thus increasing catastrophe frequency (Moores and Milligan, 2006). Kip3 is a kinesin-8 that uses its ATPase activity to walk to the microtubule end and promote catastrophe (Gardner et

al., 2011b). It is hypothesized that depolymerase activity of both motors is mediated by them tightly binding to conformations of tubulin dimers found at the microtubule end (Mulder et al., 2009)(Asenjo et al., 2013)(Arellano-Santoyo et al., 2017). Another class of MAPs that destabilize microtubules by pulling tubulin dimers out are severing enzymes. Severing enzymes are molecular machines driven by ATP hydrolysis that bind to the microtubule lattice and create holes in it by pulling out individual tubulin dimers (Kuo and Howard, 2021). If these holes are made large enough, the microtubule lattice will be severed, creating two new ends which can trigger depolymerization. While destabilization of microtubules may initially be thought of as negative, proper spatiotemporal regulation of microtubule destabilization is essential for the microtubule network to be dynamic, required for reorganization of the microtubule network.

1.3.3. Combinations of MAPs

While individual MAPs have specific effects on microtubule dynamics, MAPs can act in concert to drive complex mechanisms of microtubule dynamics regulation. The EB family of proteins is an excellent example of this; as EB recruits a number of other proteins to the microtubule tip, generating an overall stabilizing effect on the microtubule (Tirnauer et al., 2002). In addition, EB works in synergy with XMAP215 to increase microtubule growth rates to physiological rates, up to ~30-fold (Zanic et al., 2013).

Another example of MAPs working together to drive regulation of microtubule networks is the amplification of microtubule networks via severing enzymes (Vemu et al., 2018)(Kuo et al., 2019). This mechanism is dependent on the combined action of severing enzymes with other MAPs, such as SSNA1, CLASP and SPR2, that are thought to recognize and stabilize sites of microtubule damage (Nakamura et al., 2018)(Aher et al., 2020)(Lawrence et al., 2021). While severing enzymes are intrinsically destabilizers, they are an excellent example of how their function is used by the cell to elicit a different response within the microtubule network.

While the hallmark behavior of microtubules is dynamic instability, microtubules can exhibit another behavior, treadmilling. Treadmilling is a complex polymer phenomenon characterized by polymerization at one end and simultaneous depolymerization at the other, leading to overall polymer movement in one direction. Although microtubule treadmilling had been observed in cells for years, it was not known what properties of microtubule dynamics would produce treadmilling behavior. Recent work has identified that a set of four MAPs, EB1, XMAP215, CLASP, and MCAK, reconstitute microtubule treadmilling as observed in cells (Arpağ et al., 2020). This is just another example of how the cell uses the diverse function of MAPs to drive complex mechanisms of microtubule dynamics regulation.

1.4. Summary

Microtubules are highly dynamic polymers essential for a number of vital cellular processes. To carry out these functions, the microtubule network must adopt a number of diverse architectures. This plasticity is facilitated through microtubule dynamics, which is the essential property that allows the network to dynamically remodel, and regulation of dynamics through the action of MAPs. In order to understand how the microtubule network can be remodeled, it is imperative to elucidate the fundamental properties governing microtubule dynamics, and how MAPs can alter these properties.

This dissertation questions a conventional paradigm, that the size of the GTP-cap determines the microtubule stability. In Chapter 2, I discuss the *in vitro* reconstitution assay used to collect the data herein and the image analysis methods used to analyze the data. In Chapter 3, I demonstrate that increasing the microtubule growth rate by increasing tubulin concentration correlates with larger EB1 comet lengths and suppression of microtubule catastrophe, supporting the conventional paradigm. In Chapter 4, I demonstrate that although microtubule minus ends have small GTP-cap sizes, set by their slow growth rate, they are more stable. In Chapter 5, I show that the microtubule polymerase XMAP215 simultaneously increases microtubule growth rate and catastrophe frequency by perturbing the growing microtubule end. In Chapter 6, I discuss how this work relates to the current state of knowledge in the field, and future directions that need to be addressed to better understand the molecular mechanisms underlying microtubule catastrophe. In the Appendix Chapters I investigate the correlation between

microtubule tapered end structures and microtubule catastrophe, and present preliminary data on the relationship between EB1 comet length and microtubule growth rate in cells.

CHAPTER 2

2. *In vitro* reconstitution of microtubule dynamics

2.1. Introduction

The microtubule network in cells is very dense, making it difficult, or even impossible, to visualize changes at an individual microtubule level. This has resulted in challenges against interrogating the concepts of dynamic instability in living cells. Additionally, the cellular environment contains a myriad of proteins that are known to interact with microtubules, some of which have the ability to modify microtubule dynamics (Akhmanova and Steinmetz, 2008). Because of these confounding factors, many researchers have taken a biochemical reconstitution approach to studying the molecular mechanisms underlying microtubule dynamics. Biochemical reconstitution provides a controlled system to study properties of individual microtubules and how they can be regulated by different microtubule associated proteins. To date, this approach has resulted in many mechanistic discoveries facilitating further understanding of how microtubules are regulated in cells to carry out their distinct functions.

Microtubules were first observed as fibers that composed the mitotic spindle in sea urchin embryos (Inoué and Sato, 1967). Using polarized light microscopy, it was noted that this population of fibers could switch between states of polymerization and

depolymerization. Changes in fiber dynamics appeared to coincide with the phase of mitosis and could be altered by the addition of drugs or changes in buffer conditions (Inoué and Sato, 1967)(Borisy and Taylor, 1967)(Weisenberg et al., 1968). Additionally, it was hypothesized that the dynamic nature of these filaments drove chromosome separation, thus first identifying microtubules' most well-known function. Shortly after, the protein dimer tubulin, the building block of microtubules, was identified and isolated from microtubule-rich structures, such as the mitotic spindle and cilia (Shelanski and Taylor, 1967). Efficient microtubule assembly from purified tubulin *in vitro* was found to require GTP, Mg^{2+}, and a calcium chelator, such as EGTA (Weisenberg et al., 1968)(Weisenberg, 1972)(Shelanski et al., 1973)(Schilstra et al., 1991). Future studies would identify tubulin as a GTPase, with catalytic activity requiring a Mg^{2+} ion as a cofactor binding within the catalytic site in order for hydrolysis to occur(Martin et al., 1987). The requirement of a calcium chelator is still not well understood to this day; however, it is well-known that high concentrations of calcium are able to damage and promote depolymerization of microtubules, suggesting why the presence of a calcium chelator is essential for efficient microtubule polymerization (Weisenberg, 1972)(O'Brien et al., 1997). The identification of these necessary components enabled the development of a protocol for large scale tubulin purification from ungulates, primarily cows and pigs (Borisy et al., 1975). While modifications to this original protocol have been adopted, it is still the primary source of tubulin for *in vitro* studies to this day (Williams and Detrich, 1979)(Castoldi and Popov, 2003). While microtubule dynamics were first observed in living cells, the isolation of tubulin, and the discovery of its polymerization conditions, facilitated the subsequent seminal

discovery of microtubule dynamic instability (Mitchison and Kirschner, 1984). Mitchison and Kirschner utilized purified tubulin to investigate bulk polymer dynamics, identifying that microtubules coexist in growing and shrinking populations. Future studies directly observed dynamic instability at an individual microtubule level using light microscopy (Horio and Hotani, 1986)(Walker et al., 1988). Since then, *in vitro* reconstitution has facilitated numerous studies contributing to our mechanistic understanding of microtubules and MAPs' regulatory ability. As technologies and basic knowledge of fundamental processes develop, the complexity of *in vitro* reconstitution increases to better mimic the cellular environment. The vital insight gained through this approach continues to contribute to the general understanding of how biological processes are regulated.

Biochemical *in vitro* reconstitution provided us a controlled system to interrogate the fundamental relationship between microtubule stability and the GTP-cap size. We were able to regulate microtubule dynamics using purified protein components, and image the subsequent conditions using Total Internal Reflection Fluorescent (TIRF) microscopy. This approach resulted in data suitable for rigorous image analysis, allowing us to measure small changes in parameters such as microtubule growth rate fluctuations and microtubule end morphologies. While we were also interested in comparing our *in vitro* results to those from cells (see Chapter 6), *in vitro* reconstitution was the primary approach taken to obtain the majority of the data presented in this thesis. The major components of this approach are detailed in the following sections of this Chapter, while more detailed methods specific to individual Chapters can be found at their end.

2.2. Experimental Approach

2.2.1. Protein expression and purification

Purified proteins were obtained using various methods, with the chosen method for each protein being dictated by the protein's characteristics, such as charge and size. The most essential protein to this study is tubulin. Competent tubulin was purified through rounds of temperature-dependent polymerization and depolymerization in a high molarity PIPES buffer from bovine brains (Castoldi and Popov, 2003). Polymerization of competent tubulin dimers is done at a warm temperature, in polymerization promoting conditions. After polymerization, microtubule polymers are centrifuged, to remove all unwanted components. These polymers are then depolymerized in cold temperature with physical assistance, using the force of a douncer. This solution is then centrifuged to remove any polymers not competent to disassemble, and to isolate the tubulin dimers. This cycle is repeated to ensure that the final product is pure, polymerization competent, tubulin. Carrying out this process in a high molarity PIPES buffer decreases the binding affinity of MAPs to microtubules, as their interactions are electrostatic. This low-cost method yields a relatively large (micrograms) amount of tubulin, consisting of a heterogeneous population of isoforms.

Once obtained, isolated tubulin is labeled with fluorescent dyes to allow for visualization of tubulin using TIRF microscopy. Purified tubulin was polymerized and covalently labeled with either TAMRA or Alexa 647 (Invitrogen), then depolymerized (Hyman et al., 1991). Another cycle of polymerization and depolymerization was

carried out to ensure that the final population of tubulin dimers was polymerization competent. Labeling of tubulin dimers while they are in polymer form is critical to ensure that conjugation of the fluorescent dye occurred at residues of tubulin not needed to facilitate interactions between other dimers for polymerization. These methods resulted in purified tubulin used to reconstitute microtubule dynamics *in vitro*.

MAPs used in this study were obtained from expression in *E. coli* bacteria and *S. frugiperda* (Sf9), and purification using chromatography. The expression system used for each MAP was determined based on the protein's size and complexity. Large and more complex proteins, such as XMAP215, were expressed in Sf9 cells, while smaller, simpler proteins, such as EB1, were expressed in bacterial cells. While the bacterial system is faster, bacteria lack the ability to carry out certain post-translational modifications, and lack chaperons to assist in protein folding. The Sf9 system is more time consuming and costly, however, it provides a better environment for complex protein assembly. Expression of fluorescently tagged proteins yielded populations of pure protein with a 1:1 protein:tag stoichiometry. This allowed for visualization of protein localization on the microtubule in our reconstituted system using TIRF microscopy. Purification of MAPs from expression systems was done using affinity and size-exclusion chromatography. The initial type of affinity chromatography was determined based on the affinity tag attached to the expressed protein. A series of His-tags at either end of the protein was most commonly used, leading to the use of a nickel column for purification. Subsequent size-exclusion chromatography was used to clean up the protein if needed. Our ability to express and purify proteins from

different systems and utilizing different techniques provided the ability to obtain all the necessary components needed for our *in vitro* reconstitution assay in house.

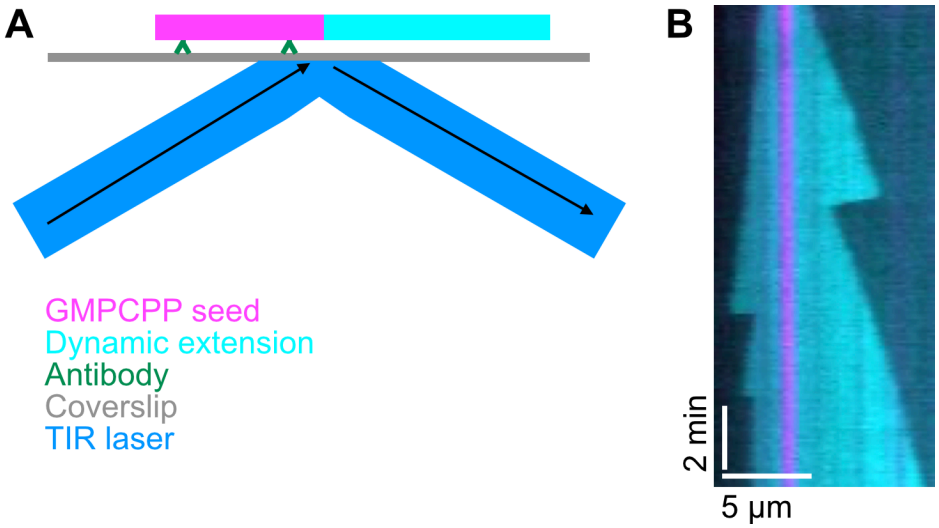

Figure 5: Schematic of microtubule dynamic assay set up and example of microtubule kymograph. (A) Stabilized GMPCPP microtubule seeds are attached to coverslips via antibodies. Soluble tubulin is introduced into reaction to visualize dynamic microtubule extensions off of stabilized seeds. Microtubule seeds and extensions are labeled with fluorophores to facilitate visualization using TIRF microscopy. (B) Example kymograph produced from dynamic assay. Microtubule dynamic parameters are quantified from kymographs.

2.2.2. Microtubule dynamics assay

The essential assay used to produce the data presented throughout this work is the microtubule dynamics assay. In brief, this assay consists of fluorescently labeled tubulin forming dynamic microtubule extensions from stabilized microtubule seeds, which are attached to a glass coverslip (Figure 5). Other MAPs, such as EB1 and

XMAP215, are included in the reaction, either as a probe or to test their effects on microtubule dynamic parameters. The assay is imaged over time using TIRF microscopy, resulting in time-lapse movies of dynamic microtubules. Fluorescently tagged MAPs facilitate visualization of their localization along these dynamic microtubules. The movies are analyzed, as detailed in the sections below, to quantify the characteristics of microtubule dynamics and localization of MAPs. While the exact experimental details depend on the question being addressed and the appropriate analytical method, the fundamental assay remains the same.

To carry out the microtubule dynamics assay, reactions containing purified protein components are incubated and imaged within an imaging channel, termed a 'flow cell'. Flow cells are constructed out of two piranha-cleaned and silanized coverslips, separated by parafilm, in custom brass holders. Piranha solution is a mixture of sulfuric acid and hydrogen peroxide that destroys organic matter, cleaning the glass coverslips. The coverslips are then coated with silane to make them hydrophobic and repel any future debris. A 22 x 22 mm coverslip is placed at the bottom of the brass holder, then three thin (1 x 22 mm) strips of parafilm are placed 2-3 mm apart from each other horizontally, creating two channels. An 18 x 18 mm coverslip is placed on top, sandwiching the parafilm, which is subsequently melted, creating a seal between the two coverslips. This process results in a flow cell consisting of two isolated flow channels. Channels are then perfused with a series of solutions to prepare the glass surface. Between solutions, channels are washed with the standard buffer microtubules polymerize in, BRB80 (80 mM PIPES/KOH, pH 6.8, 1 mM $MgCl_2$, and 1 mM EGTA). First, anti-tetramethylrhodamine (TMRA) antibody

(1:50 dilution) is nonspecifically bound to the surface, to later bind microtubule seeds labeled with TMRA. Next, the surface is passivated using Pluronic F127 to block any protein from binding non-specifically to the surface. Stabilized microtubule seeds are polymerized with a slowly-hydrolyzable GTP analogue, GMPCPP, and TMRA labeled tubulin, which facilitates seed binding to the flow cell surface. Seeds are composed of 25% TMRA -tubulin and 75% unlabeled tubulin. Polymerization with GMPCPP yields stable microtubules, as tubulin within these microtubule seeds will not undergo hydrolysis within the timeframe needed. Microtubule nucleation de novo is energetically unfavorable which results in a high energy barrier. This barrier is overcome with the use of stabilized seeds, as they provide templates for dynamic extensions to grow off of. Seeds were polymerized for 1 hour at 35°C, then ultracentrifuged at 126,000 g for 5 minutes to remove any unpolymerized dimers. The pellet of seeds was resuspended in 100 μl of BRB80, then diluted 1:10 to perfuse through the flow cell. Incubation time and volume of seeds perfused was dependent on the desired final seed density, determined based on the experimental conditions. Imaging channels were then ready for use, and were placed on the TIRF microscope for 10 minutes prior to the addition of a reaction mixture to ensure the flow cell was heated to 35°C. The basis of all reaction mixes was purified tubulin labeled with A647 dye (labeling ratio was 10% of the tubulin concentration), 1 mM GTP, and anti-fade solution (40 mM D-glucose, 40 μg/ml glucose oxidase, 16 μg/ml catalase, 0.08 mg/ml casein, 10 mM dithiothreitol (DTT)). Final salt concentration in the reaction was made to be 17-50 mM KCl, depending on the experiment. 0.01% methylcellulose was included in all reactions to help weight the microtubule polymers down and keep them

close to the surface. This basic reaction was modified to result in various buffer conditions, tubulin concentrations, nucleotide types, and the addition of MAPs at various concentrations. This microtubule dynamic assay provides a robust and controlled method to interrogate the effects of various perturbations, such as tubulin concentration, titration of individual MAPs and the combination of multiple MAPs, on microtubule dynamics. Modifications to this general method for individual experiments are described in their respective methods Chapters.

2.2.3. TIRF microscopy

In order to visualize our *in vitro* microtubule dynamics assay we utilize TIRF microscopy (Figure 5). TIRF is a modality of light microscopy that takes advantage of a specific principle: the evanescent wave. An evanescent wave is formed when total internal reflection occurs as the result of a plane wave hitting the interface between two materials with different reflective indexes at a critical angle. In light microscopy, this is manifested when the laser light passes through glass, then water, at a critical angle. The evanescent wave illuminates approximately 100 nm into the sample, exponentially decaying away from the point of interference. The advantage of this modality is that only the 100 nm closest to the coverslip is illuminated, as opposed to classic fluorescence which illuminates infinite depth of the sample. This dramatically reduces the amount of background fluorescence by not exciting fluorophores out of the 100 nm range, therefore increasing the effective signal-to-noise ratio of the

sample. Because of its characteristics, TIRF microscopy is an excellent tool for observing processes directly at the coverslip surface, such as dynamic microtubules.

For the work herein, unless otherwise specified, imaging was performed using a Nikon Eclipse Ti microscope with a 100×/1.49 NA TIRF objective; an Andor iXon Ultra EM-CCD (electron-multiplying charge-coupled device) camera; 488-nm, 561-nm, and 640-nm solid-state lasers (Nikon Lu-NA); and a Finger Lakes Instruments HS-625 high-speed emission filter wheel with standard filter sets. An objective heater was used to maintain the sample at 35°C. Images were acquired using NIS-Elements (Nikon). Time-lapse lengths varied from 1 - 15 minutes, and frame rates varied from 5 - 0.2 frames per second, depending on the question being addressed. Faster temporal imaging was used to better approximate shrinkage rates and for EB1 comet analysis.

2.3. Image Analysis

2.3.1. Microtubule dynamics analysis

Microtubule dynamic parameters (growth rate, shrinkage rate, catastrophe frequency, and rescue frequency) were analyzed by producing kymographs of dynamic microtubules over time using a custom plugin in FIJI (Figure 5)(Schindelin et al., 2012). If drift occurred in x,y space over the time-lapse, it was corrected using the Image Stabilizer plugin prior to analysis. Kymographs were formed from drawing 5-pixel-wide lines along individual microtubules on a maximum intensity projection of the time-lapse. 20 kymographs were made and analyzed per condition for dynamic

parameter analysis. Dynamic parameters were determined as previously described (Zanic, 2016). Briefly, a three-point-system was used to define coordinates of microtubule growth events with the first point being the beginning of the event, the second the point the time of catastrophe, and the third point the end of the growth event. If a microtubule did not catastrophe, but rather grew out of the field of view, the second and third point was the same. If a microtubule event rescued, the last point of that event and the first point of the subsequent event was the same. These coordinates were imported into Excel and the difference between the coordinates were used to determine the dynamic parameters. Individual growth and shrinkage rates were averaged over an experimental condition to determine an average rate and standard error. Catastrophe frequency was determined as the number of catastrophes observed within the total time spent in growth for all events. Similarly, rescue frequency was determined as the number of rescues observed within the total time spent in shrinkage for all events. Any additional analysis of microtubule growth, such as growth rate variability and instantaneous growth rate, is described in detail within the respective Chapter.

2.3.2. EB1 comet analysis

Analysis of EB1 comet lengths were used as a proxy for the size of the GTP-cap, similar to previously published work (Bieling et al., 2007)(Seetapun et al., 2012). In order to analyze EB1 comet lengths, reactions included 200 nM EB1-GFP. EB1 comet lengths were determined using a series of custom MATLAB (version R2020a,

MathWorks) scripts. These analysis scripts evolved over time as we refined our methodology. Detailed methods are provided in each subsequent Chapter to explain how comet analysis was done for each dataset. While the exact methods changed overtime, they were changed to best represent the acquired data, and the general methodology remained the same and is detailed here.

It is well known that EB1 localization resembles a comet-shape, with the brightest signal closest to the microtubule tip and exponentially decaying down the microtubule lattice. We used kymographs of microtubule growth events to take intensity profiles of EB1-GFP along each frame during a defined period of growth using a 1-pixel-wide linescan. These intensity profiles, or linescans, were then aligned based on the maximum intensity pixel, assumed to be the microtubule tip position. The background intensity for each linescan was determined by averaging the intensity in a set number of pixels in front of the microtubule tip. This background intensity was then subtracted from the linescan so that each linescan was independently background subtracted to account for any variations in the background intensity throughout the field of view. Each pixel along the background subtracted linescans was averaged, generating one averaged intensity profile per microtubule growth event. This intensity profile was then fit to an exponential decay function to determine the decay constant, or the GTP-cap size. Only microtubule growth events of an invariable growth rate were used for comet analysis so that each averaged intensity profile, thus comet length, could be correlated with a growth rate. Growth rates for each growth event were calculated by taking the difference between the start and end coordinates, determined from the same kymograph linescans were made on. This

analysis pipeline resulted in a correlation between microtubule growth rate and EB1 comet length, or GTP-cap size, as previously reported (Bieling et al., 2007).

Interestingly, this work details the observation of noncanonical EB1 comet morphologies. As explained above, EB1 typically localized in a comet-like-shape, however, we saw instances of EB1 comets splitting into two puncta. To our knowledge this is the second report of these splitting comets being observed (Aher et al., 2018). We interpret these splitting comets to indicate that a subset of the protofilaments are growing faster than the others, the leading comet, while the lagging comet signifies where the tips of the remaining protofilaments are, forming a full microtubule lattice. There are instances when the leading comet appears to curl outward, away from the lagging comet's growth trajectory; we termed these events curled comets. EB1 comet morphologies were considered while choosing microtubule growth events on which to preform comet analysis, with only growth events displaying full comets being used.

2.4. Summary

The combination of *in vitro* reconstitution with quantitative image analysis provides a robust assay for interrogating the effect of various MAPs on microtubule dynamics, including GTP-cap size, in a controlled manner. Increasing the system's complexity by increasing the number of components allows closer resemblance to a cellular system.

CHAPTER 3

3. GTP-cap size scales with microtubule growth rate *in vitro*

Adapted from:

Farmer, V., G. Arpağ, S. Hall, and M. Zanic. 2021. XMAP215 promotes microtubule catastrophe by disrupting the growing microtubule end. *J. Cell Biol.* 220:1–13. doi:10.1101/2020.12.29.424748.

3.1. Introduction

Although the concept that the GTP-cap size scales with microtubule growth rate and lifetime has been accepted by the field for decades, this hypothesis could not be tested because there was no way to visualize the GTP-cap. The identification of the EB family of proteins as markers for the GTP-cap has facilitated testing of this hypothesis, as well as a deeper investigation of the GTP-cap size under various conditions. While many of these results in this Chapter have been previously reported in the literature, these observations were essential to establish in our hands as they are the basis of this entire work.

3.1.1. Direct observation of the GTP-cap is not possible

While there are many lines of evidence to support the idea that there is a GTP-cap at the growing end of a microtubule, it has been challenging to investigate the cap's role in microtubule stability because direct visualization of the nucleotide state of tubulin within dynamic microtubules has not been possible. Structural biology techniques, such as x-ray crystallography and electron microscopy, are needed in order to have sufficiently high resolution to visualize the nucleotide state of tubulin. These techniques typically require fixed samples and averaging of images which makes visualizing dynamic microtubules almost impossible. While there have been improvements to sample preparation and image processing throughout the years, we are still unable to directly visualize the GTP-cap on the end of a dynamic microtubule and correlate it to microtubule stability. In order to correlate the GTP-cap size with microtubule stability, the GTP-cap size must be visualized on dynamic, live, microtubules.

3.1.2. The EB family of proteins are well characterized microtubule tip markers

In cells there is a myriad of MAPs that bind to microtubules, affecting microtubule dynamics directly, or acting indirectly by targeting other proteins to the microtubule. One of the most well-known families of MAP is the EB family of proteins (Su et al., 1995)(Mustyatsa et al., 2017). This family of proteins is conserved across

species with higher order organisms such as humans, having three isoforms, EB1, 2, and 3, while yeast have a single isoform, Mal3 (Lansbergen and Akhmanova, 2006). A coiled-coil motif directly prior to the C-terminal domain of the protein mediates dimerization of EB monomers (Figure 6A)(De Groot et al., 2010). The very C-terminal domain facilitates EBs interactions with other proteins, with truncation of the last 20 amino acids of the protein eliminating EB's ability to recruit other proteins to the microtubule tip (Komarova et al., 2005). The EB family of proteins is most known for its autonomous microtubule tip localization during growth (Bieling et al., 2007)(Maurer et al., 2012). This tip tracking is mediated thorough the Calponin homology (CH) domain at the N-terminus of the protein (Figure 6B). While dimerization of EB is not needed for its tip localization, it is thought to be a prerequisite in cells to tip track and to recruit other proteins to the microtubule tip (Sen et al., 2013). EB is frequently used as a marker for microtubules in cells due to its ability to clearly and specifically mark growing ends. The microtubule network is extremely dense, making visualization of the network overwhelming if looked at using a tubulin probe. However, visualization of the network using the EB proteins provides a less dense readout of microtubule ends, allowing individual microtubules to have the ability to be followed through space and time. The use of EB as a marker for microtubule tips in cells is elaborated on later in this work.

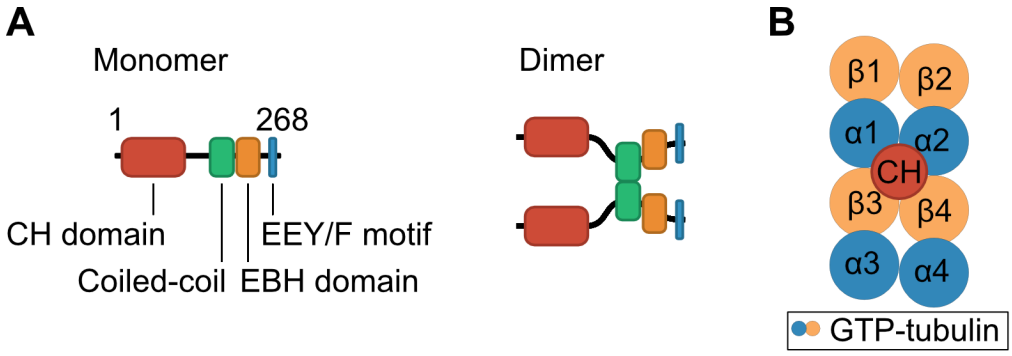

CH (Calponin homology) domain: mediates binding to the microtubule lattice
Coiled-coil: mediates dimerization of EB1
EBH (End Binding Homology) domain: mediates protein-protein interactions
EEY/F motif: mediates protein-protein interactions

Figure 6. Domain structure of EB1 facilitates its functions. (A) Major protein domains of EB1. EB1 forms a dimer through its coiled-coil domain. EB1 recruits other MAPs and proteins to the microtubule tip through interactions with its EBH domain and EEY/F motif. (B) EB binds the microtubule lattice, at the intersection of four tubulin dimers, though its CH domain.

Along with autonomously tip tracking, EB family members are known to recruit a number of other proteins to the microtubule tip. As a result, it is known to regulate a complex network of proteins called the +TIPs (Lansbergen and Akhmanova, 2006)(Mustyatsa et al., 2017). These proteins include other MAPs, signaling factors, and motor proteins. These protein complexes help anchor microtubules to the cell cortex, connect microtubule to kinetochores, and regulate microtubule dynamics. All of these activities are regulated both spatially and temporally, making the overall microtubule architecture important for acting as signaling hubs throughout various cellular processes.

3.1.3. EB proteins recognize the nucleotide state of tubulin in the microtubule lattice

The EB family of proteins was widely used as a microtubule tip marker before it was understood what drove its localization. EB localizes to the growing microtubule end in a comet-like shape, with the strongest localization at the tip, while localization exponentially decays down the lattice (Tirnauer et al., 2002)(Bieling et al., 2007)(Maurer et al., 2014). It was observed that EB only localized to growing microtubule ends, not shrinking ends, indicating that whatever it recognizes is only present during the phase of growth (Maurer et al., 2012)(Duellberg et al., 2016). Using nucleotide analogues, it was observed that EB has a higher affinity for binding microtubule lattices polymerized with GTP-like analogues over GDP-like analogues (Zanic et al., 2009)(Maurer et al., 2011). This data suggested that EB is able to recognize the nucleotide state within the microtubule lattice and has a preference for GTP-tubulin over GDP-tubulin. Structural studies support this concept, suggesting that EB is able to recognize the structural changes induced by GTP hydrolysis within the tubulin dimers in the microtubule lattice (Maurer et al., 2012)(Alushin et al., 2014)(Zhang et al., 2015). EB binds at the interface of four tubulin dimers, so it is thought that EB has to have two adjacent protofilaments present in order to complete its binding site (Maurer et al., 2012). Recent molecular dynamic simulations have suggested that EB may be able to bind to a partially formed binding site with a different affinity, thus only needing one protofilament to bind (Reid et al., 2019). The details of this localization need to be further investigated; however, it holds true that EB binds

the stabilizing region of the microtubule end. High temporal imaging of EB at the microtubule tip has demonstrated that not only does EB not localize to shrinking ends, but it is lost prior to the onset of catastrophe (Maurer et al., 2012)(Duellberg et al., 2016). This has been shown both on microtubules that undergo catastrophe naturally, and after catastrophe is artificially induced. These studies conclude that there is a threshold of EB localization that must be reached before a microtubule will undergo a catastrophe, indicating that the GTP-cap size must decrease to a critical size before it will no longer protect a microtubule against catastrophe (Maurer et al., 2012). This observation corroborates the GTP-cap model, suggesting that the GTP-cap must be lost prior to the onset of catastrophe. The culmination of all of these results lead to the field's conclusion that EB marks the GTP-cap.

3.1.4. EB proteins modulate microtubule dynamics

While it is thought that EB's tip localization is primarily used by the cell to recruit other microtubule regulatory proteins to the microtubule end, EB itself does have effects on microtubule dynamics. Modulation of EB expression levels in cells results in altered microtubule dynamics. However, these alterations in microtubule dynamics are not thought to be the direct result of EB acing on the microtubule, but thought to be driven by mislocalization of the microtubule regulators EB typically brings to the tip. The C-terminal domain of EB mediates direct binding to other proteins through cytoskeleton-associated protein-glycine-rich (CAP-Gly) and SxIP motifs (Honnappa et al., 2006)(Weisbrich et al., 2007)(Steinmetz and Akhmanova, 2008)(Bieling et al.,

2008)(Dixit et al., 2009)(Honnappa et al., 2009). C-terminal truncations of EB reveal that EB still localizes to the microtubule tips, but altered microtubule dynamics still exist, a result that is attributed to the loss of other regulators (Komarova et al., 2005). *In vitro* reconstitution was used in order to determine what direct effect EB has on microtubule dynamics. It is now understood that EB1 has the ability to increase microtubule growth rate around 1.5-fold, and increase catastrophe frequency around 2-fold on its own (Vitre et al., 2008)(Komarova et al., 2009)(Stepanova et al., 2010). In other words, EB1 is able to increase microtubule growth rate, while simultaneously decreasing microtubule lifetime. It is hypothesized that EB1 does this by promoting lateral interactions between protofilaments, and thus increasing the GTP-hydrolysis rate at the growing end. Unfortunately, to date, there is no way to fully test this hypothesis since EB is our best readout for the GTP-cap. While these effects on dynamics appear to be true, they are thought to be side-effects of EB's high specificity to the growing end, and not the primary role of the protein.

3.1.5. The GTP-cap size positively scales with microtubule growth rate, and inversely correlates with microtubule stability when microtubule growth rate is modulated with tubulin concentration

Identification of EB as a marker for the GTP-cap size has allowed the field to interrogate the relationship between microtubule growth rate and GTP-cap size proposed by the GTP-cap model. In addition, it facilitates investigation of the assumed relationship between microtubule stability and GTP-cap size, that a larger GTP-cap is

more protective than a smaller GTP-cap. It is well established in the field that increasing tubulin concentration results in faster growing microtubules (Walker et al., 1988). Using a tubulin titration and constant EB, it is demonstrated that, *in vitro*, increasing microtubule growth rate leads to larger GTP-caps and a suppression of catastrophe frequency (Bieling et al., 2007)(Farmer et al., 2021).

3.2. Results

3.2.1. Increasing the microtubule growth rate by increasing tubulin concentration correlates with an increase in GTP-cap size and suppression of microtubule catastrophe

To directly investigate the relationship between microtubule growth rate, catastrophe frequency, and GTP-cap size, we used an established *in vitro* assay (Gell et al., 2010). Dynamic microtubule extensions were polymerized from GMPCPP-stabilized seeds using a range of tubulin concentrations (12 - 60 μM), and imaged with TIRF microscopy (Figure 7A). To determine the size of the GTP-cap, we included 200 nM EB1-GFP in all conditions, and measured the EB1 comet size at growing microtubule ends over a range of growth rates. The increase in growth rate achieved with tubulin titration was accompanied by a simultaneous suppression of catastrophe frequency (Figure 7B), consistent with studies using tubulin alone (Walker et al., 1988). In addition, increasing growth rates resulted in a linear increase in the average EB1 comet size (Figure 7C), consistent with previous reports (Bieling et al., 2007). Thus, our measurements directly establish an inverse correlation between GTP-cap

size and catastrophe frequency, when increase in growth rate is achieved by increasing tubulin concentration in the presence of EB1 (Figure 7D). This finding is consistent with a model in which faster microtubule growth leads to a larger GTP-cap, which in turn provides enhanced protection against catastrophe.

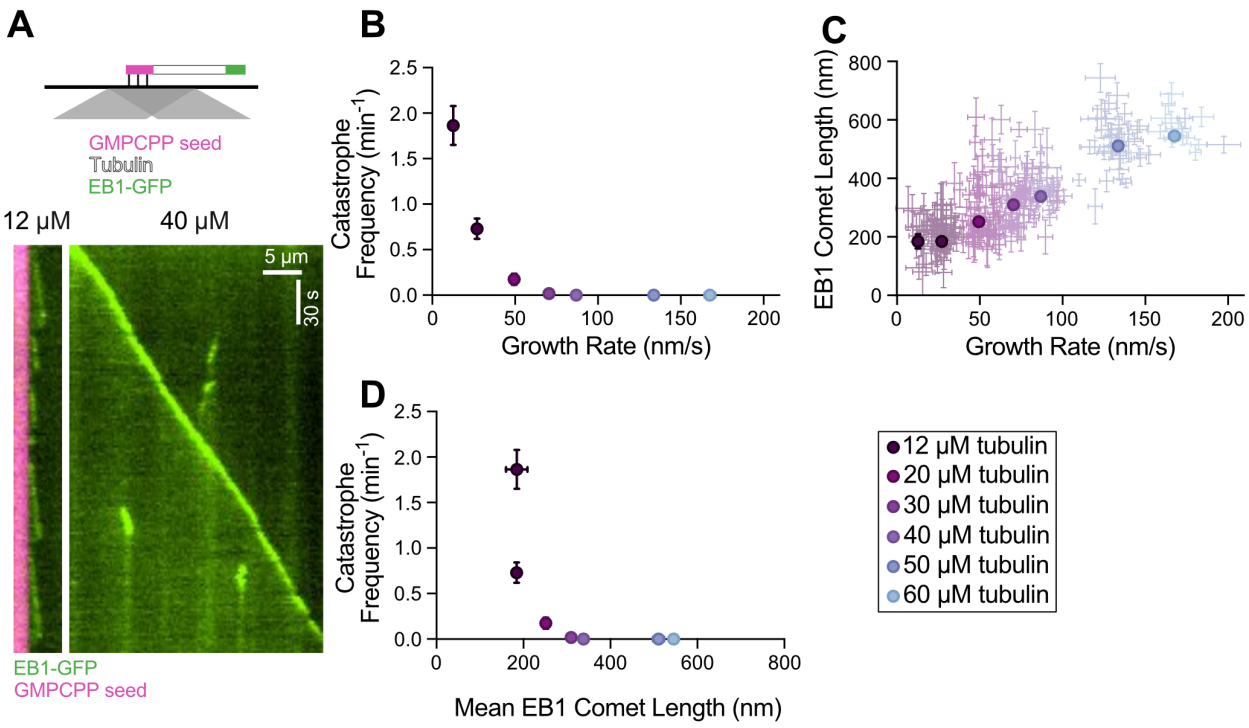

Figure 7. Increasing the microtubule growth rate by increasing tubulin concentration correlates with larger EB1 comet lengths and suppression of microtubule catastrophe. (A) Top: schematic of TIRF assay. Dynamic microtubule extensions were polymerized from GMPCPP-stabilized seeds using unlabeled tubulin in the presence of EB1-GFP. Bottom: Representative kymographs of microtubule plus ends grown with either 12 or 40 μM tubulin and 200 nM EB1-GFP. (B) Microtubule catastrophe frequency as a function of microtubule growth rate. Each point is the mean growth rate and catastrophe frequency for a single experimental condition. Error bars are SEM and CE, respectively. Any error bars that are not visible are smaller than the size of the data point. (C) EB1 comet length as a function of microtubule growth rate.

Dim points are growth rates and comet lengths for individual 30-second growth segments. Error bars are 95% CI. Bold points are weighted means for each experimental condition, with error bars being the weighted error. Any error bars that are not visible are smaller than the size of the data point. (D) Catastrophe frequency (displayed in B) replotted as a function of mean EB1 comet length (displayed in C) for each experimental condition. For all panels, 20 microtubule kymographs were analyzed for each experimental condition. All experiments were performed on the same day.

3.3. Discussion

The identification of EB1 as a marker for the GTP-cap has, for the first time, facilitated a way to interrogate the size of the GTP-cap on live, dynamic microtubules. By employing EB as a proxy for the GTP-cap, we have confirmed that, when grown with tubulin alone, increased microtubule growth rate leads to increased GTP-cap size and microtubule lifetime. Therefore, EB1 will be employed throughout the remainder of this work in order to interrogate the correlation between GTP-cap size and microtubule stability. While we cannot be sure what the GTP-cap size is in the absence of EB1, EB1 is always present in vivo, thus it is physiologically relevant. Despite the fact that very low concentrations of EBs have been reported to increase the GTP hydrolysis rate (see Chapter 6)(Maurer et al., 2011), this baseline can still be used to understand how other MAPs change the GTP-cap size of microtubules grown with EB1 (as is always the case in cells). To control for this possibility, the same saturating concentration of EB1 is used for all experiments. In addition, the hypothesis that EB1

increases the GTP hydrolysis sets a precedent for other MAPs to have the same ability.

3.4. Methods

3.4.1. Protein Purification

Bovine tubulin was purified and labeled with fluorescent dyes are previously described in Chapter 2. EB1-GFP was expressed in *Escherichia coli* and purified as previously described (Zanic et al., 2009) and stored in 10 mM Bis-Tris, 10 mM TrisHCl, 100 mM KCl, 1mM DTT, 5% glycerol, pH 6.6. Protein concentration was determined using absorbance at 280 nm.

3.4.2. Dynamics assays

Tubulin titration was performed as previously described in Chapter 2, and tubulin concentrations are indicated within the figures. For Figure 7, reactions contained imaging buffer, concentrations of tubulin ranging from 12 to 60 μM, 200 nM EB1-GFP, 1 mM GTP, 17 mM KCl, and 0.1% methylcellulose were used in the imaging reaction. Images were taken at 1.67 FPS.

3.4.3. EB1 comet length analysis

EB1 comet lengths were determined using a series of custom MATLAB (version R2020a, MathWorks) scripts. Briefly, beginnings and ends of individual growth events were manually determined on kymographs and divided into 30-second segments. The initial estimate of microtubule tip position over time was obtained assuming a constant growth rate. For each time frame, the pixel with the brightest EB1 intensity within a window (± 10 pixels, or ± 2 pixels for 12 μM condition) around the initially-estimated tip position was subsequently assigned as the microtubule tip position. The tip positions were then fit by a linear regression to assign a growth rate to each segment. Segments were then filtered to include only segments with well-defined growth rates using R^2>0.9 criterium, except for the 12 μM condition which displayed little displacement over a 30-second time period. To generate time-averaged intensity profiles, the determined tip positions from each temporal frame within the segment were aligned. The microtubule lattice intensity was determined by averaging the intensities of 5 pixels (located 5-10 pixels away from the tip for the 12 μM condition, and 15-20 pixels away from the tip elsewhere), and subsequently subtracted from the intensity of all pixels along the averaged intensity profile of a given segment.

To determine EB1 comet length, the averaged intensity profiles were fit to an exponential decay function using 20 pixels starting with the pixel immediately following the tip position (Bieling et al., 2007):

$$Ae^{(-x/\lambda)}$$

where A is the intensity at pixel 1, and λ is the comet decay length. Exclusion of the zeroth pixel intensity from the fit ensured that any potential sub-pixel perturbations in the tip structure not detected by our imaging did not affect the comet length measurement.

CHAPTER 4

4. Microtubule minus ends have long lifetimes despite small GTP-caps

Adapted from:

Strothman, C., V. Farmer, G. Arpağ, N. Rodgers, M. Podolski, S. Norris, R. Ohi, and M. Zanic. 2019. Microtubule minus-end stability is dictated by the tubulin off-rate. *J. Cell Biol.* 218:2841– 2853. doi:10.1083/jcb.201905019.

4.1 Introduction

The microtubule polymer is structurally and biochemically polarized, with the plus end growing faster than the minus end (Fan et al., 1996)(Nogales et al., 1998)(Horio and Hotani, 1986)(Walker et al., 1988). In cells, microtubule minus ends are typically anchored to microtubule organizing centers while plus ends are free to be dynamic (Dammermann et al., 2003)(Akhmanova and Steinmetz, 2015). As a result, the majority of studies investigating microtubule dynamics have been focused on the highly dynamic plus end. However, there are a number of microtubule architectures in different cell types, including neurons, meiotic spindles, and polarized epithelial cells, that contain microtubule arrays with free minus ends (Yvon and Wadsworth, 1997)(Dammermann et al., 2003)(Sanchez and Feldman, 2017)(Martin and Akhmanova, 2018). In these systems it has been demonstrated that regulation of

microtubule minus ends, both their special arrangement and dynamics, is vital for basic cellular functions (Akhmanova and Steinmetz, 2015)(Akhmanova and Hoogenraad, 2015)(Martin and Akhmanova, 2018). Early *in vitro* reconstitution studies demonstrated that, although both microtubule ends exhibited dynamic instability, minus ends had distinctly slower growth rates and undergo less frequent catastrophes (Figure 8)(Bergen and Borisy, 1980)(Mitchison and Kirschner, 1984)(Horio and Hotani, 1986)(Walker et al., 1988). These observations are in contrast to the plus end where slow growth rates lead to more frequent catastrophes, presumed to be the result of a small GTP-cap (Walker et al., 1988)(Drechsel et al., 1992)(Gardner et al., 2011b) (Duellberg et al., 2016)(Rickman et al., 2017). How are the minus ends able to grow slow but be more stable? What is the key to minus end longevity?

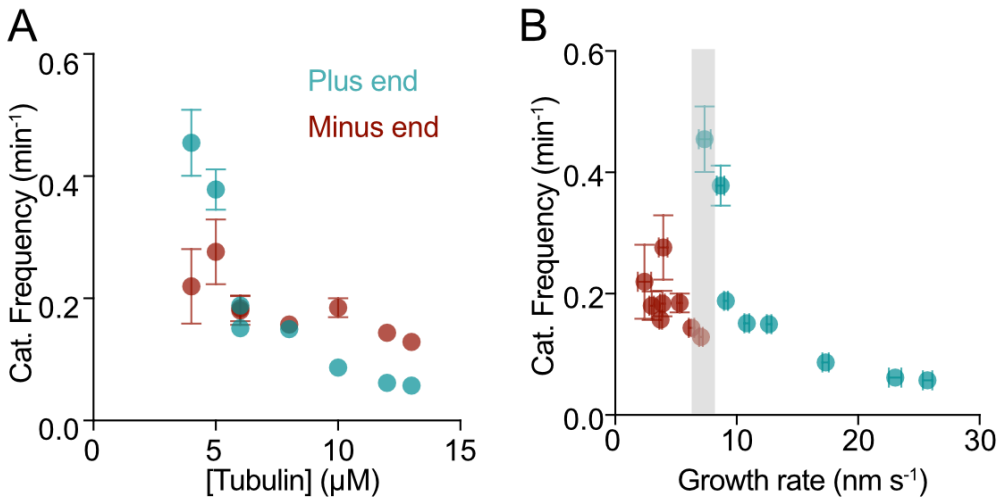

Figure 8. Minus ends grow slower and are more stable than plus ends. (A) Microtubule catastrophe frequency as a function of tubulin concentration. Error bars represent CE. Any error bars that are not visible are smaller than the size of the data point. (B) Microtubule catastrophe

frequency replotted as a function of growth rate. Error bars represent CE and SE, respectively. Shaded area indicates matching growth rates of plus and minus ends.

One logical hypothesis is that the GTP-cap size is inherently larger at the minus end compared to the plus end, yielding longer lifetimes. Despite investigation of GTP-cap size at the microtubule plus end, the size of the GTP-cap at minus ends had yet to be determined. In fact, many were under the impression that minus ends did not have EB1 comets, however, this is because microtubule minus ends are typically anchored in cells, not growing. Just like the plus ends, growing minus ends have comets. We used EB1 as a marker for GTP-cap size to determine if the enhanced stability of microtubule minus ends is a result of inherently larger GTP-caps.

4.2. Results

4.2.1. In the presence of EB1, microtubule minus ends are more stable than plus ends

EB1 is known to increase microtubule catastrophe frequency. We needed to ensure that this effect wasn't end specific and that in the presence of EB catastrophe frequency was still increased at the plus end compared to the minus end. In fact, minus ends exhibited lower frequency of catastrophe as a function of growth rate than plus ends over a range of tubulin concentrations (Figure 9). This result was important to establish before using EB1 as our proxy for GTP-cap size.

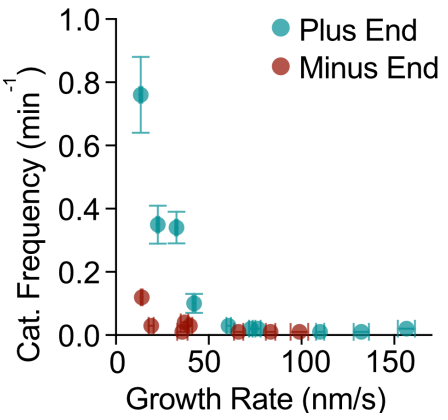

Figure 9. Minus ends are more stable than plus ends in the presence of EB1. Microtubule catastrophe frequency as a function of growth rate. Each point represents one experimental repeat. Error bars represent CE and SE, respectively. Any error bars that are not visible are smaller than the size of the data point.

4.2.2. Microtubule minus ends have small cap sizes, set by slow growth rate

To compare the size of the GTP-cap at plus and minus ends, we analyzed localization of EB1-GFP at growing microtubule ends (Figure 10). A direct comparison of EB1 comets at ends of microtubules grown with 40 μM tubulin revealed that slower-growing minus ends have on average shorter EB1 comet decay lengths (minus end: 272 ± 10 nm, 95% CI, N = 3, 865 linescans; plus end: 383 ± 20 nm, 95% CI, N = 3, 587 linescans), (Figure 10, closed circles). To investigate whether the growth rate alone sets the size of the EB1 comets at both ends, we then used 20 μM tubulin to obtain slow plus-end growth rates to match those measured at the minus ends at 40 μM tubulin (Figure 10, open circles). We found that in 20 μM tubulin, plus ends grew at the same rate (35 ± 3 nm/s, SE, N = 59) as minus ends in 40 μM tubulin (34 ± 5 nm/s, SE, N = 29), and that the corresponding average comet lengths were matched in these conditions (plus end at 20 μM tubulin: 276 ± 28 nm, 95% CI, N = 3, 1220 linescans; minus end at 40 μM tubulin: 272 ± 10 nm, 95% CI, N = 3, 865 linescans). Our results demonstrate that average EB1 comet size is set by the average growth

rate, irrespective of the microtubule end. In other words, when plus and minus ends are growing at the same growth rates (in different tubulin concentrations), their cap sizes are equivalent, yet minus ends have longer lifetimes. We thus conclude that the average size of EB1 comets alone does not define microtubule lifetime.

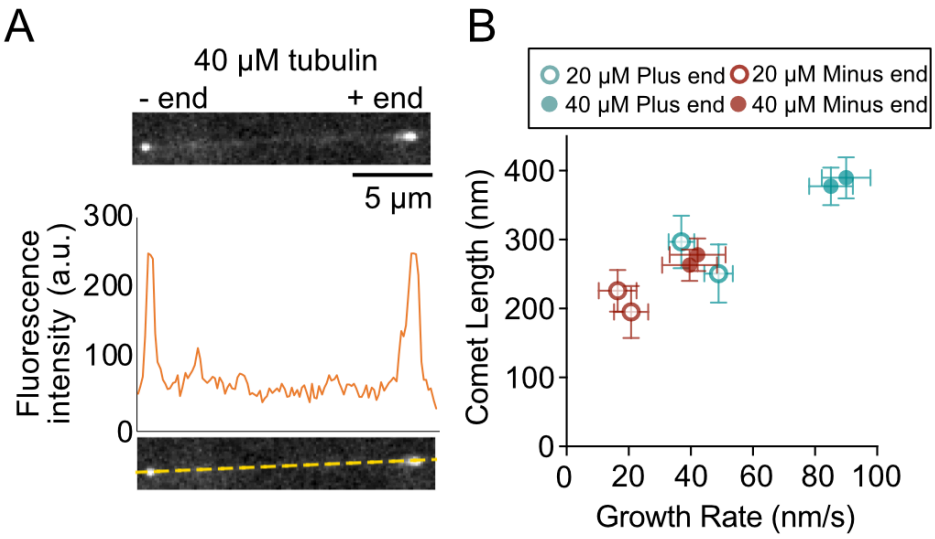

Figure 10. Minus end cap size is small and scales with growth rate. (A) Representative image of EB1-GFP at both growing ends of a single microtubule (40 μM tubulin). A line scan was drawn along this microtubule to generate intensity values along the microtubule, showing a distinct peak at each end. (B) Average EB1 comet length as a function of average growth rate of plus and minus ends in 20 or 40 μM tubulin with 200 nM EB1-GFP. Two independent repeats were done for each condition. Comet length error bars are 95% CI from the fit. Growth rate is weighted average of individual growth events and error is weighted SD. Weights are determined as the inverse of 95% CI of the linear fit to individual growth events.

4.3. Discussion

Microtubule catastrophe occurs via the loss of a protective cap of GTP-tubulin, the size of which is widely considered to be the determinant of microtubule plus-end stability. When microtubule growth rate is increased *in vitro* by increasing tubulin concentrations, the plus-end EB-comet size also increases (Bieling et al., 2007), while microtubule catastrophe is suppressed (Walker et al., 1988)(Drechsel et al., 1992)(Gardner et al., 2011b). Furthermore, larger EB comets have been directly correlated with prolonged stability against dilution-induced catastrophe at microtubule plus ends (Duellberg et al., 2016). The size of the GTP cap is set by the difference between the microtubule growth and GTP hydrolysis rates; thus, modulation of the GTP hydrolysis rate may be a potent mechanism for setting the GTP-cap size, and consequently regulating microtubule stability. Indeed, a recent study linked smaller EB comets, presumably due to a faster GTP hydrolysis rate, to increased dynamicity of *Caenorhabditis elegans* tubulin (Chaaban et al., 2018). Microtubules polymerized with recombinant tubulin mutated to have decreased GTPase activity have larger EB comets (Roostalu et al., 2020). Additionally, modulation of the GTP hydrolysis rate has been implicated in regulation of microtubule plus-end catastrophe by several microtubule-associated proteins (Maurer et al., 2014)(Zhang et al., 2017)(Zhang et al., 2018). Structural studies have proposed a mechanism of tubulin conformational changes during hydrolysis at the plus end (Nogales et al., 1998)(Nogales et al., 1999)(Alushin et al., 2014); however, it is not clear whether the minus end may have a differing mechanism or rate of GTP hydrolysis. Our results show a universal scaling between the EB1-comet size and the growth rate at both ends, suggesting that the

overall rate of GTP hydrolysis at the minus end is unlikely to be different from that at the plus end. Moreover, our finding that minus ends display the same lifetimes as plus ends with significantly smaller EB comets implies that the absolute size of the GTP-cap is not the primary determinant of microtubule lifetime.

How can minus ends maintain their stability in spite of their small GTP-caps? While our results show that an increase in minus-end growth rates also correlates with larger EB comets and enhanced stability, the sensitivity of minus ends to the GTP-cap size appears to be much lower than that of the plus ends. We do not think that potential differences in rates of GDP-tubulin dissociation at the two ends following catastrophe underlie this distinct sensitivity; we found rapid minus-end depolymerization rates to be no slower than those at plus ends upon catastrophe. Instead, based on our results, we propose that this difference is due to the significantly lower rate of GTP-tubulin dissociation at dynamic minus ends. Given that even a couple of layers of unhydrolyzed tubulin are sufficient to prevent microtubule catastrophe (Drechsel and Kirschner, 1994)(Caplow and Shanks, 1996), we conclude that the small, but stable, GTP- tubulin cap may be the key to minus-end longevity.

4.4. Methods

4.4.1. Protein Purification

Bovine tubulin was purified and labeled with fluorescent dyes are previously described in Chapter 2. EB1-GFP was expressed in Escherichia coli and purified as previously described (Zanic et al., 2009) and stored in 10 mM Bis-Tris, 10 mM TrisHCl,

100 mM KCl, 1mM DTT, 5% glycerol, pH 6.6. Protein concentration was determined using absorbance at 280 nm.

4.4.2. Dynamics assays

Tubulin titration was performed as previously described in Chapter 2, and tubulin concentrations are indicated within the figures. For microtubule dynamics assay with EB1-GFP comets, conditions were the same as described in Chapter 2 with the following exceptions: 17 mM KCl and 0.1% methylcellulose were used in the imaging reaction. Images were taken at 0.5 FPS. All experiments were imaged using the EM-CCD camera.

4.4.3. EB1-comet length analysis

Image analysis was performed by generating kymographs of microtubule growth events. For each tubulin concentration, 20 microtubules for which both plus and minus ends could be analyzed were selected to determine catastrophe frequency, average growth rate, and average EB1-comet length. The characteristic decay length of the EB1 comets was determined using custom MATLAB functions. The microtubule tip location for each time frame was estimated by fitting a line through two manually clicked points at the beginning and end of a growth event on each kymograph. The pixel with the brightest EB1 intensity within ± 5 pixels of the estimated tip location was determined for each time frame and assigned as the bona fide microtubule tip location.

Average tip intensity (I^{tip}) and its SD (σ^{tip}) of a given growth event were calculated, and any time frames with tip intensity lower than $I^{tip}-\sigma^{tip}$ were excluded. The remaining points were used to fit a linear function to approximate the growth rate. Time frames with fit residuals more than one SD away from the mean residuals were excluded. The remaining points were used to fit a linear function to determine the growth rate of the given event. For each time frame within the given growth event, the microtubule tips were aligned, and an average intensity profile was calculated. The lattice intensity was determined by averaging the intensity values between 20 and 25 pixels away from the tip. This average lattice intensity was subtracted from intensity profiles from each remaining time frame. Manual inspection was performed to remove any growth events in which the tip locations were not successfully determined by the above automated procedures. The remaining growth events were used to determine the average growth rate (v_g) and its SD (σ_{vg}) weighted with inverse of the 95% CI of the fitting procedure. Individual growth events were further excluded if they were not within $v \pm \sigma$. Individual intensity profiles from each individual time frame from the remaining growth episodes were used to generate a super-averaged intensity profile. The super-averaged intensity profile in the range of 1 pixel in the solution background and 20 pixels along the microtubule lattice was fit to an exponential decay convolved with a Gaussian function, given by

$$\frac{A}{2}\left(e^{\left(\frac{\sigma^2}{2\lambda^2}-\frac{x-x_0}{\lambda}\right)}\right)\left(1+erf\left(\frac{x-x_0}{\sigma\sqrt{2}}-\frac{\sigma}{\lambda\sqrt{2}}\right)\right)+\frac{B}{2}\left(1+erf\left(\frac{x-x_0}{\sigma\sqrt{2}}\right)\right)$$

where A is the intensity value at the tip, B is the difference between average lattice intensity and solution background, σ is the experimentally determined full width at half

maximum of the point spread function, x_0 is the offset in the tip position due to convolution, and λ is the comet decay length.

CHAPTER 5

5. XMAP215 promotes microtubule catastrophe by disrupting the growing microtubule end

Adapted from:

Farmer, V., G. Arpağ, S. Hall, and M. Zanic. 2021. XMAP215 promotes microtubule catastrophe by disrupting the growing microtubule end. *J. Cell Biol.* 220:1–13. doi:10.1101/2020.12.29.424748.

5.1. Introduction

In contrast to microtubules polymerized with purified tubulin *in vitro*, microtubules in cells can simultaneously display fast growth rates and high catastrophe frequency (Rusan et al., 2001)(Mimori-Kiyosue et al., 2005)(Akhmanova and Steinmetz, 2008)(Akhmanova and Steinmetz, 2015). In cells, microtubule dynamics are tightly regulated by a myriad of MAPs. Fast microtubule growth rates can be attributed to the action of microtubule polymerases, the most prominent belonging to the conserved XMAP215 family (Gard and Kirschner, 1987a)(Brouhard et al., 2008)(Gard et al., 2004)(Slep, 2009)(Al-Bassam and Chang, 2011). On its own, XMAP215 increases growth rates up to 10-fold (Vasquez et al., 1994; Brouhard et al., 2008), while a combination of XMAP215 and EB1 synergistically promotes up to a 30-

fold increase in growth rates, matching the fast rates observed in cells (Zanic et al., 2013). Surprisingly, although increasing growth rates by tubulin alone *in vitro* is accompanied by low catastrophe frequency, the significant increase in growth rate with XMAP215 was not accompanied by a suppression of catastrophe (Vasquez et al., 1994)(Zanic et al., 2013). Importantly, the effect of XMAP215 on the size of the GTP-cap is not known.

5.1.1. XMAP215

Proteins in the XMAP215 family — named after Xenopus microtubule assembly protein of 215 kDa — have conserved roles in promoting microtubule assembly (Figure 11). The XMAP215 family was the first to be classified as a TOG-domain protein family, after the TOG domain was identified in the human homolog of XMAP215, colon and hepatic tumor overexpression gene (ch-TOG). Members of this family localize to microtubule plus ends, microtubule- organizing centers (MTOCs), and kinetochores. Depletion of XMAP215 family proteins results in shortened microtubules with reduced growth rates, as well as characteristically small mitotic spindles (as captured in the name of the fly XMAP215 homolog, Minispindles). *In vitro* studies using recombinant XMAP215 have established that it autonomously recognizes the plus end of both growing and shrinking microtubules. XMAP215 acts as a plus-end microtubule polymerase, catalyzing the processive addition of tubulin dimers to accelerate microtubule growth rates by an order of magnitude. Furthermore, XMAP215 is involved in facilitating microtubule nucleation within the mitotic spindle.

Similar roles in promoting microtubule assembly have been established for other members of the XMAP215 protein family, all of which rely on the action of their TOG domains.

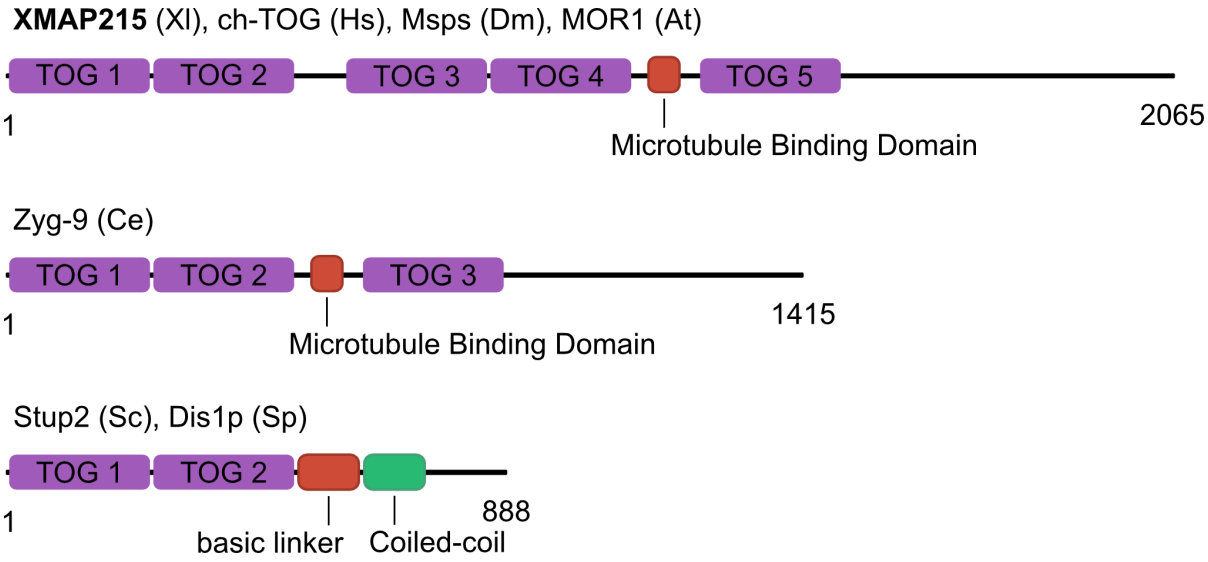

Figure 11. Domain structure of XMAP215. XMAP215 is conserved across species. XMAP215 family members vary in the number of TOG domains they have. Microtubule binding is mediated through the microtubule binding domain, or the basic linker. Stu2p and Dis1p dimerize via the coiled-coil domain.

Here, we investigate how XMAP215-promoted microtubule growth can simultaneously be fast and highly dynamic, displaying frequent microtubule catastrophes. We demonstrate that XMAP215-driven increase in microtubule growth rate is accompanied by both an increase in catastrophe frequency, as well as by an increase in EB1 comet size. Thus, the XMAP215-driven increase in catastrophe frequency is not a consequence of the GTP-cap size reduction. Rather, we

demonstrate that XMAP215 increases growth fluctuations and induces tapered and curled microtubule ends. Our results suggest that XMAP215-induced destabilization of the growing microtubule end ultimately promotes catastrophe.

5.2. Results

5.2.1. Increasing the microtubule growth rate using XMAP215 results in a simultaneous increase in microtubule catastrophe frequency

In cells, fast microtubule growth rates are achieved through the action of polymerases and other MAPs, including XMAP215 and EB1 (Akhmanova and Steinmetz, 2015). Interestingly, previous *in vitro* studies with XMAP215, either alone or in combination with EB1, reported that XMAP215-mediated increase in growth rate was not accompanied by a suppression of catastrophe frequency (Zanic et al., 2013; Vasquez et al., 1994). To investigate the relationship between catastrophe frequency and growth rate in the presence of XMAP215, we quantified microtubule dynamics over a range of XMAP215 concentrations (3.13 - 200 nM) in the background of 20 μM tubulin and 200 nM EB1-GFP (Figure 12A). As expected, microtubule growth rate increased as a function of XMAP215 concentration (Figure 12B). The increase in growth rate was accompanied by more frequent catastrophe events, even with the lowest XMAP215 concentration used (Figure 12C). This relationship between growth rate and catastrophe frequency in the presence of XMAP215 is in stark contrast to the one observed when growth rates were increased using tubulin titration (Figure 12D). Notably, XMAP215 led to a simultaneous increase in both growth rate and catastrophe

frequency even in the absence of EB1 (Figure 13), demonstrating that the observed increase in catastrophe frequency can be directly attributed to XMAP215.

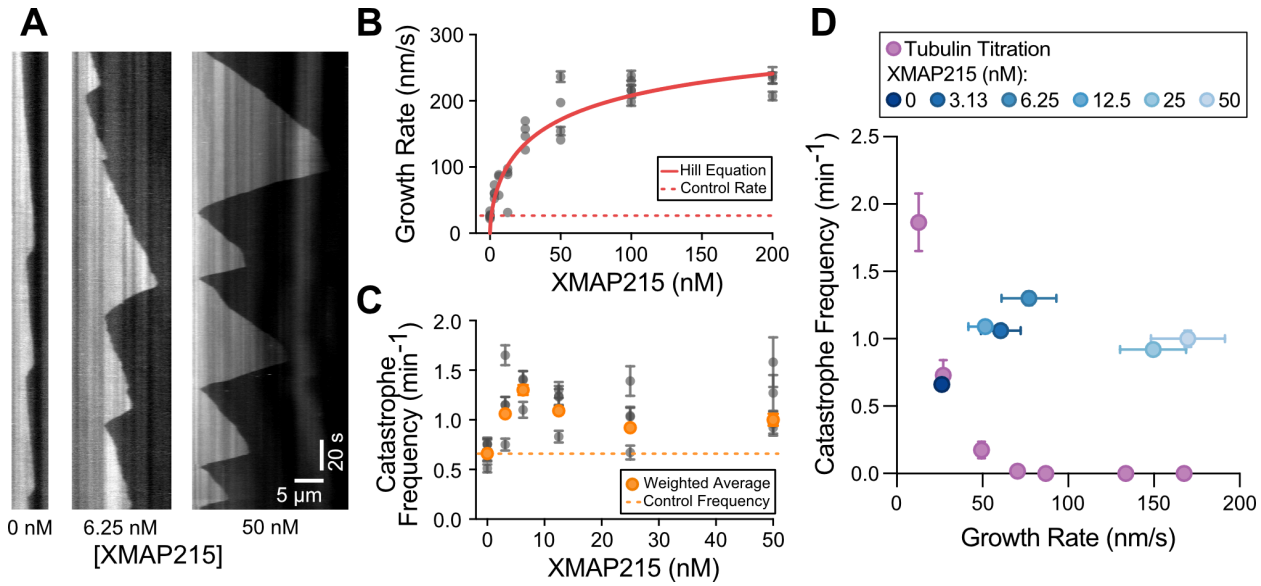

Figure 12. XMAP215 simultaneously increases microtubule growth rate and catastrophe frequency in the presence of EB1. (A) Representative kymographs of microtubule plus ends grown with 20 µM tubulin, 200 nM EB1-GFP, and corresponding amount of XMAP215 (nM). Tubulin signal is shown. (B and C) Quantification of microtubule growth rate (B) and catastrophe frequency (C) as a function of XMAP215 concentration in the presence of 20 µM tubulin and 200 nM EB1-GFP. Error bars, SEM and SE, respectively. Each point represents 20 kymographs from one experimental repeat. Number of experimental repeats per concentration, 6, 4, 3, 4, 4, 4, and 3. Dotted lines indicate the average control values (0 nM XMAP215). Solid red line in B, fit to the Hill equation. Orange points in C, weighted averages for each condition. (D) Average catastrophe frequency (from C) replotted as a function of average growth rate (from B) for the XMAP215 titration along with the tubulin titration (Chapter 3, Figure 7).

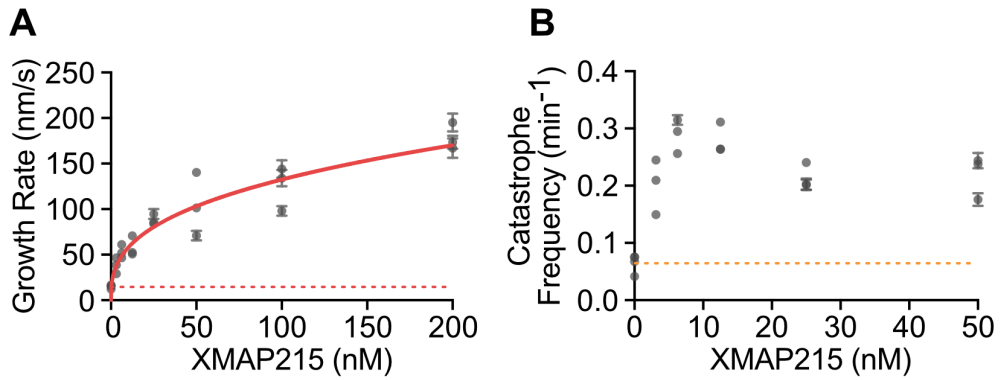

Figure 13. XMAP215 alone promotes simultaneous increase of microtubule growth rate and catastrophe frequency. Quantification of (A) microtubule growth rate and (B) catastrophe frequency as a function of XMAP215 concentration in the presence of 10 μM tubulin. Error bars represent SEM and SE, respectively. Each point represents values measured for 20 kymographs from one experimental repeat. The number of experimental repeats per concentration were: 4, 3, 3, 3, 3, 3, 3. Dotted lines indicate the average values for the control (0 nM XMAP215). Solid red line in (A) is the data fit to the Hill equation.

5.2.2. Promotion of catastrophe by XMAP215 is not achieved through a reduction in the GTP-cap size

One possible explanation for the observed increase in catastrophe frequency is that XMAP215 may be directly reducing the size of the protective GTP-cap. While a linear increase in GTP-cap size with microtubule growth rate is well established for the tubulin titration (Chapter 3, Figure 7)(Bieling et al., 2007)(Strothman et al., 2019), whether the GTP-cap size increases with XMAP215 is not known. Our measurements

of EB1 comets with XMAP215 titration revealed a direct correlation between growth rate and EB1 comet length (Figure 14A). This finding suggests that increasing growth rate by XMAP215 also results in a larger GTP-cap size, similar to what was observed when the growth rate was increased using higher tubulin concentrations (Chapter 3, Figure 7).

To directly compare the mean GTP-cap size in the presence or absence of XMAP215, we next performed growth-rate-matching experiments. We found that growth rates achieved with 60 μM tubulin and 200 nM EB1-GFP (Condition I) could be matched using 20 μM tubulin, 200 nM EB1-GFP and 25 nM XMAP215 (Condition II, Figure 14B). To precisely compare the EB1 comet sizes, we generated averaged EB1 comet intensity profiles for each of the two conditions (see Methods)(Bieling et al., 2007). Surprisingly, we found that the decay length of the EB1 comets was larger in the presence of XMAP215 (Figure 15C, 650 ± 20 nm, 95% CI; vs. 610 ± 20 nm, 95% CI, in the absence of XMAP215), in spite of the significantly higher catastrophe frequency when compared to the tubulin control (0.30 ± 0.09 min^{-1}, SE, N = 12 catastrophes in 39 min of growth over 20 kymographs; vs. 0.00 ± 0.03 min^{-1}, SE, N = 0 catastrophes in 40 min of growth over 20 kymographs). This finding directly demonstrates that promotion of catastrophe by XMAP215 is not a result of a decrease in the mean GTP-cap size.

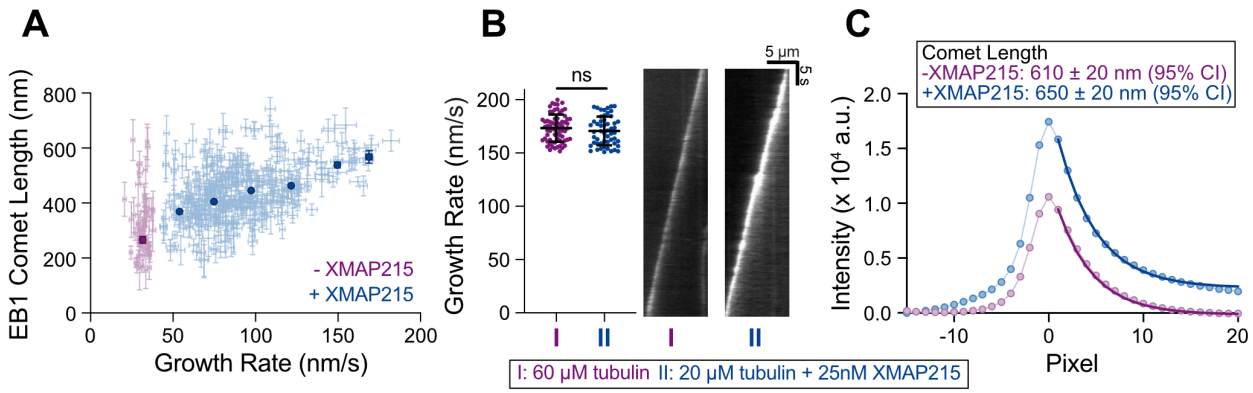

Figure 14. XMAP215 does not decrease the GTP-cap size. (A) Mean EB1 comet length as a function of microtubule growth rate over a range of XMAP215 concentrations (0–50 nM) in the presence of 20 µM tubulin and 200 nM EB1-GFP. Dim points represent individual 30-s growth segments. Error bars, 95% CI. Bold points are weighted means; error bars, weighted error. For −XMAP215 condition (0 nM XMAP215), all individual segments from a single experiment were averaged. For +XMAP215 condition (3.13–50 nM XMAP215), individual segments were binned using growth rate into 25-nm/s bins and averaged. 20 microtubule kymographs were analyzed from each condition. A total of six experimental conditions were performed over 2 days. (B) Microtubules were polymerized with either 60 µM tubulin and 200 nM EB1-GFP (condition I) or 20 µM tubulin, 200 nM EB1-GFP, and 25 nM XMAP215 (condition II) to obtain growth rate–matched conditions. Left: 69 growth segments for condition I and 53 growth segments for condition II, with no significant difference in growth rate (P = 0.28, unpaired t test), were analyzed. Means and SD are shown. Right: Representative kymographs of EB1 localization. (C) The super-average EB1 comet profiles were fitted to an exponential decay (dark lines) to determine the average comet lengths (see Methods). Error, 95% CI of the fit.

5.2.3. XMAP215 increases growth rate fluctuations and induces tapered microtubule ends

Our growth-rate-matching experiments provided an excellent dataset for a direct comparison of microtubule growth characteristics in the presence and absence of XMAP215. While the mean growth rates were matched, we wondered whether the fluctuations in growth rate may differ between the two conditions. To investigate this possibility, we tracked microtubule growth and determined deviations from the mean growth rate using linear regression (Figure 15A). We found that the sum of squared residuals (SSR) was significantly higher in the presence of XMAP215 (0.02 ± 0.01 $\mu m^2/s$, mean ± SD, N = 90) than in the tubulin control conditions (0.013 ± 0.007 $\mu m^2/s$, mean ± SD, N =103; $p < 0.0001$, unpaired Welch's t-test) (Figure 15A), despite no difference in the mean growth rate (Figure 16A). This result was further corroborated by mean squared displacement (MSD) analysis of the growing end positions in the presence and absence of XMAP215 (Figure 16B). Thus, we conclude that microtubules polymerizing with XMAP215 display a higher degree of growth rate variability than those polymerizing at the same growth rates in the absence of XMAP215.

Interestingly, our high spatiotemporal-resolution tracking of EB1-GFP localization at microtubule ends polymerized with XMAP215 also revealed a range of comet morphologies evolving over time (Figure 15B). Canonical EB localization is a single peak of fluorescence that exponentially decays along the microtubule lattice (Bieling et al., 2007), hereafter referred to as a ‘full comet’ (Figure 15B). However, in the presence of XMAP215, we observed frequent incidences of EB1 comets which

appeared to split into two distinct intensity peaks, displaying a leading and a lagging comet, both growing in the original growth direction (Figure 15B). Subsequent to comet splitting, we occasionally observed the lagging comet catching up to the leading comet, a phenomenon previously termed a ‘tip repair’ event (Aher et al., 2018)(Doodhi et al., 2016). Furthermore, we observed that a large number of split comets led to a ‘curled comet’ morphology, growing away from the original direction and resulting in polymer bending (Figure 15B). Quantification of the comet morphologies revealed that microtubules polymerized with XMAP215 were six times more likely to display a tapered end (either split or curled comet) when compared to those grown at the same growth rate without XMAP215 (Figure 15C, increase from 14 in the absence, to 85 in the presence of XMAP215 out of 110 comets quantified for each condition, $p < 0.0001$, chi-squared test). Given that the growth rates were the same between the control and XMAP215 conditions, these observations suggest that the increase in the frequency of tapered microtubule ends is a direct consequence of XMAP215.

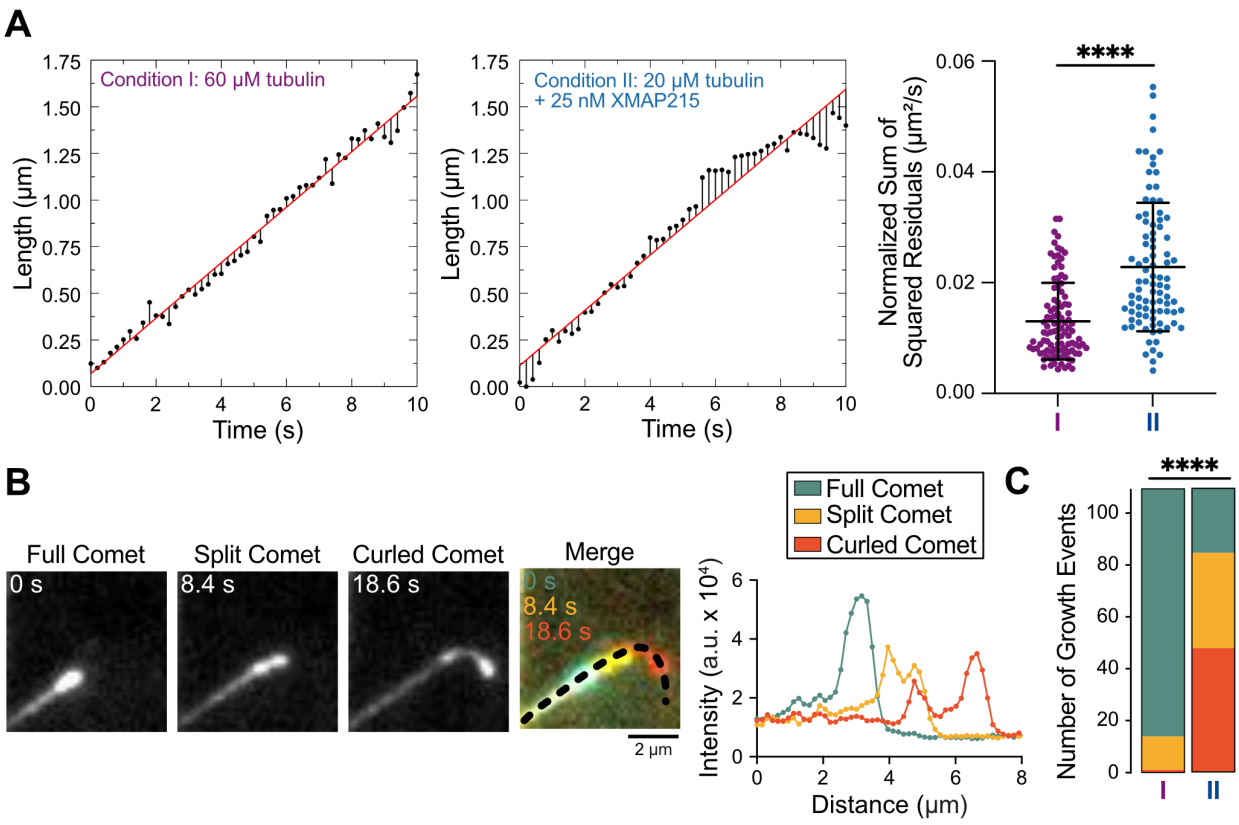

Figure 15. XMAP215 promotes microtubule growth rate fluctuations and tapered microtubule ends. Growth rate–matching conditions achieved by either 60 μM tubulin and 200 nM EB1-GFP (condition I) or 20 μM tubulin, 200 nM EB1-GFP, and 12.5/25 nM XMAP215 (condition II). (A) SSR was determined from 10-s segments that only displayed full comets. Left and center: Representative tracks showing microtubule tip position (black points), residuals for each time point (black lines), and linear regression to tip position (red line). Right: Sum of squared residuals for each segment; condition I, 0.013 ± 0.007 μm2/s (mean ± SD, n =103); condition II, 0.02 ± 0.01 μm2/s (n = 90). ****, P < 0.0001, unpaired Welch's t test. (B) An example microtubule with distinct EB1 comet morphologies: full, split, and curled. Intensity profiles along the dashed line at indicated time points. (C) Classification of 110 growth events into comet morphology categories. Condition I: 96 full, 13 split, 1 curled; condition II: 25 full, 37 split, 48 curled. ****, P < 0.0001, χ2 test.

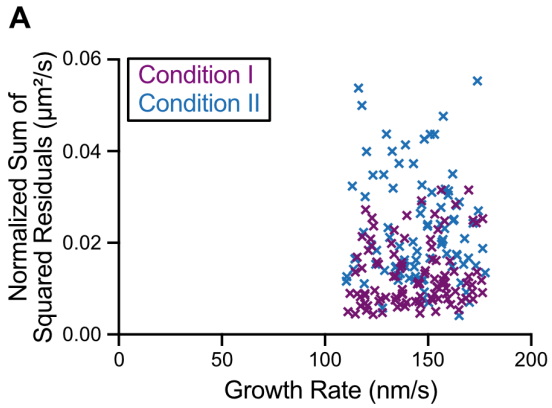

B

	Condition I	Condition II
Diffusion Coefficient (nm²/s, 95% CI)	1200 ± 100	2600 ± 100
Velocity (nm/s, 95% CI)	144 ± 1	144 ± 1
Sigma (nm, 95% CI)	49.8 ± 1.3	51.2 ± 1.4
N	103	90

Figure 16. Residual and mean squared displacement analyses indicate higher fluctuations in microtubule growth rate in the presence of XMAP215. (A) Growth events used for sum of squared residuals analysis in Figure 3A were selected to have no significant difference in growth rate: Condition I (60 μM tubulin and 200 nM EB1-GFP); 143 ± 18 nm/s (mean ± SD, N = 103), and Condition II (20 μM tubulin, 200 nM EB1-GFP, and 12.5/25 nM XMAP215); 145 ± 18 nm/s (mean ± SD, N = 90). p = 0.5352, t test. (B) Mean Squared Displacement analysis was used to determine the diffusion coefficient (D), velocity (v), and positional error (σ) of microtubule growth by fitting a quadratic function, $MSD(t) = 2Dt^2 + v^2t^2 + \sigma^2$ (Gardner et al. 2011a).

5.2.4. At the moment of catastrophe, microtubules grown with XMAP215 exhibit faster growth rates and higher EB1 localization

Our results suggested that XMAP215 disrupts the structural integrity of the GTP-cap by inducing fluctuations in growth and promoting tapered microtubule ends. We hypothesized that these disruptions make microtubules more prone to

catastrophe. To gain insight into the process of GTP-cap loss leading to catastrophe, we compared microtubule end position and EB1 intensity during catastrophe events using 0 nM and 3.13 nM XMAP215 conditions (in the background of 20 μM tubulin and 200 nM EB1-GFP), which both displayed robust, but distinct catastrophe frequencies (0 nM XMAP215: 0.76 ± 0.06 min^{-1}, SE, N = 161 catastrophes over 213 min in growth; 3.13 nM XMAP215: 1.15 ± 0.08 min^{-1}, SE, N = 205 catastrophes over 178 min in growth). Microtubules polymerized in the absence of XMAP215 experienced a slowdown in growth rate over several seconds prior to the onset of catastrophe, accompanied by a decrease in EB1 intensity at microtubule ends (Figure 17), as previously reported (Maurer et al., 2012)(Maurer et al., 2014) (Duellberg et al., 2016)(Duellberg et al., 2016)(Duellberg et al., 2016)(Duellberg et al., 2016). In contrast, the transition to catastrophe was more abrupt in the presence of XMAP215. The instantaneous growth rate at the moment of catastrophe (measured over a 1-second time window) was significantly higher for microtubules polymerized with XMAP215 (Figure 17B, 0 nM XMAP215: 4 ± 30 nm/s, mean ± SD, N = 27; vs. 3.31 nM XMAP215: 44 ± 50 nm/s, mean ± SD, N = 27, $p < 0.001$ unpaired Welch's t-test), indicating that the transition to catastrophe in the presence of XMAP215 does not require a slowdown in growth to the level observed for microtubules grown without XMAP215. Furthermore, the residual intensity of EB1 measured at the highest-intensity pixel at the moment of catastrophe was significantly larger for microtubules grown with XMAP215 (Figure 17C, 0 nM XMAP215: 9,000 ± 2,000 a.u., SD, N = 27; vs. 3.31 nM XMAP215: 12,000 ± 4,000 a.u., SD, N = 27, $p = 0.003$, unpaired Welch's t-test), suggesting that an even larger GTP-cap density is not sufficient to protect

against catastrophe in the presence of XMAP215. Overall, our results demonstrate that microtubule ends grown with XMAP215 are inherently less stable, as they undergo catastrophe at faster growth rates and with more EB1, when compared to microtubules polymerized without XMAP215.

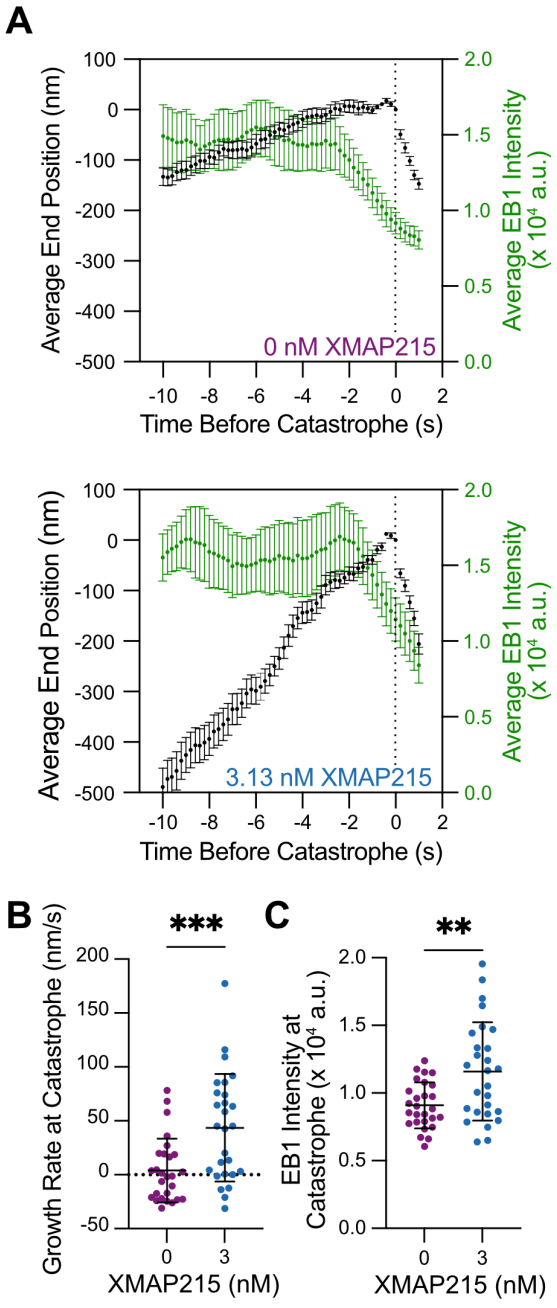

Figure 17. Microtubules grown in the presence of XMAP215 undergo catastrophe at faster growth rates and with more EB1. (A) Average microtubule end position and EB1 intensity over time. 27 events were averaged along their lifetime for both 0 and 3.13 nM XMAP215 conditions. Average EB1 intensity determined using a 1-s sliding window. Error bars, SEM. (B) Microtubule growth rate at the time of catastrophe determined for each growth event within a 1-s window before catastrophe. 0 nM XMAP215, 4 ± 30 nm/s (mean ± SD, n = 27); 3.13 nM XMAP215, 44 ± 50 nm/s (n =27). ***,P<0.001, unpaired Welch's t test. (C) EB1 intensity at the time of catastrophe. 0 nM XMAP215, 9,000 ± 2,000 a.u. (SD, n = 27); 3.13 nM XMAP215, 12,000 ± 4,000 a.u. (SD, n = 27). **, P = 0.003 unpaired Welch's t test.

5.3. Discussion

A cap of GTP-tubulin at the end of a growing microtubule is widely accepted as the determinant of microtubule stability (Mitchison and Kirschner, 1984)(Drechsel and Kirschner, 1994)(Desai and Mitchison, 1997)(Duellberg et al., 2016)(Roostalu et al., 2020). The size of the GTP-cap is defined by the balance between the rates of addition of new GTP-tubulin dimers to the growing end, and hydrolysis of GTP to GDP within the polymer. On its own, an increase in growth rate is expected to increase the size of the GTP-cap, and thus confer enhanced stability to the growing microtubule. Indeed, our results using a tubulin titration confirm that an increase in growth rate is accompanied by an increase in EB1 comet size, as well as a suppression of catastrophe (Figure 18). However, these findings raise the puzzling question of how simultaneously fast, yet highly dynamic microtubule growth, as observed in cells, can be achieved. One possible way to limit the size of the GTP-cap, and thus presumably facilitate catastrophe, is through acceleration of the GTP-hydrolysis rate. This mechanism has been proposed for EB proteins, which promote catastrophe even while inducing a slight increase in growth rate (Bieling et al., 2007)(Zhang et al., 2015)(Vitre et al., 2008). Indeed, increasing EB concentration was reported to reduce the overall length of the EB comets in a dose-dependent manner (Maurer et al., 2011). In contrast, we find that the mean length of the EB1 comets is increased when growth acceleration is achieved through the action of XMAP215. Thus, our results demonstrate that XMAP215 simultaneously promotes microtubule growth and catastrophe without accelerating the GTP-hydrolysis rate, or otherwise decreasing the mean GTP-cap size.

In addition to the nucleotide composition, the structural configuration of the microtubule end is likely to play an important role in microtubule stability. Catastrophe is a complex phenomenon that does not follow first-order kinetics; rather, the probability of catastrophe increases with time spent in growth (Odde et al., 1995)(Gardner et al., 2013)(Gardner et al., 2011b). While the exact mechanisms of this aging process are still unknown, existing models typically associate specific structural configurations with the onset of catastrophe. These may involve accumulation of permanent defects including the uncapping and/or loss of individual protofilaments (Gardner et al., 2011b) (Bowne-Anderson et al., 2013), gradual tapering of microtubule ends (Coombes et al., 2013), or dynamic evolution of stochastic end configurations involving protofilament curling (Zakharov et al., 2015). Notably, a variety of growing-end configurations have been observed by structural studies (Mcintosh et al., 2018)(Gudimchuk et al., 2020)(Chrétien et al., 1995)(Guesdon et al., 2016)(Atherton et al., 2018) (Mandelkow et al., 1991)(Reid et al., 2019), and it has been previously proposed that some of these end configurations may indeed be energetically unfavorable, leading to catastrophe (Chrétien and Fuller, 2000; Hunyadi et al., 2005). Microtubule end structures can vary with tubulin from different species (Orbach and Howard, 2019), and can be further modulated by MAPs and drugs (Chen and Hancock, 2015)(Chen et al., 2019)(Aher et al., 2018)(Doodhi et al., 2016)(Best et al., 2019)(Arnal et al., 2000). In the case of XMAP215, our observations of EB1 comet splitting and end curling demonstrate that XMAP215 perturbs the structure of the growing microtubule end.

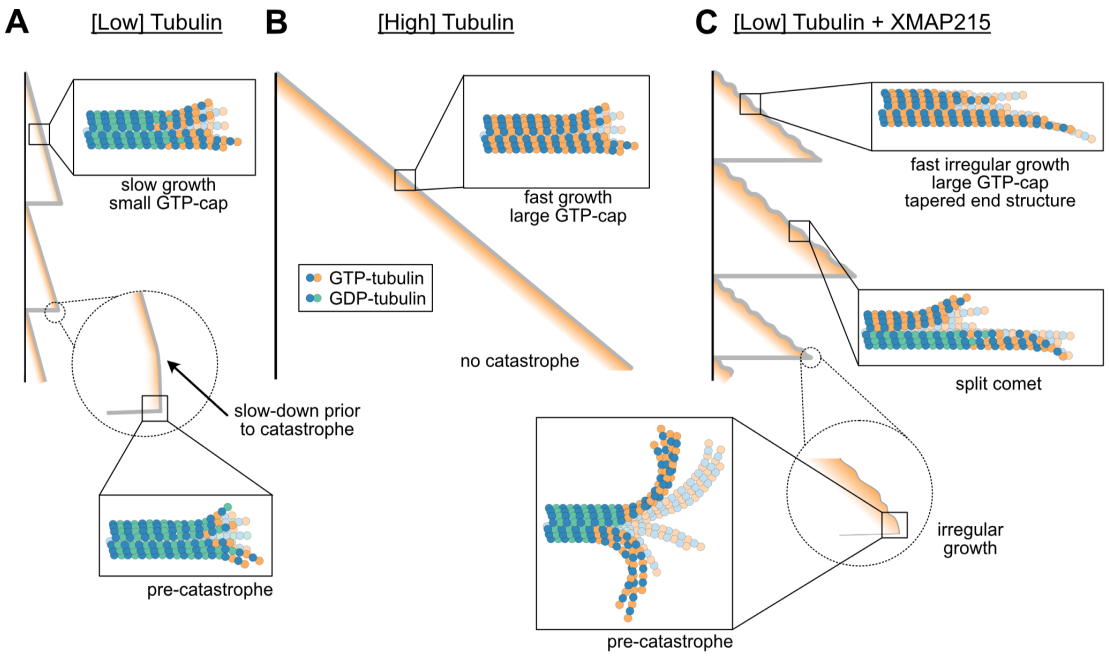

Figure 18. XMAP215 drives microtubule catastrophe by perturbing the growing microtubule end structure. (A) Microtubules polymerized with low tubulin grow slowly with small GTP-caps. Loss of GTP-tubulin triggers catastrophe. (B) Microtubules polymerized with high tubulin grow fast with large GTP- caps, resisting catastrophe. (C) Microtubules grown with XMAP215 display growth irregularities that trigger catastrophe, despite high GTP-tubulin content.

The canonical function of XMAP215 as a microtubule polymerase relies on its ability to bind curved tubulin conformation and stabilize an intermediate state in microtubule assembly (Brouhard et al., 2008) (Ayaz et al., 2012)(Brouhard and Rice, 2014). Given that XMAP215 was reported to act as a processive polymerase, with each XMAP215 molecule promoting the addition of ~25 tubulin dimers (Brouhard et

al., 2008), we speculate that XMAP215 molecules primarily drive elongation of individual protofilaments, resulting in less coordinated protofilament growth. Indeed, our observations of EB1 comet splitting and curling suggest that polymerization is not synchronized among all protofilaments. Instead, XMAP215 promotes 'sloppy' microtubule growth with some protofilaments growing faster than others, to produce an overall tapered end (Figure 18). Given that EBs localize to the interface of four tubulin dimers (Maurer et al., 2012), our observation of leading comets suggests the presence of multiple laterally-connected protofilaments within these protrusions. The existence of tapered and open ends can further facilitate EB1 targeting (Reid et al., 2019), consistent with our observations of brighter EB1 comets in the presence of XMAP215 in growth-rate-matching experiments. Importantly, although we used EB1 to visualize the nucleotide composition of growing ends, our observation of XMAP215-dependent promotion of catastrophe in the absence of EB1 demonstrates that XMAP215 on its own, rather than through enhanced targeting of EB1, promotes catastrophe.

Uncoordinated assembly of individual protofilaments in the presence of XMAP215 may be manifested by increased fluctuations in growth (Kerssemakers et al., 2006) (Howard and Hyman, 2009). Our results show that XMAP215 promotes large fluctuations in microtubule length over time even when ends display 'full' comets. We speculate that the 'sloppy' microtubule growth induced by XMAP215 is associated with a highly variable end structure, ultimately resulting in more frequent excursions into inherently unstable configurations, despite the presence of a large nucleotide cap (Figure 18). Indeed, we find that both the instantaneous growth rate and the EB1

intensity at the moment of catastrophe are significantly higher for ends polymerized with XMAP215. Our results thus imply that there is no universal GTP-cap size threshold needed for the switch to catastrophe (Duellberg et al., 2016), and rather suggest that structural changes induced by XMAP215 can override the protective effects of the nucleotide cap.

Finally, while the polymerase effects of XMAP215 are dose-dependent, such that the maximum growth promotion is reached in the ~100 nM range, we find that XMAP215's promotion of catastrophe reaches its full effect even at the lowest concentrations of XMAP215 tested. This observation provides further evidence of the distinct mechanisms regulating the absolute microtubule growth rate and overall microtubule stability. Future structural studies, combined with direct single-molecule measurements of microtubule assembly (Mickolajczyk et al., 2019), and the refinement of existing computational models (Bowne-Anderson et al., 2013)(VanBuren et al., 2002)(VanBuren et al., 2005)(Margolin et al., 2012)(Castle and Odde, 2013)(Zakharov et al., 2015)(Bollinger and Stevens, 2018)(Igaev and Grubmüller, 2018)(Kim and Rice, 2019)(Michaels et al., 2020)(Gudimchuk et al., 2020) will be necessary to unravel the full complexity of microtubule dynamics. Notwithstanding, the ability to independently control the rates of growth and catastrophe is at the very core of microtubule regulation in cells, enabling the complex, dynamic remodeling of the microtubule cytoskeleton.

5.4. Methods

5.4.1. Protein preparation

Bovine brain tubulin was purified and labeled as described in Chapter 2. For imaging purposes, labeled tubulin was used at a ratio of 10% of the final tubulin concentration. XMAP215-7his expression construct was a kind gift from G. Brouhard, McGill University, Montreal, QC, Canada. XMAP215 was expressed in Sf9 cells using the Bac-to-Bac system (Invitrogen) and purified using a HisTrap followed by gel filtration (adapted from Brouhard et al., 2008), and stored in 10 mM Bis-Tris, 10 mM TrisHCl, 100 mM KCl, 1 mM DTT, 10% glycerol, pH 6.6. EB1-GFP was expressed in *Escherichia coli* and purified as previously described (Zanic et al., 2009), and stored in 10 mM Bis-Tris, 10 mM TrisHCl, 100 mM KCl, 1 mM DTT, 5% glycerol, pH 6.6. Protein concentration was determined using absorbance at λ = 280 nm.

5.4.2. Assay conditions and imaging

Microtubule dynamics assays were performed as previously described in Chapter 2. Images were acquired using NIS-Elements (Nikon). Acquisition rates were 0.6 frames per second for tubulin titration (Figures 1D and S1), and 5 frames per second elsewhere.

The imaging buffer consisted of BRB80 supplemented with 40 mM D-glucose, 40 µg/ml glucose oxidase, 25 µg/ml catalase, 0.08 mg/ml casein, 10 mM DTT, and 0.1% methylcellulose. For tubulin titration (Figures 12D), reactions contained imaging

buffer, concentrations of tubulin ranging from 12 to 60 μM, 200 nM EB1-GFP, 1 mM GTP, and 17 mM KCl. For XMAP215 titrations, reactions contained imaging buffer, 20 μM tubulin, concentrations of XMAP215 ranging from 3.13-200 nM, 1 mM GTP and 200 nM EB1-GFP (Figures 12, 14A and 17). For the XMAP215 titration without EB1 (Figure 14), the reaction conditions were the same, except that EB1-GFP was not included. For growth-rate-matched experiments (Figures 14B-C, 15, and 16), reactions contained imaging buffer, 200 nM EB1-GFP, 1 mM GTP, and concentrations of tubulin and XMAP215 as indicated in figure legends (Condition I: 60 μM tubulin, no XMAP215; Condition II: 20 μM tubulin, 12.5 or 25 nM XMAP215). In both XMAP215 titration and growth-rate-matching experiments, XMAP215 storage buffer was consistently kept at a final concentration of 4X-dilution (2.5 mM Bis-Tris, 2.5 mM TrisHCl, 25 mM KCl, 250 nM DTT, 2.5% glycerol).

5.4.3. Microtubule dynamics analysis

Quantification of microtubule dynamics parameters was performed using microtubule kymographs generated in Fiji (Schindelin et al., 2012), as described previously (Zanic, 2016). For each experiment, 20 kymographs were generated using 5-pixel-wide lines in the tubulin channel and analyzed. In each kymograph, the faster-growing microtubule end was designated as the plus end; only plus-end dynamics were subsequently analyzed. Catastrophe events were designated as a switch from growth to shrinkage that decreased microtubule length by more than 2 pixels (320 nm). Catastrophe frequency was calculated as the total number of catastrophe events

divided by the total time spent in growth phase observed over 20 kymographs for an individual experiment, and error was determined as the counting error (square root of the number of events divided by the total time spent in growth).

5.4.4. EB1 comet length analysis

EB1 comet lengths were determined using a series of custom MATLAB (version R2020a, MathWorks) scripts as outlined in Chapter 2. Briefly, beginnings and ends of individual growth events were manually determined on kymographs and divided into 30-second segments. For the analysis in Figure 14BC only, 10-second segments (50 frames) were used to ensure highly accurate determination of segment velocities to be used in super-averaging into a single comet profile. The initial estimate of microtubule tip position over time was obtained assuming a constant growth rate. For each time frame, the pixel with the brightest EB1 intensity within a window (± 10 pixels, or ± 2 pixels for 12 μM condition in Figure 12D) around the initially-estimated tip position was subsequently assigned as the microtubule tip position. The tip positions were then fit by a linear regression to assign a growth rate to each segment. Segments were then filtered to include only segments with well-defined growth rates using R^2>0.9 criterium, except for the 12 μM condition in Figure 12D which displayed little displacement over a 30-second time period. To generate time-averaged intensity profiles, the determined tip positions from each temporal frame within the segment were aligned. The microtubule lattice intensity was determined by averaging the intensities of 5 pixels (located 5-10 pixels away from the tip for the 12 μM condition in

Figure 12D, and 15-20 pixels away from the tip elsewhere), and subsequently subtracted from the intensity of all pixels along the averaged intensity profile of a given segment. To compare comet lengths in growth-rate matching experiments in the absence and presence of XMAP215 (Figure 14BC), 10-second segments with growth velocities between 150-200 nm/s were selected and further averaged to obtain a super-averaged intensity profile for each condition.

All growth segments used for the comet length measurements displayed full EB1 comet morphologies. To determine EB1 comet length, the averaged intensity profiles were fit to an exponential decay function using 20 pixels starting with the pixel immediately following the tip position (Bieling et al., 2007):

$$\mathrm{Ae}^{(-\mathrm{x}/\lambda)}$$

where A is the intensity at pixel 1, and λ is the comet decay length. Exclusion of the zeroth pixel intensity from the fit ensured that any potential sub-pixel perturbations in the tip structure not detected by our imaging did not affect the comet length measurement.

5.4.5. Determination of variability in microtubule growth

Individual microtubule growth events from the growth-rate-matching conditions which displayed a full comet during their lifetime were subjected to automated tracking. Images were background-subtracted using a rolling ball with a 5-pixel radius in Fiji. The EB1 channel was tracked with FIESTA's single particle tracker (Ruhnow et al., 2011) using MATLAB. Then, a custom MATLAB code was used to divide the

output trajectories into continuous 10-second segments, allowing for gaps of no more than a total of 1-second within a given segment. The variations from the mean growth rate within the 10-second segments were quantified by performing residuals analysis as previously described (Lawrence et al., 2018). Briefly, using a custom MATLAB code, a linear function was fit to the length-versus-time data points to determine the mean growth rate. The sum of squared residuals (SSR) was calculated and normalized by the segment duration. For growth-rate-matching experiments, only the trajectories with mean growth rates between 110 and 180 nm/s were considered. Outliers based on normalized SSR were identified using MATLAB function "isoutlier" and subsequently discarded (12 outliers out of 115 tracks for 60 μM tubulin condition and 7 outliers out of 97 tracks for 20 μM tubulin + 12.5/25 nM XMAP215 condition). Unpaired t-test with Welch's correction was used to determine p-values for mean velocity and normalized SSR between experimental conditions. The same selected segments were subjected to Mean Squared Displacement (MSD) analysis using MATLAB-based "msdanalyzer" (Tarantino et al., 2014). A quadratic function (Gardner et al., 2011a) was fit to the first 5 seconds of the MSD curve:

$$MSD(t) = 2Dt + v^2t^2 + \sigma^2$$

where D is diffusion coefficient, v is mean growth rate, and σ is the positional error. The fit was weighted by the inverse of the standard deviation of the MSD curve determined by msdanalyzer.

5.4.6. Determination of microtubule end morphology in growth-rate-matching experiments

The microtubule end morphology was assessed from the EB1 channel for each experimental condition (Condition I: 60 μM tubulin and 200 nM EB1-GFP, Condition II: 20 μM tubulin, 200 nM EB1-GFP and 12.5/25 nM XMAP215) using timelapse movies and intensity profiles from kymographs which were produced from 7-pixel-wide (1120 nm) lines. Individual microtubule growth events were tracked for up to 2 minutes and the average microtubule growth rate was determined for each growth event. 110 growth events for each experimental condition, with no significant difference in growth rates between conditions, were scored for catastrophe and end morphology. End morphology was classified into three categories based on the EB1-GFP signal at the growing microtubule end: 'full', 'split', or 'curled' comet. If EB1 localized in a single peak at the end of a growing microtubule for the entire duration, the event was classified as having a 'full' comet. If two peaks in the intensity profile could be resolved (>2 pixels) for more than 1 second (5 frames), the comet was considered to be 'split'. A 'curled' comet was preceded by a splitting event with the leading comet having grown outside the 7-pixel-wide linescan.

5.4.7. Determination of the growth rate and EB1 intensity at the onset of catastrophe

Our methods to determine the growth rate and the EB1-GFP intensity at the onset of catastrophe were developed based on previously-published approaches(Maurer et al., 2012)(Duellberg et al., 2016). In brief, individual microtubule growth events from either 0 nM or 3.13 nM XMAP215 conditions which displayed only a full comet morphology over the 30 seconds prior to catastrophe were subjected to automated tracking. For each individual growth event, microtubule position was determined from the tubulin signal using TipTracker v3 (Prahl et al., 2014). First, both x- and y-coordinates of the microtubule end from each temporal frame, except the initial and final frames, were preprocessed to eliminate tracking noise: if the difference between coordinates of the current frame and the previous frame was larger than 1000 nm, the current coordinate value was eliminated and a new coordinate value was interpolated using the previous and subsequent frame, assuming a linear growth rate (adapted from Rickman et al., 2017). To further minimize tracking noise, the “smoothdata” function in MATLAB was used with the “movmedian” method and a 5-frame (1-second) window size. The end position was determined using smoothened coordinates. Initial determination of the time of catastrophe was performed manually and subsequently corrected using the following automated analysis: each time point in the time interval of 10 frames before and after the manually-approximated time of catastrophe was assigned an instantaneous growth rate using a linear fit over a 3-frame sliding window. Then, starting from 8 frames after catastrophe and moving backwards in time, if three consecutive frames had velocity values greater than -50 nm/s, the latest of the three temporal frames was

assigned as the time of catastrophe. After determining the time of catastrophe, the end-positions of growth events over time were aligned to generate an averaged microtubule tip position using a custom MATLAB code. For each microtubule, time and position values were offset to assign the catastrophe event to (0,0). Subsequently, the mean and standard error of the mean for the positions at each time point were calculated for the two experimental conditions. The growth rate prior to catastrophe was determined using a custom MATLAB function, performing a linear fit to the length-vs-time segments. To determine instantaneous growth rate at the time of catastrophe (T=0 seconds), a 1-second (5-frame) window size (i.e. from T=-1 seconds to T=0 seconds) was used.

EB1-GFP intensities at microtubule ends prior to catastrophe were determined using a custom MATLAB function. Briefly, for each temporal frame, the EB1-GFP-channel image was rotated centering around the end position (determined using the tubulin signal, as described above), such that the microtubule is horizontally aligned. The brightest intensity value within 5-lattice-pixels and 1-solution-pixel was assigned as maximum EB1 intensity (5-pixel thickness, i.e. 5x6 pixel^2 area). Local solution background intensity was determined by shifting the 5x6 pixel^2 area up and down by 5 pixels, and the mean intensity was calculated. Temporal frames with <25 pixels available for background determination were discarded. For each temporal frame, the mean background intensity was then subtracted from the corresponding EB1 intensity. EB1 intensities along each event were determined by averaging the intensities within a 1-second (5-frame) sliding window immediately preceding the frame of interest. The intensities corresponding to the above-determined time of catastrophe (T=0) were

defined as EB1 intensity at catastrophe. Outliers in velocity and intensity were determined using isoutlier function in MATLAB (3 outliers out of 30 events in 0 nM, and 1 outlier out of 28 events in 3.13 nM condition). The average EB1 intensities as a function of time were obtained by averaging all growth events at every time point, with error being the standard error of the mean, weighted by the inverse of squared of the propagated standard error of the mean of the solution background within the 1-second window.

CHAPTER 6

6. Conclusions & Future Directions

6.1. Microtubule lifetime is not dictated by the GTP-cap size

6.1.1. There is an inverse correlation between microtubule lifetime and GTP-cap size with tubulin alone over a small range of growth rates

Identification of EB proteins as markers for the GTP-cap has established an inverse correlation between GTP-cap size and microtubule stability over a small range of GTP-cap sizes (Chapter 3)(Duellberg et al., 2016)(Farmer et al., 2021). GTP-cap size is influenced by the microtubule growth rate, which can be modulated by changing tubulin concentration (Bieling et al., 2007). Interestingly, while there appears to be no limit on growth rate and GTP-cap length, catastrophe frequency is only sensitive in a small region of relatively slow growth rates (Farmer et al., 2021). These observations indicate that if the inverse correlation between microtubule lifetime and GTP-cap size is a direct result of the overall size of the GTP-cap, there is a critical threshold size the cap can reach beyond which the lifetime is not impacted anymore. Therefore, microtubule lifetime is only sensitive to changes in GTP-cap size over a small range of cap sizes. Thus, in order for the GTP-cap size to dictate microtubule stability, GTP-cap sizes must remain small, within the range where lifetime could be regulated. Alternatively, there may be mechanisms to actively decrease GTP-cap size, in order

to obtain a small cap that is possible of impacting lifetime. With the use of EB proteins, we can now interrogate the GTP-cap size under varying conditions and correlate it to microtubule stability. These studies have revealed a number of instances where the relationship between microtubule stability and GTP-cap size deviates from what is seen with tubulin alone at the plus end, suggesting that he GTP-cap size is not the overall determinant of microtubule lifetime (Figure 19).

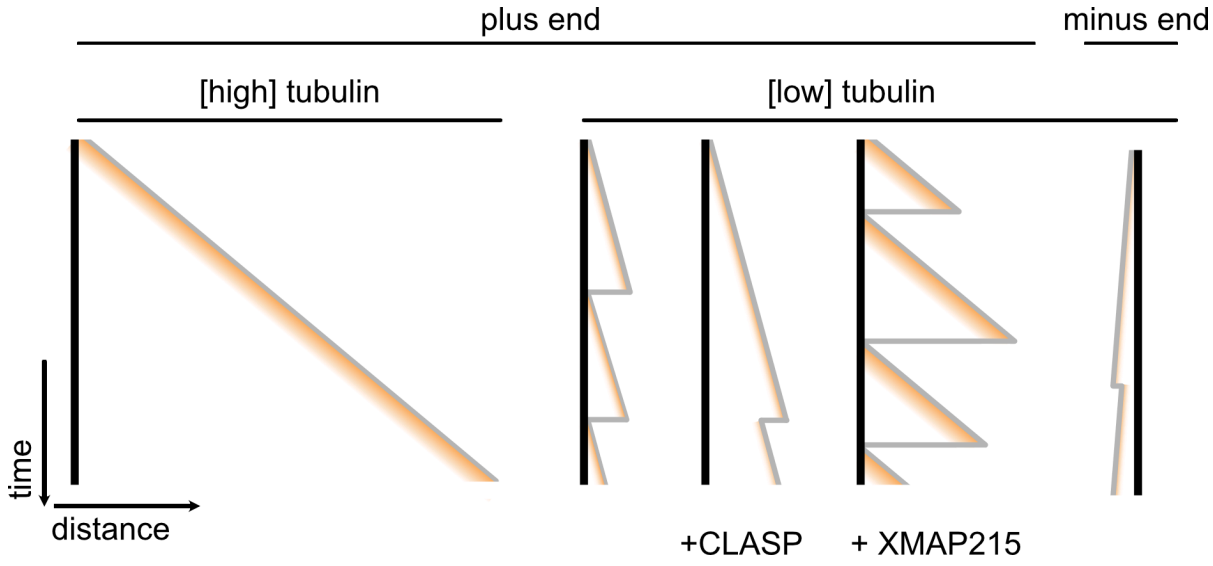

Figure 19. Microtubule lifetime is not dictated by GTP-cap size. Despite GTP-cap size (yellow) being set by the microtubule growth rate, microtubule lifetime is not determined by the GTP-cap size. The addition of MAPs, such as CLASP or XMAP215, break the canonical relationship between GTP-cap size and microtubule lifetime observed at the plus end. In addition, minus ends have small GTP-caps, but are very stable.

6.1.2. Microtubule minus ends have small GTP-caps but are very stable

In vitro quantification of microtubule dynamics has determined that at a given tubulin concentration minus ends grow slower and typically have longer lifetimes compared to their plus end counterparts (Horio and Hotani, 1986)(Walker et al., 1988)(Strothman et al., 2019). We show that the GTP-cap size at the minus end positively scales with growth rate at the minus end in the same way that it scales at the plus end, suggesting that the GTP hydrolysis rate at the two ends is the same (Chapter 4)(Strothman et al., 2019). Thus, when two populations of microtubules are grown using two different tubulin concentrations *in vitro*, microtubule minus ends polymerized at the same growth rate as plus ends have the same GTP-cap size. This reveals that the same size GTP-cap can be more protective at microtubule minus ends than at plus ends.

Models of microtubule dynamics, such as the GTP-cap model, have almost exclusively been made based on observations at the microtubule plus end. The observation that microtubule plus and minus ends can have the same GTP-cap size but different catastrophe frequencies suggests that the ability of the protective nature of the GTP-cap depends on the microtubule end (Strothman et al., 2019). This difference was determined to be a result of a lower GTP-tubulin off rate at the minus end compared to the plus end (Strothman et al., 2019). This is a clear example of the GTP-cap size not being the single determinant of microtubule stability. Additionally, the finding that the minus end is stable with a small GTP-cap emphasizes the importance of taking into account both ends of the microtubule when developing

models of dynamic instability. This is important, not only because the models may be different at the two ends, but because differential regulation of the two ends could help reveal mechanisms by which microtubule dynamics could be regulated by MAPs.

6.1.3. XMAP215 decreases microtubule lifetime despite the presence of large GTP-caps

In cells, fast microtubule growth rates are achieved through the action of microtubule polymerases, the most prominent belonging to the conserved XMAP215 family (Gard and Kirschner, 1987b)(Gard et al., 2004)(Brouhard et al., 2008)(Slep, 2009)(Al-Bassam and Chang, 2011). XMAP215 family members contain an array of tubulin binding-tumor overexpressing gene (TOG) domains at their N-terminus (Widlund et al., 2011)(Farmer and Zanic, 2021). Mutations in TOG domains disrupt their ability to bind free tubulin and promote polymerization (Ayaz et al., 2012)(Ayaz et al., 2014). While the number of TOG domains present varies between XMAP215 family members, and the exact role of each TOG domain is unclear, it has been shown that an array of TOG domains is necessary for the polymerase activity of XMAP215 family members (Widlund et al., 2011)(Ayaz et al., 2014)(Geyer et al., 2018). The minimal polymerase unit has been identified to contain two arrayed TOG domains and a microtubule targeting region (Widlund et al., 2011). The observation that a TOG array is necessary for polymerization suggests that tethering of unpolymerized tubulin dimers to the microtubule end is needed for XMAP215's polymerization mechanism.

In vitro, XMAP215 can promote microtubule growth rates up to 10-fold alone, and it works in synergy with EB1 to accelerate growth rates up to 30-fold, matching growth rates observed in cells (Brouhard et al., 2008)(Zanic et al., 2013)(Farmer et al., 2021). Interestingly, XMAP215 promotes microtubule growth rate without a significant increase in microtubule lifetime, as would be expected based on the GTP-cap model (Vasquez et al., 1994)(Zanic et al., 2013)(Farmer et al., 2021). A logical hypothesis to explain this is that XMAP215 decreases the GTP-cap size, by increasing the GTP hydrolysis rate, resulting in fast-growing microtubules with small protective caps. Polymerizing microtubules at the same growth rate, by either using high tubulin concentrations or low tubulin concentrations with the addition of XMAP215, revealed that XMAP215 does not decrease the average EB comet length. This result suggests that XMAP215 does not decrease the GTP-cap size by increasing the GTP hydrolysis rate in order to increase microtubule catastrophe frequency. Instead, XMAP215 promotes irregularities in microtubule growth by increasing growth rate fluctuations and disrupted end configurations (Farmer et al., 2021). Disruption of the growing end makes microtubules more prone to catastrophe, resulting in microtubules undergoing a more abrupt transition to catastrophe, and with a larger GTP-tubulin content. This work demonstrates the importance of the microtubule end structure in defining microtubule lifetime, indicating that GTP-cap size is not the only factor.

6.1.4. CLASP promotes microtubule lifetime without increasing the GTP-cap size

In cells there is a myriad of MAPs that work to regulate microtubule dynamics. The cytoplasmic linker-associated protein (CLASP) family is a well conserved protein family known to regulate individual microtubule dynamics and spial organization of microtubule networks (Lemos et al., 2000)(Inoue et al., 2000)(Akhmanova et al., 2001)(Lawrence et al., 2020). CLASPs localizes to the tips of microtubules at the leading edge of migrating cells and are necessary for proper cell migration (Akhmanova et al., 2001)(Wittmann and Waterman-Storer, 2005)(Drabek et al., 2006). They also localize to kinetochores and along the mitotic spindle during mitosis in order to regulate microtubule dynamics within the spindle to achieve proper spindle formation, as depletion of CLASPs results in severe spindle defects (Maiato et al., 2003)(Maiato et al., 2005). Additionally, CLASPs play a role in promoting microtubule nucleation and increasing microtubule density at microtubule organizing centers, including both the centrosome and the Golgi (Efimov et al., 2007)(Miller et al., 2009).

Similar to the XMAP215 family, CLASP family members have an array of TOG domains that facilitate their ability to regulate microtubule dynamics (Al-Bassam et al., 2006)(Al-Bassam et al., 2007)(Slep and Vale, 2007). Unlike XMAP215, it has been shown that when targeted to the tips of microtubules, a single TOG domain from CLASP2 is sufficient to impact microtubule dynamics similarly to full length CLASP (Aher et al., 2018)(Majumdar et al., 2018). This is in contrast to XMAP215, which needs an array of TOG domains to carry out its functions, highlighting a difference between the mechanisms of the two MAPs.

CLASP's regulation of microtubule dynamics is known to facilitate its essential roles in cells (Lawrence et al., 2020). *In vitro* studies have demonstrated that CLASP regulates microtubule dynamics by suppressing catastrophe frequency, and promoting rescue and pausing during periods of growth, overall stabilizing microtubules (Aher et al., 2018)(Lawrence et al., 2018). It would be reasonable to hypothesize that a possible mechanism employed by CLASP to stabilize microtubules is to increase the GTP-cap size, either by increasing microtubule growth rate, or decreasing the GTP-hydrolysis rate. Measurements of microtubule dynamics report that CLASP's effect on catastrophe and rescue is accompanied by no significant change in average growth or shrinkage rates, indicating that microtubule stabilization is not a consequence of changes in these rates (Aher et al., 2018)(Lawrence et al., 2018). Interrogation of GTP-cap size using EB family members as a proxy for the GTP-cap size reveal that CLASP does not increase the GTP-cap size (Majumdar et al., 2018)(Lawrence et al., 2018). Interestingly, in the presence of CLASP, instances of EB comet repair are observed more frequently compared to when microtubules are grown in the absence of CLASP (Aher et al., 2018). EB comet repair is the phenomenon observed when there are two EB comets on a single growth event, and the lagging one catches up to the leading to form a single comet (Aher et al., 2018). XMAP215 induces comet split comets that are occasionally able to repair (Chapter 5)(Farmer et al., 2021). It is thought that these two comets represent two subsets of protofilaments; the leading comet being a subset of protofilaments growing faster than the remaining protofilaments, the lagging comet. CLASP's ability to increase the frequency of split comet events suggests that it stabilizes incomplete lattices, to the

extent that it gives the microtubule a chance to repair itself, instead of undergoing a catastrophe as a result of a disrupted end.

The molecular mechanism behind CLASP's stabilization of microtubules is still not understood. The observation that a single TOG domain of CLASP is able to reproduce the regulatory effects of the full-length protein refutes the hypothesis that CLASP simply tethers unpolymerized tubulin dimers to the end of a microtubules, such that they are available when needed, either to protect against catastrophe or promote rescue. Instead, CLASP must stabilize the microtubule by directly acting on the inter- and/or intra-dimer interactions within the polymer. However, it should be noted that these effects have to be temporary, or occur at a protofilament level, such that they do not affect the overall rate of microtubule shrinkage. Despite CLASP's exact mechanism remaining elusive, it is clear that CLASP does not stabilize microtubules by increasing the GTP-cap size. Thus, similar to the microtubule minus ends, and XMAP215, CLASP is able to break the canonical relationship between GTP-cap size and microtubule stability.

6.1.5. Summary

There are many lines of evidence indicating that the GTP-cap is protective, however it has become clear that its size does not dictate microtubule stability. Although with tubulin alone microtubule lifetime is correlated with microtubule growth rate, this relationship can easily be changed through the action of MAPs. Beyond

XMAP215 and CLASP, there are other MAPs that modulate microtubule growth rate and/or catastrophe frequency. Some of these MAPs have been suggested to disrupt the relationship between GTP-cap size and microtubule stability (van Haren and Wittmann, 2019). Without interrogating the size of the GTP-cap under all of these conditions, we cannot confidently conclude if any of these MAPs change the relationship between GTP-cap size and microtubule lifetime.

While the concept that the GTP-cap being a stabilizing structure remains true, it is now clear that the same GTP-cap size is consistent with a variety of microtubule lifetimes, indicating that there must be additional characteristics that impact microtubule stability. The other regulators of microtubule stability are still being determined, and when they overtake the protective nature of the GTP-cap remain to be understood. We must explore what other polymer characteristics contribute to instability in order to fully understand how microtubule dynamics can be regulated.

6.2. Microtubule stability can be regulated through the GTP hydrolysis rate

The GTP-cap size is the difference between the microtubule growth rate and the GTP hydrolysis rate. Thus, modulation of the GTP hydrolysis rate is a logical mechanism to regulate the GTP-cap size, and microtubule stability. Assuming a constant growth rate, increasing the GTP hydrolysis rate is predicted to decrease the cap size, while decreasing the GTP hydrolysis rate is predicted to increase the cap size (Figure 20). Despite it being clear that GTP-cap size does not define stability, a

GTP-cap is still necessary to protect a growing microtubule from shrinkage. Therefore, large fluctuations in GTP-cap size would be expected to impact overall stability of a microtubule.

The catalytic residues of tubulin needed for GTP hydrolysis have been well characterized. Mutations to key residues have been made to produce tubulin mutants with a decreased GTP hydrolysis rate (Roostalu et al., 2020)(Lafrance et al., 2022). Microtubules polymerized with this mutant tubulin have larger EB comets and decreased catastrophe frequency compared to wild-type microtubules. These results suggest that modulation of the GTP hydrolysis rate does indeed impact microtubule stability. In fact, microtubules polymerized with purified *C. elegans* tubulin have smaller EB comets when grown at the same rate as bovine tubulin, suggesting they have a faster GTP hydrolysis rate (Chaaban et al., 2018). It is thought that the increase in catastrophe frequency that *C. elegans* tubulin displays is, at least in part, a result of the decrease in GTP-cap size. This is yet another example linking microtubule stability to the GTPase activity of the tubulin dimer.

Modulation of the GTP hydrolysis rate has been proposed as a mechanism used by MAPs that impact microtubule catastrophe frequency. While this hypothesis has been rejected in the case of XMAP215 and CLASP, previous reports using EB proteins suggest this is the mechanism by which they increase catastrophe frequency. Increasing EB concentration has been reported to decrease the EB comet length, indicating a decrease in the GTP-cap size (Maurer et al., 2011). This is interpreted as

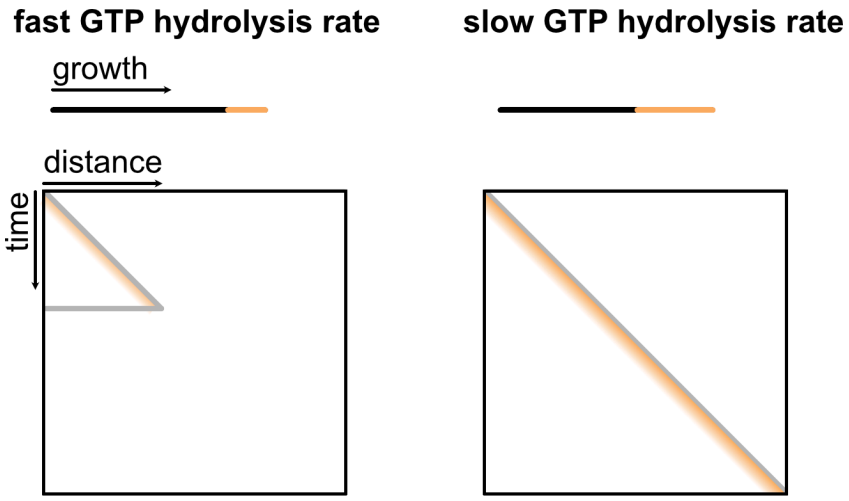

Figure 20. Modulation of the GTP hydrolysis rate can be used as a mechanism to regulate microtubule lifetime. Assuming the same growth rate, one microtubule with a faster GTP hydrolysis rate (left) will have a smaller GTP-cap size and higher catastrophe frequency compared to a microtubule with a slower hydrolysis rate (right) which will have a larger GTP-cap size and lower catastrophe frequency.

a concentration-dependent increase in the GTP hydrolysis rate. Whether this is true or not has been difficult to prove since EB is the only proxy for the GTP-cap size on dynamic microtubules. Nevertheless, EB is thought to always be present in the cellular environment, thus it's impact on microtubules is always relevant. It would be novel if

another MAP proved to modulate the GTP-cap size in the presence of EB. While other MAPs, such as TPX2, have been predicted to modulate the GTP hydrolysis rate, beyond EB, it has yet to be concluded that other MAPs regulate microtubule stability through modulation of the GTP hydrolysis rate. The correlation between microtubule stability and the GTP hydrolysis rate with tubulin alone suggests an intrinsic relationship between the two. Not only can this relationship can be disrupted through the action of MAPs, but through the microtubule tip structure as well.

6.3. Microtubule stability can be regulated by the microtubule tip structure

One emerging concept in the field is that the structure of the microtubule end plays a role in determining microtubule stability. This association seems somewhat obvious, however, due to the diffraction-limited nature and the dynamicity of the microtubule tip, it has been challenging to directly interrogate how end structure plays a role in regulating microtubule stability.

6.3.1. The structure of the growing microtubule end is complex

The architecture of the microtubule end has been debated for decades. Visualization of microtubule end structures using fluorescence has provided limited information due to the small size of microtubule ends. Microtubules are below the diffraction limit of light; they are 25 nm in diameter, with individual protofilaments being

only 4 nm wide. The most information regarding the structure of growing microtubule ends that fluorescence has been able to provide is that the growing end can exist as tapered (Demchouk et al., 2011)(Coombes et al., 2013)(Reid et al., 2019). Differences in taper length can be predicted based on model convolution of simulated images of set tapered lengths with the point spread function (Demchouk et al., 2011)(Coombes et al., 2013). In order to more directly visualize the growing microtubule end, structural biology techniques, such as electron microscopy, must be used. However, to gain the contrast needed to resolve what is going on at a dimer level, averaging techniques must be used. This is less problematic for the microtubule lattice, which typically displays specific patterns and repeats, but for the diverse and constantly evolving structures at the microtubule tip this is not an option. Nevertheless, these structural techniques have provided insight into what the growing microtubule end may look like. These structures have been incorporated into molecular models to try and gain a better understand of how microtubule dynamics are regulated.

Currently, there are three views of what the growing end looks like, based on the conflicting results of structural studies to date (Figure 21). Early work using either negative stain or cryo-electron microscopy (cryo-EM) of frozen hydrated dynamic microtubules resulted in detection of blunt or tapered growing ends (Mandelkow et al., 1991). These studies suggest that protofilaments at the growing end are relatively straight. This end structure could be achieved through cooperative assembly, as explained by the ‘cozy corner’ model of microtubule assembly (Erickson and Pantaloni, 1981). The cozy corner model states that an incoming subunit is more likely to bind in a location where it can form both a longitudinal and lateral bond with adjacent

subunits because the formation of two bonds is more energetically favorable than formation of one (Erickson and Pantaloni, 1981)(Erickson, 1989). Computational models have taken into account this end structure and cooperative binding, resulting in a relatively simple model of microtubule dynamics that is able to reproduce many experimental observations (VanBuren et al., 2002)(Castle and Odde, 2013)(Gardner et al., 2011a) (Zakharov et al., 2015)(Coombes et al., 2013). While these models are attractive because of their simplicity, they do not account for all of the observed dynamics, and do not agree with other structural studies.

Other studies of dynamic growing ends *in vitro* using cryo-EM and cryo-electron tomography (cryo-ET) report long, gently curved sheets of protofilaments at growing ends (Chrétien et al., 1995)(Guesdon et al., 2016). These data suggest that lateral bonds between protofilaments are strong enough to hold protofilaments together, and are able to contribute to protofilament straightening, eventually closing the polymer. How protofilament sheets would impact microtubule dynamics and GTP hydrolysis remains unclear. One computational model predicts sheets are an intermediate state of growth and the result of transiently bound GDP-tubulin subunits at the ends of protofilaments (Stewman et al., 2020). This model also predicts that dimer straightening is a prerequisite for GTP hydrolysis, thus GTP hydrolysis cannot occur in a sheet because all dimers in a sheet are curved. However, it is not known that a dimer must straighten prior to hydrolysis, and is inconsistent with the idea of split comets which can be observed in experimental data (Aher et al., 2018)(Farmer et al., 2021). While these studies report the observation of sheets at the ends of growing microtubes, some argue that these structures are simply a result of the sample

preparation and imaging technique. Although sheet structures have never explicitly been visualized using fluorescence, the split comets that can be seen using EB1 suggest that there may be sheet-like structures present during periods of microtubule growth.

Recent advances in cryo-EM technologies and sample preparation have facilitated the visualization of the growing microtubule end in three dimensions using axial tomography. These studies have created 3D models of growing microtubule end structures *in vitro* and in cells (Mcintosh et al., 2018)(Atherton et al., 2018). Regardless of the environment, the majority of growing ends were composed of individual protofilaments curving outwards. It was previously thought that this end architecture was only present during shrinkage (Kirschner et al., 1974)(Simon and Salmon, 1990)(Mandelkow et al., 1991). These new studies suggest that protofilaments at the growing end individually elongate, and then rely on the formation of lateral bonds to come together and close the microtubule lattice (Gudimchuk et al., 2020). Computational modeling of this microtubule growth mechanism has resulted in a new model in which thermal fluctuations cause the formation of lateral bonds and drive protofilament straightening (Chen et al., 2021). Combining this aspect of microtubule growth with a model for GTP hydrolysis results in accurate reproduction of microtubule dynamics observed over a range of conditions *in vitro* (Margolin et al., 2012) (Gudimchuk et al., 2020). Visualization of microtubule ends from many angles has facilitated identification and tracking of individual protofilaments, leading to yet another mechanism of how microtubule ends look during grow. The observation of

diverse end structures could point to the possibility that the microtubule end structure is constantly evolving, exhibiting a number of different morphologies over time.

While structural studies have been very informative, each result represents a single snapshot of many conformations a protein can adopt. It is difficult, if not impossible, to be certain of the exact dynamic state at the moment the structures were fixed. However, the ability to instantaneously freeze, then image, samples in vitrified ice has been an advancement in sample preparation that provides better temporal and temperature control of sample state at the time of fixation. Future studies using techniques such as correlative light and electron microscopy (CLEM) will come the closest to linking structure to dynamic state. It will be important to understand how individual points in time relate to microtubule stability to provide more insight on how microtubule dynamics can be regulated. One example of an area of research that lack understanding is how the microtubule end can dynamically change structure over time, and how these structures relate to stability.

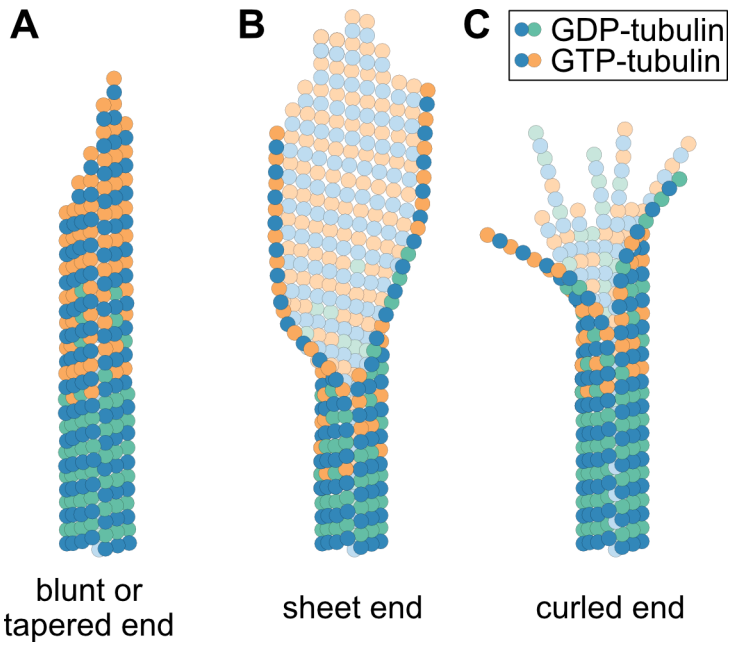

Figure 21. Three models of microtubule end structure during growth. (A) Model of microtubule growth with straight protofilaments. The end structure of these protofilaments is either blunt or tapered. (B) Model of microtubule growth with open sheet-like structures. It is thought that open sheets are able to curl together to form an intact lattice. (C) Model of microtubule growth with curled protofilaments. This model predicts that individual protofilaments grow and are able to then form lateral interactions to stitch together the lattice.

6.3.2. EB localization suggests microtubule ends can split and repair throughout growth

While it has been challenging to learn anything about the microtubule end structure from tubulin-based probes, the localization of MAPs on microtubule tips may be able to provide some new insights on the end structure. Recent work using EB

proteins as markers for the growing microtubule ends reveals the presence of splitting comets, suggesting that the microtubule end is not blunt, but ragged. Assuming EBs localizes to the interface of four tubulin dimers, between two protofilaments (Figure 6), the presence of two EB comets at a microtubule end suggests that a subset of protofilaments are growing faster than the rest (Maurer et al., 2012)(Aher et al., 2018)(Farmer et al., 2021). The idea that EB marks the GTP-cap reveals that the GTP-cap can be split into two parts, and that a full lattice is not a prerequisite for hydrolysis to occur. Whether these disrupted ends are able to disrupt the microtubule lattice enough to destabilize the polymer and promote catastrophe is unknown. Although microtubules with split ends have been observed to undergo catastrophe (Appendix Figure 1), it is unknown if these catastrophes occurred as a result of the end morphology. One can predict that the impact split ends have on microtubule lifetime is dependent on the number of protofilaments growing faster than the rest. For example, if more than half of the protofilaments are growing faster, the fate of the leading end may dictate the fate of the rest of the polymer. If only a few protofilaments are growing faster, the full microtubule lattice might be able to overpower the fate of the leading end. These are only speculations; careful correlation of EB comet morphology, protofilament number, and microtubule lifetime will lead to a better understanding of how end structure plays into microtubule stability. It may also provide insight into how other regulators of microtubule end structure, such as microtubule age, impact stability.

6.3.3. Microtubule aging has been linked to microtubule stability

Another characteristic that is thought to play a role in defining overall microtubule stability is microtubule age. The distribution of microtubule lifetimes is best fit to a Gama distribution rather than an exponential decay (Odde et al., 1995). This observation suggests that catastrophe is a multistep process (Odde et al., 1995)(Gardner et al., 2013). It is thought that the step to precede catastrophe involves microtubule aging (Odde et al., 1995) (Gardner et al., 2013). While the regulators of microtubule aging and the exact definition of microtubule aging remain unclear, one element may be the microtubule end structure (Brouhard, 2015). The microtubule end structure becomes more tapered *in vitro* as a function of time, tubulin concentration, and growth rate (Coombes et al., 2013). These *in vitro* approximations were applied to computational models and the results corroborate that microtubule aging plays a role in defining lifetime (Coombes et al., 2013) (Zakharov et al., 2015). Another parameter that is thought to impact microtubule aging is the accumulation of defects, either along the microtubule lattice or concentrated at the tip (Bowne-Anderson et al., 2013). How and if lattice damage is propagated to affect catastrophe, which occurs at the microtubule tip, is not well understood. We determined that XMAP215 is able to increase the frequency of end disruptions, which play a role in increasing the catastrophe frequency (Chapter 5) (Farmer et al., 2021). XMAP215 is able to promote catastrophe at fast growth rates and with a higher GTP-tubulin content compared to controls, suggesting a more unstable microtubule tip. Thus, XMAP215 can be viewed as an aging accelerator.

Despite knowing some players involved in microtubule aging, the exact mechanism by which this process happens remains yet to be understood. Continued interrogation of the relationships between microtubule growth, stability, and GTP-cap size will be imperative to uncover how these parameters are linked to one another and the contributors to microtubule aging. Regulators of microtubule dynamics will continue to be used as probes for gaining insight into the basic parameters governing dynamic instability, such as microtubule aging.

6.3.4. Summary

While we have gained insight into the link between end structure and microtubule lifetime, there is still much to be discovered. Unfortunately, a lot of these unknowns are at the molecular detail of the microtubule structure. With advances in sample preparation, development of new microscopy techniques, and innovations in data analysis, we will gain insight into how these details impact microtubule stability. A challenge to addressing how these molecular details impact stability is that they need to be interrogated on dynamic microtubules. Many methods that increase resolution take advantage of fixed samples or slow processes. Microtubule dynamics is a fast, dynamic process. This is one of the major reasons detailed investigations into the size of GTP-cap in cells are challenging and have yet to be done.

6.4. The GTP-cap in cells

While there have been many advances and discoveries thanks to studies using *in vitro* reconstitution, it is imperative to compare the *in vitro* results to those observed in cells. Because individual microtubules are difficult to image live in cells, there are limited number of investigations and questions that have been answered in this system. Morphological changes to the microtubule network are frequently reported, however, it is often underlying changes in microtubule dynamics that drive these changes. It has been difficult to gain information regarding how individual microtubule dynamics are regulated to drive these morphologic changes due to the challenges surrounding visualization of individual microtubules in cells. MAPs are known to regulate microtubule dynamics in cells. Modulating the microtubule network is cells is not only driven by these MAPs that directly impact microtubule dynamics, but also other proteins that indirectly interact with microtubules. This is one of the major reasons why it is advantageous to isolate elements of the system, in order to interrogate how each element works, so they can be put together to build the microtubule networks we see in cells. It has been shown that microtubule dynamics change with the phase of the cell cycle, with microtubules in mitosis being more dynamic overall, exhibiting increased growth rates and number of catastrophes (Rusan et al., 2001). Microtubule dynamics also change with morphological changes, such as differentiation, polarization, and migration. Future studies investigating exactly how, and by what mechanisms, microtubule dynamics are changing to facilitate these morphological changes are required for a better understanding of the microtubule network in cells.

6.4.1. EB is a microtubule TIP organizer

Microtubule dynamics in cells are regulated by a myriad of MAPs, one group being the well-known EB family of proteins. In mammalian cells there are three EB family members, EB1, 2, and 3. While all family members autonomously track growing microtubule ends, they have distinct localization profiles, suggesting slightly different nucleotide sensing mechanisms (Komarova et al., 2009)(Roth et al., 2019). EB1 and EB3 display near indistinguishable localization, localizing closest to the microtubule tip with localization exponentially decaying down the microtubule lattice, while EB2 localizes slightly behind the others with a broader peak of intensity. Recent work has speculated that there is a slight change in nucleotide sensing ability in EB2 to drive its differential localization (Roth et al., 2019). Despite this, all family members autonomously tip track and thus provide excellent markers for growing microtubule ends in cells.

Along with autonomously tip tracking, EB family members are known to recruit a number of other proteins to the microtubule tip. As a result, EBs are known to regulate a complex network of proteins called the +TIPs (Lansbergen and Akhmanova, 2006)(Mustyatsa et al., 2017). Depletion of EB in cells results in aberrant microtubule dynamics, thought to be mainly driven by mislocalization of the microtubule regulators it typically brings to the tip. These proteins include other MAPs, signaling factors, and motor proteins. These protein complexes are regulated both spatially and temporally to help anchor microtubules to the cell cortex, connect microtubule to kinetochores, and regulate microtubule dynamics.

6.4.2. EB is primarily used as a marker for growing microtubule ends in cells

EBs are commonly used to mark the growing microtubule ends in cells due to their localization to the microtubule tip, thus only marking a fraction of the dense microtubule network in cell. This results in increased ability to approximate polymer amount and growth characteristics of the microtubule network, even just in 2D. In contrast, due to the high density of the microtubule network, it is near impossible to distinguish individual polymers when using a tubulin signal to mark the microtubule network. The ability to image tubulin in 3D slightly overcomes this, but it frequently eliminates the possibility of imaging through time, thus limiting acquisition of dynamic information. For these reasons, EBs have frequently been used to mark the ends of microtubules in cells. Despite its wide-use as a microtubule marker, the number of studies that have tried to quantify characteristics of its localization in cells is a small fraction of the studies that have used it.

6.4.3. GTP-cap size in cells

While GTP-cap sizes have been used *in vitro* to correlate with microtubule stability, this correlation has yet to be drawn in cells. While some studies have resorted to quantifying the relative EB intensity at the tip to microtubule as a way of comparing comet ‘size’ (Maurer et al., 2011)(Maurer et al., 2012)(Mohan et al., 2013)(Duellberg et al., 2016)(Ramirez-Rios et al., 2016)(Rickman et al., 2017)(Roostalu et al., 2020)(Ye et al., 2020)(Hahn et al., 2021), it is widely known that there are a number

of factors that impact EB localization, such as microtubule growth rate (Hahn et al., 2021). Based on fitting EB comets to exponential decay functions, as done *in vitro*, the GTP-cap size in cells has been approximated to be on the order of magnitude of hundreds of subunits long (Seetapun et al., 2012)(Mustyatsa et al., 2019). This approximation is in line with what would be expected if microtubule growth rate sets EB comet length in cells similar to how it does *in vitro* (Bieling et al., 2007)(Farmer et al., 2021). Of the few studies that have attempted to measure the size of the GTP-cap in cells, none of them have correlated the size with a range of microtubule growth rates, meaning, it is not known if GTP-cap size, as measured by EB comet length, scales with microtubule growth rate in cells. How comet lengths dictate microtubule stability in cells is also unknown. We set out to measure EB comet size over a range of microtubule growth rates in cells to determine if similar to *in vitro*, microtubule growth rate sets the GTP-cap size.

6.4.4. EB comet sizes scale with microtubule growth rate in cells but differently compared to microtubules in vitro

Our results indicate that, similar to *in vitro*, EB comet length positively scales with microtubule growth rate in cells. Interestingly, the relationship between microtubule growth rate and EB comet size in cells appears to be different from that *in vitro* such that a microtubule will have a smaller EB comet length *in vitro* compared to in cells for a given growth rate (Appendix Figure 2). These results suggest that the GTP-cap length in cells is restricted, or that the GTP hydrolysis rate is increased, thus

producing a smaller GTP-cap for a given growth rate. Our immediate future direction is to acquire time lapses of EB comets growing *in vitro* and in cells using instant structured illumination microscope (iSIM). These datasets can then be analyzed for microtubule growth rate and EB comet length to determine if EB comets *in vitro* are truly larger than those in cells.

6.4.5. Summary

While there has been significant work *in vitro* detailing the relationships between microtubule growth rate, stability, and GTP-cap size, it is essential to interrogate these relationships in cells to determine if our *in vitro* system mimics what is seen in cells. When growth rates observed in cells are reconstituted *in vitro* by increasing tubulin concentration, no catastrophe is observed (Farmer et al., 2021). However, in cells, microtubules growing at these growth rates undergo frequent catastrophe (Rusan et al., 2001). How are microtubules in cells able to grow fast but undergo frequent catastrophes? It remains unclear what the relationship is between microtubule growth rate and GTP-cap size in cells, however preliminary data suggest that cells may have an inherent mechanism to keep the GTP-cap smaller than *in vitro*. Future interrogation into this relationship will help elucidate whether GTP-cap sizes in cells are similar to what is observed *in vitro*.

APPENDIX CHAPTER 1

A1. Microtubule lifetime does not correlate with tapered ends in the presence of XMAP215

A1.1. Introduction

The presence of split comets raised the question, do split comets correlate with microtubule lifetime? In other words, are split comets a predictor of microtubule fate? We wondered if XMAP215's catastrophe-promoting activity was a direct consequence of XMAP215-mediated disruption of the microtubule end structure.

A1.2. Results

To determine if microtubule catastrophe correlated with the presence of a split comets, we analyzed growth-rate-matching experiments and XMAP215 titration for end structure and catastrophe. Growth-rate-matched events from Chapter 5, Figure 15C were tracked until they underwent a catastrophe, up to two minutes. They were then scored as having a tapered end if they displayed a split or curled comet at any point during their lifetime. In the control condition (-XMAP215), no catastrophe events were observed, however 13% of microtubules displayed a ragged end (Appendix Figure 1A, left). About half of the microtubules polymerized in the presence of

XMAP215 (+XMAP215) underwent a catastrophe within two minutes, and while most of them displayed a ragged end (77%), a similar percentage of microtubules did not undergo a catastrophe within the observed period even after displaying a ragged end (81%) (Appendix Figure 1A, left). These data suggest that microtubules polymerized with XMAP215 have a similar probability of undergoing a catastrophe within two minutes, regardless of end structure. In addition, microtubules polymerized at similar growth rates with tubulin that display a tapered end are not more likely to undergo catastrophe.

We extended this analysis to microtubules grown over a range of XMAP215 concentrations, reasoning that if tapered ends lead to catastrophe, microtubule growth events that display a ragged end should have, on average, a smaller lifetime compared to those that do not display a tapered end. We analyzed 65 growth events from each XMAP215 concentration tested on one experimental day (Chapter 5, Figure 12). Growth events were tracked until they underwent a catastrophe, or up to two minutes, and scored as having a tapered end if one occurred at any point during the growth event. Surprisingly, there was not a correlation between the presence of tapered ends and shorter lifetime at any concentration of XMAP215 tested (Appendix Figure 1B).

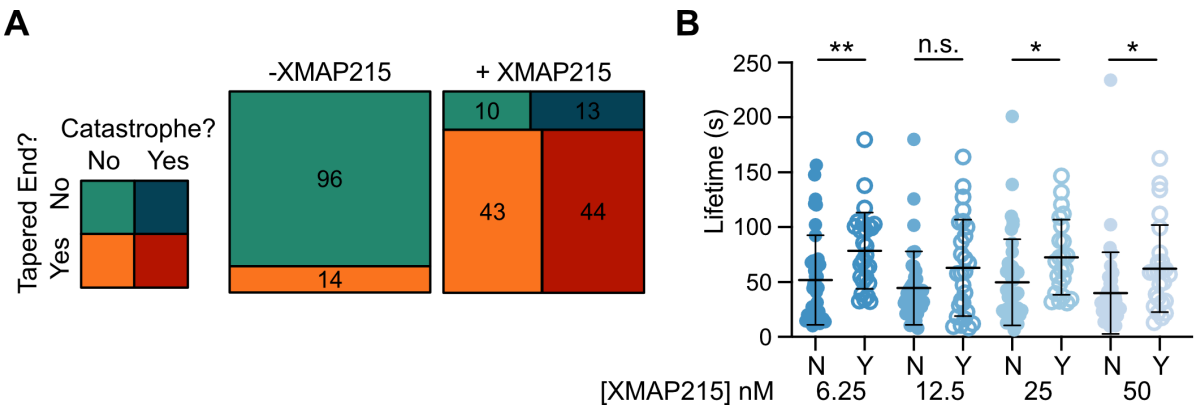

Appendix Figure 1. Catastrophe frequency does not correlate with the presence of tapered ends. A) Microtubules were either polymerized with 60 μM tubulin, 200 nM EB1GFP (- XMAP215), or with 20 μM tubulin, 200 nM EB1GFP, and 12.5/25 nM XMAP215 (+ XMAP215). 110 microtubule growth events, which did not have significant difference in growth rates, were tracked. Growth events were scored to be tapered if they displayed a split or curl at any point during their lifetime, and scored as a catastrophe if one was observed within two minutes. B) Growth events from one experimental day of the XMAP215 titration in Figure 12 were analyzed for end disruption and plotted against their lifetime. 65 growth events per condition were analyzed. Student's t-test were performed to determine significance within XMAP215 concentrations.

A1.3. Discussion

Our analysis revealed no obvious correlation between tapered ends and microtubule catastrophe. These results emphasize that microtubules are able to catastrophe with and without a, detectable, tapered end. It is important to note that we cannot detect tapered end events that are below the diffraction limit, meaning there

may be many tapered ends in both condition that could not be detected. That being said, these results make it clear that microtubule end structure is very dynamic, constantly evolving overtime, and the presence of a disruption does not always lead to a catastrophe.

A1.4. Methods

A1.4.1. Protein preparation and assay conditions and imaging

Performed as described in Chapter 5.

A1.4.2. Determination of microtubule end morphology and microtubule lifetime

End morphology was determined as described in Chapter 5. For growth-rate-matching data, microtubule growth events were tracked for up to 2 minutes and scored for tapered ends and catastrophe. Microtubule lifetime for the XMAP215 titration (Appendix Figure 1B) was determined as the total time a growth event spent in a period of growth prior to catastrophe. The same 110 microtubule growth events that did not differ significantly in growth rate analyzed in Chapter 5, Figure 15C were also scored for catastrophe.

APPENDIX CHAPTER 2

A2. Preliminary data suggests EB1 comet length scales with microtubule growth rate in cells

A2.1. Introduction

While EB is commonly used at a microtubule tip marker in cells, only a handful of studies have attempted to measure the size of the GTP-cap in cells. Additionally, none of them have measured the GTP-cap size over a range of microtubule growth rates, thus, it is not known if GTP-cap size scales with microtubule growth rate in cells. It is unknown if our *in vitro* system models the relationship between microtubule growth rate and EB comet length in cells because the relationship in cells is not known.

A2.2. Results

In order to determine if GTP-cap size scales with microtubule growth rate in cells similarly to how it does *in vitro*, we set out to determine the EB comet size in cells over a range of microtubule growth rates. We imaged microtubules in live cells using spinning disk confocal and used EB1-GFP as our probe for both microtubule growth rate and GTP-cap size. The growth rate of microtubule growth events that could be

tracked in time for at least 5 seconds were determined and the average EB comet length over the course of that lifetime was determined (Methods). Growth events from cells in interphase or mitosis were analyzed to determine if there were cell-cycle specific effects. These data reveal a positive correlation between microtubule growth rate and EB comet length (Appendix Figure 2). On average, microtubule growth events in mitosis are faster than growth events in interphase, consistent with previously published data (Rusan et al., 2001). While there is a range of EB comet lengths for a given growth rate, there is no evidence that the relationship between growth rate and EB comet length changes depending on the phase of the cell cycle (Appendix Figure 2). The data was then plotted with a previously acquired *in vitro* tubulin titration to compare EB comet lengths from microtubules growing at the same growth rate (Appendix Figure 2). This reveals that for a given growth rate, EB comet size appears to be larger *in vitro* than in cells.

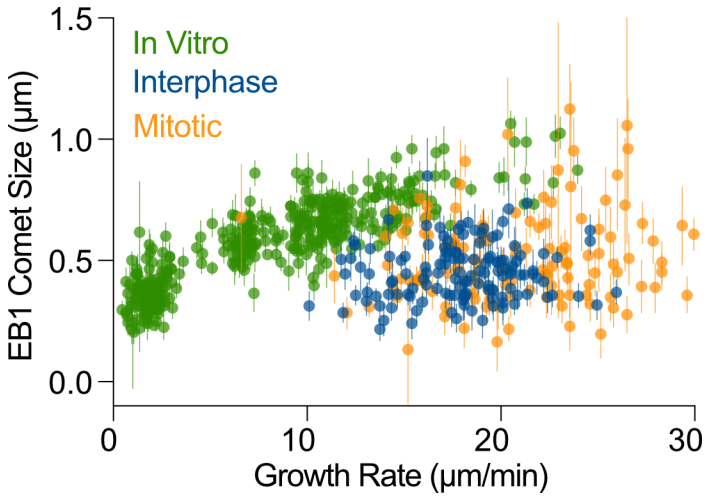

Appendix Figure 2. EB1 comet length scales with microtubule growth rate *in vitro* and in cells. Preliminary results suggest that EB1 comet size positively scales with microtubule growth rate in cells. Each point is the

average EB1 comet length and microtubule growth rate for a given growth event. Error bars are 95% CI of the fit.

A2.3. Discussion

Our preliminary data not only suggest that EB comet length scales with microtubule growth rate in cells, it suggests that EB comet length is shorter for a given growth rate when compared to microtubules grown *in vitro*. This observation suggests that the cell may employ mechanism to limit the GTP-cap size. However, the in vitro and cellular data were acquired using different imaging parameters and systems, which could affect the measured comet length. In order to more directly address if EB comet size differs in these two systems, the cell and *in vitro* data need to be acquired using the same microscope and the same imaging parameters.

A2.4. Methods

A2.4.1. Cell culture

LLC-PK1 cells stably over-expressing EB1-GFP were a gift from R. Ohi (Piehl and Cassimeris, 2003). Cells were cultured in a 1:1 mixture of Opti-MEM and F-10 media supplemented with 10% fetal bovine serum, 1% Penn/Step, and 1% L-Glutamine (Invitrogen). Cells were grown in a 5% CO_2 atmosphere at 37°C. For use in experiments, cells were either plated on glass-bottomed dishes (MatTek Corp).

A2.4.2. Protein Purification

Bovine tubulin was purified and labeled with fluorescent dyes are previously described in Chapter 2. EB1-GFP was expressed in *Escherichia coli* and purified as previously described (Zanic et al., 2009) and stored in 10 mM Bis-Tris, 10 mM TrisHCl, 100 mM KCl, 1mM DTT, 5% glycerol, pH 6.6. Protein concentration was determined using absorbance at 280 nm.

A2.4.3. Dynamics assays

In vitro tubulin titration was performed as previously described in Chapter 2, and tubulin concentrations used were the same as for the tubulin titration in Chapter 3. For microtubule dynamics assay with EB1-GFP comets, conditions were the same as described in Chapter 2 with 17 mM KCl and 0.1% methylcellulose were used in the imaging reaction. Images were taken at 1.67 FPS.

A2.4.4. Imaging

In vitro data was acquired as previous described in Chapter 3. Cell images were acquired using a Nikon spinning disk confocal system outfitted with an Apo TIRF Oil 100X 1.49 NA objective, Yokogawa CSU-X1 spinning disk head, Andor DU-897 EMCCD, high-speed piezo z stage, live cell incubator (TokiHit), and four-line

high-power solid-state laser launch (405, 488, 561, and 647 lines). Cells were kept at 37°C with 5% CO_2 during imaging.

A2.4.5. EB1-comet length analysis

Each microtubule growth event was assigned a mean microtubule growth rate and EB comet length. EB comet analysis was done as explained in Chapter 4.

REFERENCES

Aher, A., M. Kok, A. Sharma, A. Rai, N. Olieric, R. Rodriguez-Garcia, E.A. Katrukha, T. Weinert, V. Olieric, L.C. Kapitein, M.O. Steinmetz, M. Dogterom, and A. Akhmanova. 2018. CLASP Suppresses Microtubule Catastrophes through a Single TOG Domain. *Dev. Cell*. 46:40–58. doi:10.1016/j.devcel.2018.05.032.

Aher, A., D. Rai, L. Schaedel, J. Gaillard, K. John, Q. Liu, M. Altelaar, L. Blanchoin, M. Thery, and A. Akhmanova. 2020. CLASP Mediates Microtubule Repair by Restricting Lattice Damage and Regulating Tubulin Incorporation. *Curr. Biol.* 30:2175-2183.e6. doi:10.1016/j.cub.2020.03.070.

Akhmanova, A., and C.C. Hoogenraad. 2015. Microtubule minus-end-targeting proteins. *Curr. Biol.* 25:R162–R171. doi:10.1016/j.cub.2014.12.027.

Akhmanova, A., C.C. Hoogenraad, K. Drabek, T. Stepanova, B. Dortland, T. Verkerk, W. Vermeulen, B.M. Burgering, C.I. De Zeeuw, F. Grosveld, and N. Galjart. 2001. Clasps are CLIP-115 and -170 associating proteins involved in the regional regulation of microtubule dynamics in motile fibroblasts. *Cell*. 104:923–935.

Akhmanova, A., and M.O. Steinmetz. 2008. Tracking the ends: a dynamic protein network controls the fate of microtubule tips. *Nat. Rev. Mol. Cell Biol.* 9:309–322. doi:10.1038/nrm2369.

Akhmanova, A., and M.O. Steinmetz. 2015. Control of microtubule organization and dynamics: two ends in the limelight. *Nat. Rev. Mol. Cell Biol.* 16:711–26.

doi:10.1038/nrm4084.

Al-Bassam, J., M. Van Breugel, S.C. Harrison, and A. Hyman. 2006. Stu2p binds tubulin and undergoes an open-to-closed conformational change. *J. Cell Biol.* 172:1009–1022. doi:10.1083/jcb.200511010.

Al-Bassam, J., and F. Chang. 2011. Regulation of microtubule dynamics by TOG-domain proteins XMAP215/Dis1 and CLASP. *Trends Cell Biol.* 21:604–614. doi:10.1016/j.tcb.2011.06.007.

Al-Bassam, J., N.A. Larsen, A.A. Hyman, and S.C. Harrison. 2007. Crystal Structure of a TOG Domain: Conserved Features of XMAP215/Dis1-Family TOG Domains and Implications for Tubulin Binding. *Structure*. 15:355–362. doi:10.1016/j.str.2007.01.012.

Aldaz, H., L.M. Rice, T. Stearns, and D.A. Agard. 2005. Insights into microtubule nucleation from the crystal structure of human γ-tubulin. *Nature*. 435:523–527. doi:10.1038/nature03586.

Alushin, G.M., G.C. Lander, E.H. Kellogg, R. Zhang, D. Baker, and E. Nogales. 2014. High-Resolution microtubule structures reveal the structural transitions in ab-tubulin upon GTP hydrolysis. *Cell*. 157:1117–1129. doi:10.1016/j.cell.2014.03.053.

Arellano-Santoyo, H., E.A. Geyer, E. Stokasimov, G.Y. Chen, X. Su, W. Hancock, L.M. Rice, and D. Pellman. 2017. A Tubulin Binding Switch Underlies

Kip3/Kinesin-8 Depolymerase Activity. *Dev. Cell*. 42:37-51.e8. doi:10.1016/j.devcel.2017.06.011.

Arnal, I., E. Karsenti, and A.A. Hyman. 2000. Structural transitions at microtubule ends correlate with their dynamic properties in Xenopus egg extracts. *J. Cell Biol.* 149:767–774. doi:10.1083/jcb.149.4.767.

Arpağ, G., E.J. Lawrence, V.J. Farmer, S.L. Hall, and M. Zanic. 2020. Collective effects of XMAP215, EB1, CLASP2, and MCAK lead to robust microtubule treadmilling. *PNAS*. 117:12847–12855. doi:10.1073/pnas.2003191117.

Asenjo, A.B., C. Chatterjee, D. Tan, V. DePaoli, W.J. Rice, R. Diaz-Avalos, M. Silvestry, and H. Sosa. 2013. Structural model for tubulin recognition and deformation by kinesin-13 microtubule depolymerases. *Cell Rep.* 3:759–768. doi:10.1016/j.celrep.2013.01.030.

Atherton, J., K. Jiang, M.M. Stangier, Y. Luo, S. Hua, K. Houben, J.J.E. Van Hoff, A.-P. Joseph, G. Scarabelli, B.J. Grant, A.J. Roberts, M. Topf, M.O. Steinmetz, M. Baldus, C.A. Moores, and A. Akhmanova. 2017. A structural model for microtubule minus-end recognition and protection by CAMSAP proteins. *Nat. Struct. Mol. Biol.* in press. doi:10.1038/nsmb.3483.

Atherton, J., M. Stouffer, F. Francis, and C.A. Moores. 2018. Microtubule architecture in vitro and in cells revealed by cryo-electron tomography. *Acta Crystallogr. Sect. D Struct. Biol.* 74:1–13. doi:10.1107/S2059798318001948.

Ayaz, P., S. Munyoki, E.A. Geyer, F.A. Piedra, E.S. Vu, R. Bromberg, Z. Otwinowski, N. V. Grishin, C.A. Brautigam, and L.M. Rice. 2014. A tethered delivery mechanism explains the catalytic action of a microtubule polymerase. *Elife*. 3:1–19. doi:10.7554/eLife.03069.

Ayaz, P., X. Ye, P. Huddleston, C.A. Brautigam, and L.M. Rice. 2012. A TOG : αβ-tubulin Complex Structure Reveals Conformation-Based Mechanisms for a Microtubule Polymerase. *Science (80-.).* 337:857–60. doi:10.1126/science.1221698.

Bergen, L.G., and G.G. Borisy. 1980. Head-to-tail polymerization of microtubules in vitro: Electron microscope analysis of seeded assembly. *J. Cell Biol.* 84:141–150. doi:10.1083/jcb.84.1.141.

Best, R.L., N.E. LaPointe, J. Liang, K. Ruan, M.F. Shade, L. Wilson, and S.C. Feinstein. 2019. Tau isoform–specific stabilization of intermediate states during microtubule assembly and disassembly. *J. Biol. Chem.* 294:12265–12280. doi:10.1074/jbc.ra119.009124.

Bieling, P., S. Kandels-Lewis, I.A. Telley, J. Van Dijk, C. Janke, and T. Surrey. 2008. CLIP-170 tracks growing microtubule ends by dynamically recognizing composite EB1/tubulinbinding sites. *J. Cell Biol.* 183:1223–1233. doi:10.1083/jcb.200809190.

Bieling, P., L. Laan, H. Schek, E.L. Munteanu, L. Sandblad, M. Dogterom, D. Brunner, and T. Surrey. 2007. Reconstitution of a microtubule plus-end tracking system in

vitro. *Nature*. 450:1100–1105. doi:10.1038/nature06386.

Bollinger, J.A., and M.J. Stevens. 2018. Catastrophic Depolymerization of Microtubules Driven by Subunit Shape Change. *Soft Matter*. doi:2018/SM/C7SM02033C.

Borisy, G.G., J.M. Marcum, J.B. Olmsted, D.B. Murphy, and K.A. Johnson. 1975. Purification of Tubulin and Associated High Molecular Weight Proteins From Porcine Brain and Characterization of Microtubule Assembly in Vitro. *Ann. N. Y. Acad. Sci.* 253:107–132. doi:10.1111/j.1749-6632.1975.tb19196.x.

Borisy, G.G., and E.W. Taylor. 1967. The mechanism of action of colchicine. Binding of colchincine-3H to cellular protein. *J. Cell Biol.* 34:525–533. doi:10.1083/jcb.34.2.525.

Bowne-Anderson, H., M. Zanic, M. Kauer, and J. Howard. 2013. Microtubule dynamic instability: A new model with coupled GTP hydrolysis and multistep catastrophe. *BioEssays*. 35:452–461. doi:10.1002/bies.201200131.

Brouhard, G.J. 2015. Dynamic instability 30 years later: Complexities in microtubule growth and catastrophe. *Mol. Biol. Cell*. 26:1207–1210. doi:10.1091/mbc.E13-10-0594.

Brouhard, G.J., and L.M. Rice. 2014. The contribution of αβ-tubulin curvature to microtubule dynamics. *J. Cell Biol.* 207:323–334. doi:10.1083/jcb.201407095.

Brouhard, G.J., J.H. Stear, T.L. Noetzel, J. Al-Bassam, K. Kinoshita, S.C. Harrison, J.

Howard, and A.A. Hyman. 2008. XMAP215 Is a Processive Microtubule Polymerase. *Cell*. 132:79–88. doi:10.1016/j.cell.2007.11.043.

Caplow, M., and J. Shanks. 1996. Evidence that a single monolayer tubulin-GTP cap is both necessary and sufficient to stabilize microtubules. *Mol. Biol. Cell*. 7:663–675. doi:10.1091/MBC.7.4.663.

Carlier, M.-F., D. Didry, C. Simon, and D. Pantaloni. 1989. Mechanism of GTP hydrolysis in tubulin polymerization: characterization of the kinetic intermediate microtubule-GDP-Pi using phosphate analogues. *Biochemistry*. 28:1783–1791. doi:10.1021/bi00430a054.

Carlier, M.-F., and D. Pantaloni. 1981. Kinetic analysis of guanosine 5'-triphosphate hydrolysis associated with tubulin polymerization. *Biochemistry*. 20:1918–1924. doi:10.1021/bi00510a030.

Castle, B.T., and D.J. Odde. 2013. Brownian dynamics of subunit addition-loss kinetics and thermodynamics in linear polymer self-assembly. *Biophys. J.* 105:2528–2540. doi:10.1016/j.bpj.2013.10.009.

Castoldi, M., and A. V. Popov. 2003. Purification of brain tubulin through two cycles of polymerization- depolymerization in a high-molarity buffer. *Protein Expr. Purif.* 32:83–88. doi:10.1016/S1046-5928(03)00218-3.

Chaaban, S., S. Jariwala, C.T. Hsu, S. Redemann, J.M. Kollman, T. Müller-Reichert, D. Sept, K.H. Bui, and G.J. Brouhard. 2018. The Structure and Dynamics of C.

elegans Tubulin Reveals the Mechanistic Basis of Microtubule Growth. *Dev. Cell*. 47:191-204.e8. doi:10.1016/j.devcel.2018.08.023.

Chabin-Brion, K., J. Marceiller, F. Perez, C. Settegrana, A. Drechou, G. Durand, and C. Poüs. 2001. The Golgi complex is a microtubule-organizing organelle. *Mol. Biol. Cell*. 12:2047–2060. doi:10.1091/mbc.12.7.2047.

Chen, G.-Y., J.M. Cleary, A.B. Asenjo, Y. Chen, J.A. Mascaro, D.F.J. Arginteanu, H. Sosa, and W.O. Hancock. 2019. Kinesin-5 Promotes Microtubule Nucleation and Assembly by Stabilizing a Lattice-Competent Conformation of Tubulin. *Curr. Biol.* 29:2259-2269.e4. doi:10.1016/j.cub.2019.05.075.

Chen, J., E. Kholina, A. Szyk, V.A. Fedorov, I. Kovalenko, N. Gudimchuk, and A. Roll-Mecak. 2021. A-Tubulin Tail Modifications Regulate Microtubule Stability Through Selective Effector Recruitment, Not Changes in Intrinsic Polymer Dynamics. *Dev. Cell*. 56:2016-2028.e4. doi:10.1016/j.devcel.2021.05.005.

Chen, Y., and W.O. Hancock. 2015. Kinesin-5 is a microtubule polymerase. *Nat. Commun.* 6:8160. doi:10.1038/ncomms9160.

Chrétien, D., and S.D. Fuller. 2000. Microtubules switch occasionally into unfavorable configurations during elongation. *J. Mol. Biol.* 298:663–676. doi:10.1006/jmbi.2000.3696.

Chrétien, D., S.D. Fuller, and E. Karsenti. 1995. Structure of growing microtubule ends: Two-dimensional sheets close into tubes at variable rates. *J. Cell Biol.*

129:1311–1328. doi:10.1083/jcb.129.5.1311.

Coombes, C.E., A. Yamamoto, M.R. Kenzie, D.J. Odde, and M.K. Gardner. 2013. Evolving tip structures can explain age-dependent microtubule catastrophe. *Curr. Biol.* 23:1342–1348. doi:10.1016/j.cub.2013.05.059.

Cyr, R.J. 1994. Microtubules in plant morphogenesis: Role of the cortical array. *Annu. Rev. Cell Biol.* 10:153–180. doi:10.1146/annurev.cb.10.110194.001101.

Dammermann, A., A. Desai, and K. Oegema. 2003. The minus end in sight. *Curr. Biol.* 13:614–624. doi:10.1016/S0960-9822(03)00530-X.

Datta, A., S. Deng, V. Gopal, K.C.H. Yap, C.E. Halim, M.L. Lye, M.S. Ong, T.Z. Tan, G. Sethi, S.C. Hooi, A.P. Kumar, and C.T. Yap. 2021. Cytoskeletal dynamics in epithelial-mesenchymal transition: Insights into therapeutic targets for cancer metastasis. *Cancers (Basel).* 13:1–27. doi:10.3390/cancers13081882.

David-Pfeuty, T., H.P. Erickson, and D. Pantaloni. 1977. Guanosinetriphosphatase activity of tubulin associated with microtubule assembly. *Proc. Natl. Acad. Sci. U. S. A.* 74:5372–5376. doi:10.1073/pnas.74.12.5372.

Dehmelt, L., and S. Halpain. 2004. Protein family review The MAP2 / Tau family of microtubule-associated proteins. *Genome Biol.* 6:1–10.

Demchouk, A.O., M.K. Gardner, and D.J. Odde. 2011. Microtubule tip tracking and tip structures at the nanometer scale using digital fluorescence microscopy. *Cell. Mol. Bioeng.* 4:192–204. doi:10.1007/s12195-010-0155-6.

Desai, A., and T.J. Mitchison. 1997. Microtubule Polymerization Dynamics. *Annu. Rev. Cell Dev. Biol.* 13:83–117. doi:10.1146/annurev.cellbio.13.1.83.

Dixit, R., B. Barnett, J.E. Lazarus, M. Tokito, Y.E. Goldman, and E.L.F. Holzbaur. 2009. Microtubule plus-end tracking by CLIP-170 requires EB1. *Proc. Natl. Acad. Sci. U. S. A.* 106:492–497. doi:10.1073/pnas.0807614106.

Doodhi, H., A.E. Prota, L.C. Kapitein, A. Akhmanova, and M.O. Steinmetz. 2016. Termination of Protofilament Elongation by Eribulin Induces Lattice Defects that Promote Microtubule Catastrophes. *Curr. Biol.* 26:1713–1721. doi:10.1016/j.cub.2016.04.053.

Drabek, K., M. van Ham, T. Stepanova, K. Draegestein, R. van Horssen, C.L. Sayas, A. Akhmanova, T. ten Hagen, R. Smits, R. Fodde, F. Grosveld, and N. Galjart. 2006. Role of CLASP2 in Microtubule Stabilization and the Regulation of Persistent Motility. *Curr. Biol.* 16:2259–2264. doi:10.1016/j.cub.2006.09.065.

Drechsel, D.N., A.A. Hyman, M.H. Cobb, and M.W. Kirschner. 1992. Modulation of the dynamic instability of tubulin assembly by the microtubule-associated protein tau. *Mol. Biol. Cell*. 3:1141–54. doi:10.1091/mbc.3.10.1141.

Drechsel, D.N., and M.W. Kirschner. 1994. The minimum GTP cap required to stabilize microtubules. *Curr. Biol.* 4:1053–1061. doi:10.1016/S0960-9822(00)00243-8.

Duellberg, C., N.I. Cade, D. Holmes, and T. Surrey. 2016. The size of the EB cap

determines instantaneous microtubule stability. *Elife*. 5:1–23. doi:10.7554/eLife.13470.

Efimov, A., A. Kharitonov, N. Efimova, J. Loncarek, P.M. Miller, N. Andreyeva, P. Gleeson, N. Galjart, A.R.R. Maia, I.X. McLeod, J.R. Yates, H. Maiato, A. Khodjakov, A. Akhmanova, and I. Kaverina. 2007. Asymmetric CLASP-Dependent Nucleation of Noncentrosomal Microtubules at the trans-Golgi Network. *Dev. Cell*. 12:917–930. doi:10.1016/j.devcel.2007.04.002.

Erickson, H.P. 1989. Co-operativity in protein-protein association. The structure and stability of the actin filament. *J. Mol. Biol.* 206:465–474. doi:10.1016/0022-2836(89)90494-4.

Erickson, H.P., and D. Pantaloni. 1981. The role of subunit entropy in cooperative assembly. Nucleation of microtubules and other two-dimensional polymers. *Biophys. J.* 34:293–309. doi:10.1016/S0006-3495(81)84850-3.

Fan, J., A.D. Griffiths, A. Lockhart, R.A. Cross, and L.A. Amos. 1996. Microtubule minus ends can be labelled with a phage display antibody specific to alpha-tubulin. *J. Mol. Biol.* 259:325–330. doi:10.1006/jmbi.1996.0322.

Farmer, V., G. Arpağ, S. Hall, and M. Zanic. 2021. XMAP215 promotes microtubule catastrophe by disrupting the growing microtubule end. *J. Cell Biol.* 220:1–13. doi:10.1101/2020.12.29.424748.

Farmer, V.J., and M. Zanic. 2021. TOG-domain proteins. *Curr. Biol.* 31:R499–R501.

doi:10.1016/j.cub.2021.01.039.

Flyvbjerg, H., T. Holy, and S. Leibler. 1996. Microtubule dynamics: Caps, catastrophes, and coupled hydrolysis. *Phys. Rev. E*. 54:5538–5560. doi:10.1103/PhysRevE.54.5538.

Gard, D.L., B.E. Becker, and S. Josh Romney. 2004. MAPping the eukaryotic tree of life: Structure, function, and evolution of the MAP215/Dis1 family of microtubule-associated proteins. *Int. Rev. Cytol.* doi:10.1016/S0074-7696(04)39004-2.

Gard, D.L., and M.W. Kirschner. 1987a. A microtubule-associated protein from Xenopus eggs that specifically promotes assembly at the plus-end. *J. Cell Biol.* 105:2203–2215. doi:10.1083/jcb.105.5.2203.

Gard, D.L., and M.W. Kirschner. 1987b. A Microtubule-associated Protein from Xenopus Eggs That Specifically Promotes Assembly at the Plus-End. 105:2203–2215. doi:10.1083/jcb.105.5.2203.

Gardner, M.K., B.D. Charlebois, I.M. Janosi, J. Howard, A.J. Hunt, and D.J. Odde. 2011a. Rapid microtubule self-assembly kinetics. *Cell*. 146:582–592. doi:10.1016/j.cell.2011.06.053.

Gardner, M.K., M. Zanic, C. Gell, V. Bormuth, and J. Howard. 2011b. Depolymerizing kinesins Kip3 and MCAK shape cellular microtubule architecture by differential control of catastrophe. *Cell*. 147:1092–1103. doi:10.1016/j.cell.2011.10.037.

Gardner, M.K., M. Zanic, and J. Howard. 2013. Microtubule catastrophe and rescue.

Curr. Opin. Cell Biol. 25:1–9. doi:10.1016/j.ceb.2012.09.006.

Gell, C., V. Bormuth, G.J. Brouhard, D.N. Cohen, S. Diez, C.T. Friel, J. Helenius, B. Nitzsche, H. Petzold, J. Ribbe, E. Schaffer, J.H. Stear, A. Trushko, V. Varga, P.O. Widlund, M. Zanic, and J. Howard. 2010. Microtubule dynamics reconstituted in vitro and imaged by single-molecule fluorescence microscopy. 95. First edit. Elsevier. 221–245 pp.

Geyer, E.A., M.P. Miller, C.A. Brautigam, S. Biggins, and L.M. Rice. 2018. Design principles of a microtubule polymerase. *Elife*. 7. doi:10.7554/eLife.34574.

Goodson, H. V, and E.M. Jonasson. 2018. Microtubules and Microtubule-Associated Proteins. *Cold Spring Harb. Perspect. Biol.* 1–20.

De Groot, C.O., I. Jelesarov, F.F. Damberger, S. Bjelić, M.A. Schärer, N.S. Bhavesh, I. Grigoriev, R.M. Buey, K. Wüthrich, G. Capitani, A. Akhmanova, and M.O. Steinmetz. 2010. Molecular insights into mammalian end-binding protein heterodimerization. *J. Biol. Chem.* 285:5802–5814. doi:10.1074/jbc.M109.068130.

Gudimchuk, N.B., E. V Ulyanov, E.O. Toole, C.L. Page, D.S. Vinogradov, G. Morgan, G. Li, J.K. Moore, E. Szczesna, A. Roll-mecak, F.I. Ataullakhanov, and J.R. Mcintosh. 2020. Mechanisms of microtubule dynamics and force generation examined with computational modeling and electron cryotomography. *Nat. Commun.* 1–15. doi:10.1038/s41467-020-17553-2.

Guesdon, A., F. Bazile, R.M. Buey, R. Mohan, S. Monier, R.R. García, M. Angevin, C. Heichette, R. Wieneke, R. Tampé, L. Duchesne, A. Akhmanova, M.O. Steinmetz, and D. Chrétien. 2016. EB1 interacts with outwardly curved and straight regions of the microtubule lattice. *Nat. Cell Biol.* 1. doi:10.1038/ncb3412.

Gupta, K.K., C. Li, A. Duan, E.O. Alberico, O. V. Kim, M.S. Alber, and H. V. Goodson. 2013. Mechanism for the catastrophe-promoting activity of the microtubule destabilizer Op18/stathmin. *Proc. Natl. Acad. Sci. U. S. A.* 110:20449–20454. doi:10.1073/pnas.1309958110.

Hahn, I., A. Voelzmann, J. Parkin, J.B. Fülle, P.G. Slater, L.A. Lowery, N. Sanchez-Soriano, and A. Prokop. 2021. Tau, XMAP215/Msps and Eb1 co-operate interdependently to regulate microtubule polymerisation and bundle formation in axons. *PLoS Genet.* 17:1–30. doi:10.1371/journal.pgen.1009647.

Hannak, E., K. Oegema, M. Kirkham, P. Gönczy, B. Habermann, and A.A. Hyman. 2002. The kinetically dominant assembly pathway for centrosomal asters in Caenorhabditis elegans is γ-tubulin dependent. *J. Cell Biol.* 157:591–602. doi:10.1083/jcb.200202047.

van Haren, J., and T. Wittmann. 2019. Microtubule Plus End Dynamics − Do We Know How Microtubules Grow? *BioEssays*. 1800194:1800194. doi:10.1002/bies.201800194.

Heald, R., R. Tournebize, T. Blank, R. Sandaltzopoulos, P. Becker, A.A. Hyman, and E. Karsenti. 1996. Self-organization of microtubules into bipolar spindles around

artificial chromosomes in Xenopus egg extracts. *Nature*. 382:420–5. doi:10.1038/382420a0.

Honnappa, S., S.M. Gouveia, A. Weisbrich, F.F. Damberger, N.S. Bhavesh, H. Jawhari, I. Grigoriev, F.J.A. van Rijssel, R.M. Buey, A. Lawera, I. Jelesarov, F.K. Winkler, K. Wuthrich, A. Akhmanova, and M.O. Steinmetz. 2009. An EB1-Binding Motif Acts as a Microtubule Tip Localization Signal. *Cell*. 138:366–376. doi:10.1016/j.cell.2009.04.065.

Honnappa, S., O. Okhrimenko, R. Jaussi, H. Jawhari, I. Jelesarov, F.K. Winkler, and M.O. Steinmetz. 2006. Key Interaction Modes of Dynamic +TIP Networks. *Mol. Cell*. 23:663–671. doi:10.1016/j.molcel.2006.07.013.

Horio, T., and H. Hotani. 1986. Visualization of the dynamic instability of individual micortubules by dark-field microscopy. *Nature*. 320:264–265. doi:10.1038/323646a0.

Howard, J., and A.A. Hyman. 2009. Growth, fluctuation and switching at microtubule plus ends. *Nat. Rev. Mol. Cell Biol.* 10:569–574. doi:10.1038/nrm2713.

Hunyadi, V., D. Chrétien, and I.M. Jánosi. 2005. Mechanical stress induced mechanism of microtubule catastrophes. *J. Mol. Biol.* 348:927–938. doi:10.1016/j.jmb.2005.03.019.

Hyman, A.A., D.N. Drechsel, D. Kellogg, S. Salser, K. Sawin, P. Steffen, L. Wordeman, and T.J. Mitchison. 1991. Preparation of Modified Tubulins. *Methods*

Enzymol. 196:478–485.

Hyman, A.A., S. Salser, D.N. Drechsel, N. Unwin, and T.J. Mitchison. 1992. Role of GTP Hydrolysis in Microtubule Dynamics : Information from a Slowly Hydrolyzable Analogue , GMPCPP. *Mol. Biol. Cell*. 3:1155–1167.

Igaev, M., and H. Grubmüller. 2018. Microtubule assembly governed by tubulin allosteric gain in flexibility and lattice induced fit. *Elife*. 7:1–21. doi:10.7554/eLife.34353.

Inoué, S., and H. Sato. 1967. Cell Motility by Labile Association of Molecules: The nature of mitotic spindle fibers and their role in chromosome movement. *J. Gen. Physiol.* 50:259–292. doi:10.1085/jgp.50.6.259.

Inoue, Y.H., M.D.C. Avides, M. Shiraki, P. Deak, M. Yamaguchi, Y. Nishimoto, A. Matsukage, and D.M. Glover. 2000. Orbit, a novel microtubule-associated protein essential for mitosis in 3Drosophila melanogaster. *J. Cell Biol.* 149:153–165. doi:10.1083/jcb.149.1.153.

Jacobs, M., H. Smith, and T.E. W. 1974. Tubulin : Nucleotide Binding and Enzymic Activity. *J. Mol. Biol.* 89:455–468. doi:10.1016/0022-2836(72)90401-9.

Kerssemakers, J.W.J., E.L. Munteanu, L. Laan, T.L. Noetzel, M.E. Janson, and M. Dogterom. 2006. Assembly dynamics of microtubules at molecular resolution. *Nature*. 442:709–712. doi:10.1038/nature04928.

Khodjakov, A., and C.L. Rieder. 1999. The sudden recruitment of γ-tubulin to the

centrosome at the onset of mitosis and its dynamic exchange throughout the cell cycle, do not require microtubules. *J. Cell Biol.* 146:585–596. doi:10.1083/jcb.146.3.585.

Kim, T., and L.M. Rice. 2019. Long-range, through-lattice coupling improves predictions of microtubule catastrophe. *Mol. Biol. Cell*. 30:mbc.E18-10-0641. doi:10.1091/mbc.E18-10-0641.

Kirschner, M.W., R.C. Williams, M. Weingarten, and J.C. Gerhart. 1974. Microtubules from mammalian brain: some properties of their depolymerization products and a proposed mechanism of assembly and disassembly. *Proc. Natl. Acad. Sci. U. S. A.* 71:1159–1163. doi:10.1073/pnas.71.4.1159.

Kobayashi, T. 1975. Dephosphorylation of Tubulin-bound Guanosine Triphosphate during Microtuble Assembly. *J. Biochem.* 77:1193–1197.

Kollman, J.M., A. Merdes, L. Mourey, and D.A. Agard. 2011. Microtubule nucleation by γ-tubulin complexes. *Nat. Rev. Mol. Cell Biol.* 12:709–721. doi:10.1038/nrm3209.

Kollman, J.M., J.K. Polka, A. Zelter, T.N. Davis, and D.A. Agard. 2010. Microtubule nucleating γ-TuSC assembles structures with 13-fold microtubule-like symmetry. *Nature*. 466:879–882. doi:10.1038/nature09207.

Komarova, Y.A., C.O. De Groot, I. Grigoriev, S.M. Gouveia, E.L. Munteanu, J.M. Schober, S. Honnappa, R.M. Buey, C.C. Hoogenraad, M. Dogterom, G.G. Borisy,

M.O. Steinmetz, and A. Akhmanova. 2009. Mammalian end binding proteins control persistent microtubule growth. *J. Cell Biol.* 184:691–706. doi:10.1083/jcb.200807179.

Komarova, Y.A., G. Lansbergen, N. Galjart, F. Grosveld, G.G. Borisy, and A. Akhmanova. 2005. EB1 and EB3 Control CLIP Dissociation from the Ends of Growing Microtubules. *Mol. Biol. Cell*. 16:5356–5372. doi:10.1091/mbc.E05.

Kuo, Y.-W., O. Trottier, M. Mahamdeh, and J. Howard. 2019. Spastin is a dual-function enzyme that severs microtubules and promotes their regrowth to increase the number and mass of microtubules. *Proc. Natl. Acad. Sci. U. S. A.* doi:10.1073/pnas.1818824116.

Kuo, Y.W., and J. Howard. 2021. Cutting, Amplifying, and Aligning Microtubules with Severing Enzymes. *Trends Cell Biol.* 31:50–61. doi:10.1016/j.tcb.2020.10.004.

Lafrance, B.J., J. Roostalu, G. Henkin, B.J. Greber, R. Zhang, D. Normanno, C. McCollum, T. Surrey, and E. Nogales. 2022. Structural transitions in the GTP cap visualized by cryo-EM of catalytically inactive microtubules. *Proc. Natl. Acad. Sci.* 119:1–12. doi:10.1073/pnas.2114994119/-/DCSupplemental.Published.

Lansbergen, G., and A. Akhmanova. 2006. Microtubule plus end: A hub of cellular activities. *Traffic*. 7:499–507. doi:10.1111/j.1600-0854.2006.00400.x.

Lawrence, E.J., G. Arpag, C. Arnaiz, and M. Zanic. 2021. Ssna1 stabilizes dynamic microtubules and detects microtubule damage. *Elife*. 10:1–21.

doi:10.7554/eLife.67282.

Lawrence, E.J., G. Arpag, S.R. Norris, and M. Zanic. 2018. Human CLASP2 specifically regulates microtubule catastrophe and rescue. *Mol. Biol. Cell*. 29:1168–1177. doi:10.1091/mbc.E18-01-0016.

Lawrence, E.J., M. Zanic, and L.M. Rice. 2020. CLASPs at a glance. *J. Cell Sci.* 133:1–7. doi:10.1242/jcs.243097.

Lemos, C.L., P. Sampaio, H. Maiato, M. Costa, L. V. Omel'yanchuk, V. Liberal, and C.E. Sunkel. 2000. Mast, a conserved microtubule-associated protein required for bipolar mitotic spindle organization. *EMBO J.* 19:3668–3682. doi:10.1093/emboj/19.14.3668.

Linse, K., and E.-M. Mandelkow. 1988. The GTP-binding Peptide of &Tubulin. *J. Biol. Chem.* 263:15205–15210.

Liu, P., M. Würtz, E. Zupa, S. Pfeffer, and E. Schiebel. 2021. Microtubule nucleation: The waltz between γ-tubulin ring complex and associated proteins. *Curr. Opin. Cell Biol.* 68:124–131. doi:10.1016/j.ceb.2020.10.004.

Löwe, J., H. Li, K.H. Downing, and E. Nogales. 2001. Refined structure of αβ-tubulin at 3.5 Å resolution. *J. Mol. Biol.* 313:1045–1057. doi:10.1006/jmbi.2001.5077.

Maccioni, R., and N.W. Seeds. 1977. Stoichiometry of GTP hydrolysis and tubulin polymerization. *Proc. Natl. Acad. Sci.* 74:462–466.

Maiato, H., E.A.L. Fairley, C.L. Rieder, J.R. Swedlow, C.E. Sunkel, and W.C. Earnshaw. 2003. Human CLASP1 is an outer kinetochore component that regulates spindle microtubule dynamics. *Cell*. 113:891–904. doi:10.1016/S0092-8674(03)00465-3.

Maiato, H., A. Khodjakov, and C.L. Rieder. 2005. Drosophila CLASP is required for the incorporation of microtubule subunits into fluxing kinetochore fibres. *Nat. Cell Biol.* 7:42–47. doi:10.1038/ncb1207.

Maiato, H., C.L. Rieder, and A. Khodjakov. 2004. Kinetochore-driven formation of kinetochore fibers contributes to spindle assembly during animal mitosis. *J. Cell Biol.* 167:831–840. doi:10.1083/jcb.200407090.

Majumdar, S., T. Kim, Z. Chen, S. Munyoki, S.-C. Tso, C.A. Brautigam, and L.M. Rice. 2018. An isolated CLASP TOG domain suppresses microtubule catastrophe and promotes rescue. *Mol. Biol. Cell*. 0–1. doi:10.1111/cbdd.13316.

Mandelkow, E.-M., E. Mandelkow, and R.A. Milliganll. 1991. Microtubule dynamics and microtubule caps: a time-resolved cryo- electron microscopy study. *J. Cell Biol.* 114:977–991. doi:10.1083/jcb.114.5.977.

Margolin, G., I. V. Gregoretti, T.M. Cickovski, C. Li, W. Shi, M.S. Alber, and H. V. Goodson. 2012. The mechanisms of microtubule catastrophe and rescue: Implications from analysis of a dimer-scale computational model. *Mol. Biol. Cell*. 23:642–656. doi:10.1091/mbc.E11-08-0688.

Margolis, R.L., and L. Wilson. 1978. Opposite end assembly and disassembly of microtubules at steady state in vitro. *Cell*. 13:1–8. doi:10.1016/0092-8674(78)90132-0.

Martin, M., and A. Akhmanova. 2018. Coming into Focus: Mechanisms of Microtubule Minus-End Organization. *Trends Cell Biol.* 28:574–588. doi:10.1016/j.tcb.2018.02.011.

Martin, S.R., F.M.M. Butler, D.C. Clark, J.-M. Zhou, and P.M. Bayley. 1987. Magnesium ion effects on microtubule nucleation in vitro. *Biochim. Biophys. Acta*. 914:96–100.

Maurer, S.P., P. Bieling, J. Cope, A. Hoenger, and T. Surrey. 2011. GTPγS microtubules mimic the growing microtubule end structure recognized by end-binding proteins (EBs). *Proc. Natl. Acad. Sci.* 108:3988–3993. doi:10.1073/pnas.1014758108.

Maurer, S.P., N.I. Cade, G. Bohner, N. Gustafsson, E. Boutant, and T. Surrey. 2014. EB1 accelerates two conformational transitions important for microtubule maturation and dynamics. *Curr. Biol.* 24:372–384. doi:10.1016/j.cub.2013.12.042.

Maurer, S.P., F.J. Fourniol, G. Bohner, C.A. Moores, and T. Surrey. 2012. EBs recognize a nucleotide-dependent structural cap at growing microtubule ends. *Cell*. 149:371–382. doi:10.1016/j.cell.2012.02.049.

McAlear, T.S., and S. Bechstedt. 2022. The mitotic spindle protein CKAP2 potently increases formation and stability of microtubules. *Elife*. 11:1–15. doi:10.7554/elife.72202.

Mcintosh, J.R., E.O. Toole, G. Morgan, J. Austin, E. Ulyanov, F.I. Ataullakhanov, and N.B. Gudimchuk. 2018. Microtubules grow by the addition of bent guanosine triphosphate tubulin to the tips of curved protofilaments. *J. Cell Biol.* 1–25.

Michaels, T.C.T., S. Feng, H. Liang, and L. Mahadevan. 2020. Mechanics and kinetics of dynamic instability. *Elife*. e54077. doi:10.7554/eLife.54077.

Mickolajczyk, K.J., E.A. Geyer, T. Kim, L.M. Rice, and W.O. Hancock. 2019. Direct observation of individual tubulin dimers binding to growing microtubules. *PNAS*. 1–15. doi:10.1101/418053.

Miller, P.M., A.W. Folkmann, A.R.R. Maia, N. Efimova, A. Efimov, and I. Kaverina. 2009. Golgi-derived CLASP-dependent microtubules control Golgi organization and polarized trafficking in motile cells. *Nat. Cell Biol.* 11:1069–1080. doi:10.1038/ncb1920.

Mimori-Kiyosue, Y., I. Grigoriev, G. Lansbergen, H. Sasaki, C. Matsui, F. Severin, N. Galjart, F. Grosveld, I.A. Vorobjev, S. Tsukita, and A. Akhmanova. 2005. CLASP1 and CLASP2 bind to EB1 and regulate microtubule plus-end dynamics at the cell cortex. *J. Cell Biol.* 168:141–153. doi:10.1083/jcb.200405094.

Mitchison, T.J., and M.W. Kirschner. 1984. Dynamic instability of microtubule growth.

Nature. 310:237–242.

Mogensen, M.M., and J.B. Tucker. 1987. Evidence for microtubule nucleation at plasma membrane-associated sites in Drosophila. *J. Cell Sci.* 88 (Pt 1):95–107. doi:10.1242/jcs.88.1.95.

Mohan, R., E.A. Katrukha, H. Doodhi, I. Smal, E. Meijering, L.C. Kapitein, M.O. Steinmetz, and A. Akhmanova. 2013. End-binding proteins sensitize microtubules to the action of microtubule-targeting agents. *Proc. Natl. Acad. Sci. U. S. A.* 110:8900–5. doi:10.1073/pnas.1300395110.

Moores, C.A., and R.A. Milligan. 2006. Lucky 13 - Microtubule depolymerisation by kinesin-13 motors. *J. Cell Sci.* 119:3905–3913. doi:10.1242/jcs.03224.

Moritz, M., M.B. Braunfeld, V. Guénebaut, J. Heuser, and D.A. Agard. 2000. Structure of the γ-tubulin ring complex: A template for microtubule nucleation. *Nat. Cell Biol.* 2:365–370. doi:10.1038/35014058.

Mulder, A.M., A. Glavis-Bloom, C.A. Moores, M. Wagenbach, B. Carragher, L. Wordeman, and R.A. Milligan. 2009. A new model for binding of kinesin 13 to curved microtubule protofilaments. *J. Cell Biol.* 185:51–57. doi:10.1083/jcb.200812052.

Mustyatsa, V. V., A. V. Boyakhchyan, F.I. Ataullakhanov, and N.B. Gudimchuk. 2017. EB-family proteins: Functions and microtubule interaction mechanisms. *Biochem.* 82:791–802. doi:10.1134/S0006297917070045.

Mustyatsa, V. V., A. V. Kostarev, A. V. Tvorogova, F.I. Ataullakhanov, N.B. Gudimchuk, and I.A. Vorobjev. 2019. Fine structure and dynamics of EB3 binding zones on microtubules in fibroblast cells. *Mol. Biol. Cell*. 30:2105–2114. doi:10.1091/mbc.e18-11-0723.

Nakamura, M., J.J. Lindeboom, M. Saltini, B.M. Mulder, and D.W. Ehrhardt. 2018. SPR2 protects minus ends to promote severing and reorientation of plant cortical microtubule arrays. *J. Cell Biol.* 217:915–927. doi:10.1083/jcb.201708130.

Nogales, E., M. Whittaker, R.A. Milligan, and K.H. Downing. 1999. High-resolution model of the microtubule. *Cell*. 96:79–88. doi:10.1016/S0092-8674(00)80961-7.

Nogales, E., S.G. Wolf, and K.H. Downing. 1998. Structure of the ab-tubulin dimer by electron crystallography. *Nature*. 391:199–204. doi:10.1007/1-4020-3920-4.

O'Brien, E.T., E.D. Salmon, and H.P. Erickson. 1997. How calcium causes microtubule depolymerization. *Cell Motil. Cytoskeleton*. 36:125–135. doi:10.1002/(SICI)1097-0169(1997)36:2<125::AID-CM3>3.0.CO;2-8.

O'Brien, E.T., W.A. Voter, and H.P. Erickson. 1987. GTP hydrolysis during microtubule assembly. *Biochemistry*. 26:4148–4156. doi:10.1021/bi00387a061.

Odde, D.J., L. Cassimeris, and H.M. Buettner. 1995. Kinetics of microtubule catastrophe assessed by probabilistic analysis. *Biophys. J.* 69:796–802. doi:10.1016/S0006-3495(95)79953-2.

Orbach, R., and J. Howard. 2019. The dynamic and structural properties of axonemal

tubulins support the high length stability of cilia. *Nat. Commun.* 10:1–11. doi:10.1038/s41467-019-09779-6.

Ori-McKenney, K.M., L.Y. Jan, and Y.N. Jan. 2012. Golgi Outposts Shape Dendrite Morphology by Functioning as Sites of Acentrosomal Microtubule Nucleation in Neurons. *Neuron*. 76:921–930. doi:10.1016/j.neuron.2012.10.008.

Petry, S., A.C. Groen, K. Ishihara, T.J. Mitchison, and R.D. Vale. 2013. Branching microtubule nucleation in xenopus egg extracts mediated by augmin and TPX2. *Cell*. 152:768–777. doi:10.1016/j.cell.2012.12.044.

Petry, S., and R.D. Vale. 2015. Microtubule nucleation at the centrosome and beyond. *Nat. Cell Biol.* 17:1089–1093. doi:10.1038/ncb3220.

Piehl, M., and L. Cassimeris. 2003. Organization and Dynamics of Growing Microtubule Plus Ends during Early Mitosis. *Mol. Biol. Cell*. 14:916–925. doi:10.1091/mbc.E02.

Prahl, L.S., B.T. Castle, M.K. Gardner, and D.J. Odde. 2014. Quantitative analysis of microtubule self-assembly kinetics and tip structure. 540. 1st ed. Elsevier Inc. 35–52 pp.

Ramirez-Rios, S., E. Denarier, E. Prezel, A. Vinit, V. Stoppin-Mellet, F. Devred, P. Barbier, V. Peyrot, C.L. Sayas, J. Avila, L. Peris, A. Andrieux, L. Serre, A. Fourest-Lieuvin, and I. Arnal. 2016. Tau antagonizes end-binding protein tracking at microtubule ends through a phosphorylation-dependent mechanism. *Mol. Biol.*

Cell. 27:2924–2934. doi:10.1091/mbc.E16-01-0029.

Reid, T.A., C. Coombes, S. Mukherjee, R.R. Goldblum, K. White, S. Parmar, M. Mcclellan, M. Zanic, N. Courtemanche, and M.K. Gardner. 2019. Structural state recognition facilitates tip tracking of EB1 at growing microtubule ends. *Elife*. 1–32. doi:10.1101/636092.

Rickman, J., C. Duellberg, N.I. Cade, L.D. Griffin, and T. Surrey. 2017. Steady-state EB cap size fluctuations are determined by stochastic microtubule growth and maturation. *Proc. Natl. Acad. Sci.* 201620274. doi:10.1073/pnas.1620274114.

Roostalu, J., N.I. Cade, and T. Surrey. 2015. Complementary activities of TPX2 and chTOG constitute an efficient importin-regulated microtubule nucleation module. *Nat. Cell Biol.* doi:10.1038/ncb3241.

Roostalu, J., and T. Surrey. 2017. Microtubule nucleation: Beyond the template. *Nat. Rev. Mol. Cell Biol.* 18:702–710. doi:10.1038/nrm.2017.75.

Roostalu, J., C. Thomas, N.I. Cade, S. Kunzelmann, I.A. Taylor, and T. Surrey. 2020. The speed of GTP hydrolysis determines GTP cap size and controls microtubule stability. *Elife*. 9:1–22. doi:10.7554/eLife.51992.

Roth, D., B.P. Fitton, N.P. Chmel, N. Wasiluk, and A. Straube. 2019. Spatial positioning of EB family proteins at microtubule tips involves distinct nucleotide-dependent binding properties. *J. Cell Sci.* 132. doi:10.1242/jcs.219550.

Ruhnow, F., D. Zwicker, and S. Diez. 2011. Tracking single particles and elongated

filaments with nanometer precision. *Biophys. J.* 100:2820–2828. doi:10.1016/j.bpj.2011.04.023.

Rusan, N.M., C.J. Fagerstrom, A.-M.C. Yvon, and P. Wadsworth. 2001. Cell cycle-dependent changes in microtubule dynamics in living cells expressing green fluorescent protein-alpha tubulin. *Mol. Biol. Cell*. 12:971–80.

Sanchez, A.D., and J.L. Feldman. 2017. Microtubule-organizing centers: from the centrosome to non-centrosomal sites. *Curr. Opin. Cell Biol.* 44:93–101. doi:10.1016/j.ceb.2016.09.003.

Sanders, A.A.W.M., and I. Kaverina. 2015. Nucleation and dynamics of Golgi-derived microtubules. *Front. Neurosci.* 9:1–7. doi:10.3389/fnins.2015.00431.

Schilstra, M.J., P.M. Bayley, and S.R. Martin. 1991. The effect of solution composition on microtubule dynamic instability. *Biochem. J.* 277:839–847.

Schindelin, J., I. Arganda-Carreras, E. Frise, V. Kaynig, M. Longair, T. Pietzsch, S. Preibisch, C. Rueden, S. Saalfeld, B. Schmid, J.Y. Tinevez, D.J. White, V. Hartenstein, K. Eliceiri, P. Tomancak, and A. Cardona. 2012. Fiji: An open-source platform for biological-image analysis. *Nat. Methods*. 9:676–682. doi:10.1038/nmeth.2019.

Seetapun, D., B.T. Castle, A.J. McIntyre, P.T. Tran, and D.J. Odde. 2012. Estimating the microtubule GTP cap size in vivo. *Curr. Biol.* 22:1681–1687. doi:10.1016/j.cub.2012.06.068.

Sen, I., D. Veprintsev, A. Akhmanova, and M.O. Steinmetz. 2013. End Binding Proteins Are Obligatory Dimers. *PLoS One*. 8:1–7. doi:10.1371/journal.pone.0074448.

Shelanski, M.L., F. Gaskin, and C.R. Cantor. 1973. Microtubule assembly in the absence of added nucleotides. *Proc. Natl. Acad. Sci. U. S. A.* 70:765–8. doi:10.1073/pnas.70.3.765.

Shelanski, M.L., and E.W. Taylor. 1967. Isolation of a protein subunit from microtubules. *J. Cell Biol.* 34:549–554. doi:10.1083/jcb.34.2.549.

Simon, J.R., and E.D. Salmon. 1990. The structure of microtubule ends during the elongation and shortening phases of dynamic instability examined by negative-stain electron microscopy. *J. Cell Sci.* 96 (Pt 4):571–82. doi:10.1109/TSP.2003.822287.

Slep, K.C. 2009. The role of TOG domains in microtubule plus end dynamics. *Biochem. Soc. Trans.* 37:1002–1006. doi:10.1042/BST0371002.

Slep, K.C., and R.D. Vale. 2007. Structural Basis of Microtubule Plus End Tracking by XMAP215, CLIP-170, and EB1. *Mol. Cell*. 27:976–991. doi:10.1016/j.molcel.2007.07.023.

Steinmetz, M.O., and A. Akhmanova. 2008. Capturing protein tails by CAP-Gly domains. *Trends Biochem. Sci.* 33:535–545. doi:10.1016/j.tibs.2008.08.006.

Stepanova, T., I. Smal, J. Van Haren, U. Akinci, Z. Liu, M. Miedema, R. Limpens, M.

Van Ham, M. Van Der Reijden, R. Poot, F. Grosveld, M. Mommaas, E. Meijering, and N. Galjart. 2010. History-dependent catastrophes regulate axonal microtubule behavior. *Curr. Biol.* 20:1023–1028. doi:10.1016/j.cub.2010.04.024.

Stewman, S.F., K.K. Tsui, and A. Ma. 2020. Dynamic Instability from Non-equilibrium Structural Transitions on the Energy Landscape of Microtubule. *Cell Syst.* 11:608-624.e9. doi:10.1016/j.cels.2020.09.008.

Strome, S., J. Powers, M. Dunn, K. Reese, C.J. Malone, J. White, G. Seydoux, and W. Saxton. 2001. Spindle dynamics and the role of γ-tubulin in early Caenorhabditis elegans embryos. *Mol. Biol. Cell*. 12:1751–1764. doi:10.1091/mbc.12.6.1751.

Strothman, C., V. Farmer, G. Arpağ, N. Rodgers, M. Podolski, S. Norris, R. Ohi, and M. Zanic. 2019. Microtubule minus-end stability is dictated by the tubulin off-rate. *J. Cell Biol.* 218:2841–2853. doi:10.1083/jcb.201905019.

Su, L.-K., M. Burrell, D.E. Hill, J. Gyuris, R. Brent, R. Wiltshire, J. Trent, B. Vogelstein, and K.W. Kinzler. 1995. APC Binds to the Novel Protein EB1. *Cancer Res.* 55:2972–2977.

Tarantino, N., J.Y. Tinevez, E.F. Crowell, B. Boisson, R. Henriques, M. Mhlanga, F. Agou, A. Israël, and E. Laplantine. 2014. Tnf and il-1 exhibit distinct ubiquitin requirements for inducing NEMO-IKK supramolecular structures. *J. Cell Biol.* 204:231–245. doi:10.1083/jcb.201307172.

Tassin, A.M., B. Maro, and M. Bornens. 1985. Fate of microtubule-organizing centers during myogenesis in vitro. *J. Cell Biol.* 100:35–46. doi:10.1083/jcb.100.1.35.

Tilney, L.G., J. Bryan, D.J. Bush, K. Fujiwara, M.S. Mooseker, D.B. Murphy, and D.H. Snyder. 1973. Microtubules: evidence for 13 protofilaments. *J. Cell Biol.* 59:267–275. doi:10.1083/jcb.59.2.267.

Tirnauer, J.S., S. Grego, E.D. Salmon, and T.J. Mitchison. 2002. EB1 – Microtubule Interactions in Xenopus Egg Extracts : Role of EB1 in Microtubule Stabilization and Mechanisms of Targeting to Microtubules. *Mol. Biol. Cell*. 13:3614–3626. doi:10.1091/mbc.E02.

Tran, P.T., R.A. Walker, and E.D. Salmon. 1997. A metastable intermediate state of microtubule dynamic instability that differs significantly between plus and minus ends. *J. Cell Biol.* 138:105–117. doi:10.1083/jcb.138.1.105.

VanBuren, V., L. Cassimeris, and D.J. Odde. 2005. Mechanochemical model of microtubule structure and self-assembly kinetics. *Biophys. J.* 89:2911–2926. doi:10.1529/biophysj.105.060913.

VanBuren, V., D.J. Odde, and L. Cassimeris. 2002. Estimates of lateral and longitudinal bond energies within the microtubule lattice. *Proc. Natl. Acad. Sci.* 99:6035–6040. doi:10.1073/pnas.092504999.

Vasquez, R.J., D.L. Gard, and L. Cassimeris. 1994. XMAP from Xenopus Eggs Promotes Rapid Plus End Assembly of Microtubules and Rapid Microtubule

Polymer Turnover. *J. Cell Biol.* 127:985–993.

Vemu, A., E. Szczesna, E.A. Zehr, J.O. Spector, N. Grigorieff, A.M. Deaconescu, and A. Roll-Mecak. 2018. Severing enzymes amplify microtubule arrays through lattice GTP-tubulin incorporation. *Science (80-.).* 361:eaau1504. doi:10.1126/science.aau1504.

Vitre, B., F.M. Coquelle, C. Heichette, C. Garnier, D. Chrétien, and I. Arnal. 2008. EB1 regulates microtubule dynamics and tubulin sheet closure in vitro. *Nat. Cell Biol.* 10:415–421. doi:10.1038/ncb1703.

Walker, R.A., S. Inoué, and E.D. Salmon. 1989. Asymmetric behavior of severed microtubule ends after ultraviolet-microbeam irradiation of individual microtubules in vitro. *J. Cell Biol.* 108:931–937. doi:10.1083/jcb.108.3.931.

Walker, R.A., E.T. O'Brien, N.K. Pryer, M.F. Soboeiro, W.A. Voter, H.P. Erickson, and E.D. Salmon. 1988. Dynamic Instability of Individual Microtubules. *J. Cell Biol.* 107:1437–1448.

Walker, R.A., N.K. Pryer, and E.D. Salmon. 1991. Dilution of individual microtubules observed in real time in vitro: Evidence that cap size is small and independent of elongation rate. *J. Cell Biol.* 114:73–81. doi:10.1083/jcb.114.1.73.

Weisbrich, A., S. Honnappa, R. Jaussi, O. Okhrimenko, D. Frey, I. Jelesarov, A. Akhmanova, and M.O. Steinmetz. 2007. Structure-function relationship of CAP-Gly domains. *Nat. Struct. Mol. Biol.* 14:959–967. doi:10.1038/nsmb1291.

Weisenberg, R.C. 1972. Microtubule formation in vitro in solutions containing low calcium concentrations. *Science (80-.).* 177:1104–1105.

Weisenberg, R.C., G.G. Borisy, and E.W. Taylor. 1968. The Colchicine-Binding Protein of Mammalian Brain and Its Relation to Microtubules. *Biochemistry*. 7:4466–4479. doi:10.1021/bi00852a043.

Weisenberg, R.C., W.J. Deery, and P.J. Dickinson. 1976. Tubulin-nucleotide interactions during the polymerization and depolymerization of microtubules. *Biochemistry*. 15:4248–4254. doi:10.1021/bi00664a018.

Widlund, P.O., J.H. Stear, A. Pozniakovsky, M. Zanic, S. Reber, G.J. Brouhard, A.A. Hyman, and J. Howard. 2011. XMAP215 polymerase activity is built by combining multiple tubulin-binding TOG domains and a basic lattice-binding region. *Proc. Natl. Acad. Sci.* 108:2741–2746. doi:10.1073/pnas.1016498108.

Williams, R.C., and H.W. Detrich. 1979. Separation of Tubulin from Microtubule-Associated Proteins on Phosphocellulose. Accompanying Alterations in Concentrations of Buffer Components. *Biochemistry*. 18:2499–2503. doi:10.1021/bi00579a010.

Wittmann, T., and C.M. Waterman-Storer. 2005. Spatial regulation of CLASP affinity for microtubules by Rac1 and GSK3β in migrating epithelial cells. *J. Cell Biol.* 169:929–939. doi:10.1083/jcb.200412114.

Ye, X., T. Kim, E.A. Geyer, and L.M. Rice. 2020. Insights into allosteric control of

microtubule dynamics from a buried β-tubulin mutation that causes faster growth and slower shrinkage. *Protein Sci.* 29:1429–1439. doi:10.1002/pro.3842.

Yuba-Kubo, A., A. Kubo, M. Hata, and S. Tsukita. 2005. Gene knockout analysis of two γ-tubulin isoforms in mice. *Dev. Biol.* 282:361–373. doi:10.1016/j.ydbio.2005.03.031.

Yvon, A.M.C., and P. Wadsworth. 1997. Non-centrosomal microtubule formation and measurement of minus end microtubule dynamics in A498 cells. *J. Cell Sci.* 110:2391–2401. doi:10.1242/jcs.110.19.2391.

Zakharov, P., N.B. Gudimchuk, V. Voevodin, A. Tikhonravov, F.I. Ataullakhanov, and E.L. Grishchuk. 2015. Molecular and Mechanical Causes of Microtubule Catastrophe and Aging. *Biophys. J.* 109:2574–2591. doi:10.1016/j.bpj.2015.10.048.

Zanic, M. 2016. Measuring the Effects of Microtubule-Associated Proteins on Microtubule Dynamics In Vitro. *Methods Mol. Biol.* 1413:47–61. doi:10.1007/978-1-4939-3542-0_4.

Zanic, M., J.H. Stear, A.A. Hyman, and J. Howard. 2009. EB1 recognizes the nucleotide state of tubulin in the microtubule lattice. *PLoS One*. 4:1–5. doi:10.1371/journal.pone.0007585.

Zanic, M., P.O. Widlund, A.A. Hyman, and J. Howard. 2013. Synergy between XMAP215 and EB1 increases microtubule growth rates to physiological levels.

Nat. Cell Biol. 15:688–693. doi:10.1038/ncb2744.

Zhang, R., G.M. Alushin, A. Brown, and E. Nogales. 2015. Mechanistic origin of microtubule dynamic instability and its modulation by EB proteins. *Cell*. 162:849–859. doi:10.1016/j.cell.2015.07.012.

Zhang, R., B. LaFrance, and E. Nogales. 2018. Separating the effects of nucleotide and EB binding on microtubule structure. *Proc. Natl. Acad. Sci.* 115:E6191–E6200. doi:10.1073/pnas.1802637115.

Zhang, R., J. Roostalu, T. Surrey, and E. Nogales. 2017. Structural insight into TPX2-stimulated microtubule assembly. *Elife*. 6:e30959. doi:10.7554/eLife.30959.

Zheng, Y., M.L. Wong, B. Alberts, and T. Mitchison. 1995. Nucleation of microtubule assembly by a y-tubulin-containing ring complex. *Nature*. 378:578–583.

Zhu, X., R. Hu, M. Brissova, R.W. Stein, A.C. Powers, G. Gu, and I. Kaverina. 2015. Microtubules Negatively Regulate Insulin Secretion in Pancreatic β Cells. *Dev. Cell*. 34:656–668. doi:10.1016/j.devcel.2015.08.020.